ACOUSTIC SENSORS USING 0-3 NANOCOMPOSITES

LAU SIEN TING

M.PHIL.

THE HONG KONG POLYTECHNIC UNIVERSITY

2001

Table of Contents

Acknowledgements iii

Abstract iv

List of Tables vi

List of Figures vii

Chapter One – Introduction

1.1 Background 1-1

1.2 Piezoelectric Ceramic/Polymer Composite 1-4

1.3 Scope of the Work 1-15

Chapter Two – Sample Preparation

2.1 Materials Used

2.1.1 Nanocrystallite Lead Titanate Powder 2-1

2.1.2 P(VDF-TrFE) Copolymer 2-5

2.2 Fabrication of PT/P(VDF-TrFE) 0-3 Composites 2-7

2.3 Fabrication of P(VDF-TrFE) Copolymer 2-8

2.4 PT Volume Fraction of 0-3 Composites 2-10

2.5 Microstructure of PT/P(VDF-TrFE) 0-3 Composites 2-10

2.6 Sample Poling 2-12

Chapter Three – Characterization of PT/P(VDF-TrFE) 0-3 Composites

3.1 Introduction 3-1

3.2 Estimation of the Degree of Poling in the 0-3 Composites

3.2.1 X-ray Diffraction Method 3-1

3.2.2 Hysteresis Measurement 3-4
3.3 Measurement of Relative Permittivity 3-5
3.4 Measurement of Piezoelectric Coefficient 3-6
3.5 Measurement of Pyroelectric Coefficient 3-11
3.6 Results and Discussion
3.6.1 Degree of Poling of the Composites 3-14
3.6.2 Relative Permittivity of the Composites 3-19
3.6.3 Piezoelectric Coefficient of the Composites 3-23
3.6.4 Pyroelectric Coefficient of the Composites 3-29
3.7 Summary 3-32

Chapter Four – Fabrication of Hydrophones

4.1 Introduction 4-1
4.2 Construction of Needle-type Hydrophone 4-2
4.3 Construction of 8-element Hydrophone Array 4-4

Chapter Five – Evaluation of Hydrophones

5.1 Introduction 5-1
5.2 Experimental Techniques
5.2.1 Receiving Sensitivity Measurement 5-4
5.2.2 Angular Response Measurement 5-9
5.3 Results and Discussion
5.3.1 Receiving Sensitivity of Hydrophones 5-11
5.3.2 Angular Response of Hydrophones 5-25
5.4 Summary 5-34

Chapter Six – Conclusion 6-1

References R-1

List of Publications P-1

Acknowledgments

I would like to take this opportunity to express my deepest appreciation to my supervisors Dr. K. W. Kwok and Prof. H. L. W. Chan for their excellent guidance and constant encouragement during my work and the preparation of this thesis.

I would like to thank Dr. Bernd Ploss, Dr. Beatrix Ploss and the technicians in Department of Applied Physics for their helpful discussion and technical supports throughout the work.

I gratefully acknowledge the financial support from Research Grants Council (RGC). Finally, I would like to thank my family for their support.

Abstract

This thesis describes the optimum conditions for poling 0-3 nanocomposite thin films to obtain high piezoelectric and low pyroelectric activities. The design and the performance of piezoelectric hydrophones with such materials as the sensing elements have been evaluated.

Piezoceramic/piezopolymer 0-3 composites with nanosized lead titanate (PT) ceramic powders imbedded in a vinylidene fluoride-trifluoroethylene (P(VDF-TrFE) 70/30 mole%) copolymer have been fabricated. The ceramic powder was prepared using the sol-gel method, and the average crystallite diameter was about 60 nm. The powder was blended into a solution containing dissolved P(VDF-TrFE) to form a composite suspension, which was then fabricated into thin films of thickness 5 μm using the spin-coating technique.

The two phases of the composite film were poled either in opposite directions or in the same direction using a two-step procedure. The ceramic phase was first poled under a dc electric field at a temperature above the ferroelectric-to-paraelectric phase transition temperature of the copolymer. The copolymer phase was then poled under an ac field at 70 °C. By controlling the field direction in the last half-cycle of the ac field, the copolymer phase was poled either in opposite directions or in the same direction to the ceramic phase. Hence, composites of different polarization states were then prepared.

The relative permittivity, piezoelectric and pyroelectric properties of the composite films were studied. Composite with two phases poled in opposite directions has enhanced piezoelectric response and reduced pyroelectric response. It is because the piezoelectric coefficients of the ceramic and the copolymer phase have opposite signs, while their pyroelectric coefficients are of the same sign. As its piezoelectric response is about 30 % larger than that of the copolymer, such composite material can be fabricated into hydrophones with good receiving sensitivity.

The composite and the copolymer films were used to fabricate single element needle-type hydrophones. Besides, an 8-element hydrophone array was also fabricated using the composite with two phases poled in opposite directions as sensing element. The receiving sensitivity and the angular response of the needle-type hydrophones and the hydrophone array were evaluated in water. It is found that the sensitivity of the hydrophone is approximately proportional to the piezoelectric coefficient d_{33} of the sensing element. Composite hydrophone with two phases poled in opposite directions shows better receiving response than the copolymer hydrophone. The hydrophone array also has good sensitivity with low inter-element coupling. Both the needle-type hydrophones and the hydrophone array have good angular responses that can be predicted accurately using the unbaffled piston model.

List of Tables

Table 1.1	Properties of PT and P(VDF-TrFE) (70/30 mole %) copolymer	1-15
Table 2.1	Temperatures of melting T_m, solidification T_s and transition T_c	2-7
Table 2.2	Poling conditions of the composite and copolymer samples	2-18
Table 3.1	The poling ratio of the ceramic phase α_c for the composites of different polarization states	3-14
Table 3.2	The poling ratio of the copolymer phase α_p for the composites of different polarization states	3-18
Table 3.3	Effective piezoelectric coefficients of the composite and copolymer samples measured at room temperature	3-29
Table 3.4	Pyroelectric coefficients of the composite and copolymer samples measured at room temperature	3-31
Table 5.1	The capacitances at 5 MHz of the hydrophones, the sensing elements and the loading	5-19
Table 5.2	The -3 dB and -6 dB angular response angles for the eight elements at 5 MHz	5-33

List of Figures

Figure 1.1	Ten different connectivity patterns of diphasic materials	1-5
Figure 1.2	Piezoelectric d (d_{33}, d_h and d_{31}) coefficients of 0-3 composite consisting chloroprene rubber and ceramic powder mixture of PZT and PT with ceramic volume percent of 50 % as a function of ceramic powder mixture ratio	1-7
Figure 1.3	Variation of acoustic sensitivity as a function of frequency for three types of hydrophones	1-8
Figure 1.4	Schematic representation of the processes commonly employed to obtain piezoelectrically and pyroelectrically active PVDF film	1-9
Figure 1.5	DSC thermodiagrams of VDF-TrFE copolymers, PTrFE and PVDF	1-12
Figure 1.6	The piezoelectric and pyroelectric properties of the PT/P(VDF-TrFE) 0-3 composites with two phases poled in the same direction as a function of ceramic volume fraction	1-13
Figure 2.1	XRD pattern of the annealed PT powder	2-3
Figure 2.2	Particle size distribution of the PT powder	2-4
Figure 2.3	DSC thermograms of P(VDF-TrFE) (70/30 mole%) copolymer (a) for the first heating and (b) for the first cooling	2-6
Figure 2.4	Procedure for preparing the PT/P(VDF-TrFE) 0-3 composite films	2-9
Figure 2.5	Structure of the thin film spin-coated on a glass substrate	2-9

Figure 2.6	SEM micrograph of the fracture surface of the PT/P(VDF-TrFE) composite film sample	2-11
Figure 2.7	Maxwell-Wagner model for a diphasic composite	2-13
Figure 2.8	Schematic diagram of the setup for dc poling	2-15
Figure 2.9	Step-wise process for dc poling of 0-3 composites	2-16
Figure 2.10	Schematic diagram of the setup for ac poling	2-17
Figure 3.1	Schematic diagram of 180° and 90° domain switching	3-3
Figure 3.2	Schematic diagram of the setup for piezoelectric coefficient measurement	3-9
Figure 3.3	Frequency spectrum recorded by a spectrum analyzer	3-10
Figure 3.4	Schematic diagram of the setup for pyroelectric coefficient measurement	3-13
Figure 3.5	XRD patterns of the composite (sample A) before and after poling	3-15
Figure 3.6	Hysteresis loops of (a) PT/P(VDF-TrFE) composite (sample B) and (b) P(VDF-TrFE) copolymer (sample E) measured at 10 Hz and 70 °C	3-17
Figure 3.7	Variation of the remanent polarization P_r with the electric field E for the composite (sample B), ---●---; and copolymer (sample E), ---■---	3-18
Figure 3.8	Relative permittivity against temperature of unpoled composite and P(VDF-TrFE) copolymer upon heating and cooling (solid: heating; open: cooling)	3-21

Figure 3.9 Relative permittivity against frequency for the composites and the copolymer before and after poling 3-22

+ : Unpoled composite
× : Unpoled copolymer
▲ : Composite with only the ceramic phase poled (sample A)
◇ : Composite with only the copolymer phase poled (sample B)
▼ : Composite with two phases poled in opposite directions (sample C)
● : Composite with both phases poled in the same direction (sample D)
■ : Poled copolymer (sample E)

Figure 3.10 Variation of the amplitude of vibration across the sample surface measured at 15 kHz 3-26

Figure 3.11 The surface displacement of the film sample at different measuring frequencies 3-27

Figure 3.12 Variation of the displacement with driving voltage at 15 kHz for sample E 3-28

Figure 4.1 Schematic diagram of the needle head of the needle-type hydrophone 4-3

Figure 4.2 Photograph of the needle-type hydrophone 4-3

Figure 4.3 Schematic diagram of the 8-element hydrophone array 4-5

Figure 4.4 Photograph of the 8-element hydrophone array 4-6

Figure 5.1 Schematic diagram of the setup for measuring receiving sensitivity of a hydrophone 5-7

Figure 5.2 The calibration curve for the end-of-cable loaded sensitivity with gain = 5 of the PVDF membrane hydrophone (National Physical Laboratory, UK) 5-8

Figure 5.3 Schematic diagrams for measuring the angular response of (a) needle-type hydrophone and (b) hydrophone array 5-10

Figure 5.4 End-of-cable capacitance of the needle-type hydrophones with different sensing elements as a function of frequency: PT/P(VDF-TrFE) composite with only the ceramic phase poled, ▽; PT/P(VDF-TrFE) composite with two phases poled in opposite directions, ◇; and P(VDF-TrFE), △ 5-12

Figure 5.5 Receiving waveforms of the needle-type hydrophones with different sensing elements to a tone burst at 5 MHz: (a) PT/P(VDF-TrFE) composite with only the ceramic phase poled, (b) PT/P(VDF-TrFE) composite with two phases poled in opposite directions; and (c) P(VDF-TrFE) 5-13

Figure 5.6 End-of-cable open-circuit sensitivities M_o of the hydrophones with different sensing elements as a function of frequency: PT/P(VDF-TrFE) composite with only the ceramic phase poled, ▼; PT/P(VDF-TrFE) composite with two phases poled in opposite directions, ◆; and P(VDF-TrFE), ▲ 5-16

Figure 5.7 Schematic diagram of a needle-type hydrophone 5-18

Figure 5.8 Simplified equivalent electrical circuit of a needle-type hydrophone 5-18

Figure 5.9 End-of-cable capacitance of the array elements as a function of frequency (element 1, □; element 2, ×; element 3, +; element 4, ▽; element 5, O; element 6, ▲; element 7, △ and element 8, ◇) 5-21

Figure 5.10 Receiving waveform of the array element 4 to a tone burst at 5 MHz 5-22

Figure 5.11 End-of-cable open-circuit sensitivity M_o of the array element 4 as a function of frequency (open: with short-circuit of other elements; solid: without short-circuit of other elements) 5-23

Figure 5.12 End-of-cable open-circuit sensitivities M_o of the eight elements as a function of frequency (element 1, □; element 2, ×; element 3,+; element 4,▽; element 5,O; element 6,▲; element 7,△ and element 8, ◇) 5-24

Figure 5.13 Angular response of the needle-type hydrophones with different sensing elements at 5 MHz: (a) PT/P(VDF-TrFE) composite with only the ceramic phase poled, (b) PT/P(VDF-TrFE) composite with two phases poled in opposite directions and (c) P(VDF-TrFE) 5-27

Theoretical values:
- - - - - : Rigid baffle model
——— : Unbaffled piston model
—·— : Soft baffle model

Figure 5.14 Angular response of the composite needle-type hydrophone with two phases poled in opposite directions at (a) 2.25, (b) 7.5 and (c) 10 MHz 5-29

Theoretical values:
- - - - - : Rigid baffle model
——— : Unbaffled piston model
—·— : Soft baffle model

Figure 5.15 Angular response of the array element 4 at (a) 2.25, (b) 5 and (c) 10 MHz 5-31

Theoretical values:

- - - - - : Rigid baffle model

——— : Unbaffled piston model

—·— : Soft baffle model

Chapter One

Introduction

1.1 Background

The increasing sophistication of ultrasonic techniques for nondestructive testing (NDT) of various materials, including human body, has brought an increasing concern for precise measurements of the ultrasonic fields used in the megahertz range of frequencies. Non-destructive testing procedure can often be optimized when spatial distribution of the acoustic field is known. In medical applications, it is of great interest to study not only the acoustic field distribution, but also the absolute value of the acoustic pressure amplitude generated by diagnostic devices. It is because excessive acoustic outputs may lead to undesirable biological effects. Hence, considerable effort has been put into the development of high performance hydrophones. Ideally, a hydrophone should have a small geometrical size compared to the wavelength of acoustic wave, adequate sensitivity and signal-to-noise ratio, and a wideband response to the acoustic wave field to be measured. In general, particular attention is focused on the hydrophones making use of piezoelectric effect.

The piezoelectric effect was first reported by the Curie Brothers in 1880. The original discovery, that polarization charges are induced in response to an external

mechanical stress, is known as direct piezoelectric effect. The converse piezoelectric effect is a dimensional change result from an applied electric field. For evaluating piezoelectric materials for use in hydrophones working in thickness mode, the piezoelectric (voltage) coefficient g_{33} is a useful parameter, which relates the electric field appearing across the material to the applied stress. Another frequently used parameter is the piezoelectric (charge) coefficient d_{33}, which describes the polarization resulting from a change in mechanical stress. The g_{33} coefficient is related to the d_{33} coefficient by the relative permittivity ε_r ($g_{33} \sim d_{33}/\varepsilon_o\varepsilon_r$, where ε_o is the permittivity of free space).

Since 1950's, piezoelectric ceramics such as barium titanate ($BaTiO_3$) and lead zirconate titanate (PZT) have been the dominant materials for the active elements of hydrophones [Hill, 1970; Colbert *et al.*, 1973; Lewin and Chivers, 1981; Aindow and Chivers, 1982]. These ceramics offer high d_{33} value ranged from 100 to 600 pC/N, a wide range of relative permittivity ($\varepsilon/\varepsilon_o \sim 100$ to 2400) and low electrical and mechanical losses. However, there are some drawbacks making them inappropriate for hydrophone applications. Due to their high relative permittivities, the g_{33} values of ceramics are generally low, and this limits their receiving sensitivities. Besides, the acoustic impedances of ceramics (Z_o = density × velocity of sound) are much larger than those of the subjects under test. For example, the density of PZT is about 7900 kg/m^3 and its acoustic impedance is about 35 Mrayl (1 Mrayl = 10^6 kg $m^{-2}s^{-1}$) while the acoustic impedances of body tissue (in medical diagnosis) and water (in hydrophone application) are about 1.5 Mrayl. Such a large acoustic mismatch causes much of the

signal to be reflected at the interface between the ceramic and the subject under test, reducing the overall sensitivity of the hydrophone. Moreover, ceramics are ionically bonded crystalline materials, which are stiff but very brittle. Therefore, it is difficult to re-shape them after they have been sintered at high temperature (>1000 °C).

At the beginning of the 1960's, piezoelectric polymers such as polyvinylidene difluoride (PVDF) and its copolymer with trifluroethylene (TrFE) began to attract special attention from researchers [Kawai, 1969; Sessler, 1981; Furukawa *et al.*, 1984; Kimura and Ohigashi, 1987] as they possess certain properties better than those of ceramics. The polymers have high degree of flexibility, low density, and low acoustic impedance (~ 4 Mrayl) which facilitates impedance matching with the subject under test. Because of the low relative permittivity ($\varepsilon/\varepsilon_0 \sim$ 10-12), they exhibit high voltage coefficient g_{33}. Hence, they have been widely used for fabricating high frequency probe hydrophones [Lewin, 1981; Platte, 1985; Chan *et al.*, 1991] and membrane hydrophones [Shotton *el al.*, 1980; Preston *et al.*, 1983; Galbraith and Hayward, 1998]. However, their performances are not good enough because their high electrical losses lead to a low signal-to-noise ratio. The small value of their relative permittivities are also not preferred for device applications because the output signal of the sensing element will be greatly reduced by the stray capacitance associated with long hydrophone cable.

1.2 Piezoelectric Ceramic/Polymer Composite

Fabrication of piezoelectric ceramic/polymer diphasic composites is a way to reduce the limitations of both phases and attain their complementary properties [Yamada *et al.*, 1982; Ting, 1986; Han *et al.*, 1991; Marra *el al.*, 1999]. The piezoelectic, pyroelectric, electrical and mechanical properties of a composite can be adjusted by using constitute phases of different properties, varying the fraction of the phases, and changing the connectivities of the phases (i.e. how they are interconnected with each other) [Newnham *et al.*, 1978]. In a diphasic system, each phase may be self-connected in zero, one, two, or three dimensions. There are ten different combinations of phase connectivity: 0-0, 0-1, 0-2, 0-3, 1-1,1-2, 1-3, 2-2, 2-3 and 3-3 (Figure 1.1). In practice, the first letter represents the connectivity of the ceramic phase, while the second represents that of the polymeric phase. For example, in a 0-3 composite, the ceramic phase is in particulate form while the polymeric phase is continuous in all 3 directions. Among the different types of composites, 0-3 composites have been widely used as piezoelectric and pyroelectric sensor materials [Murphy *et al.*, 1992; Tandon *et al.*, 1992; Dias and Das-Gupta, 1993] because they are relatively easy to prepare and can be fabricated into different forms including thin sheets, extruded bars and fibers.

Early attempts to produce 0-3 composites using piezoelectrically active ceramic powder PZT as an inclusion and piezoelectrically passive polymer polyurethane as a matrix were made by Pauer [1973] and Harrison [1976]. It was reported that the d_{33} coefficients of these composites were comparable with that of PVDF, but the values of the hydrostatic piezoelectric coefficient d_h were lower than those of PZT and PVDF.

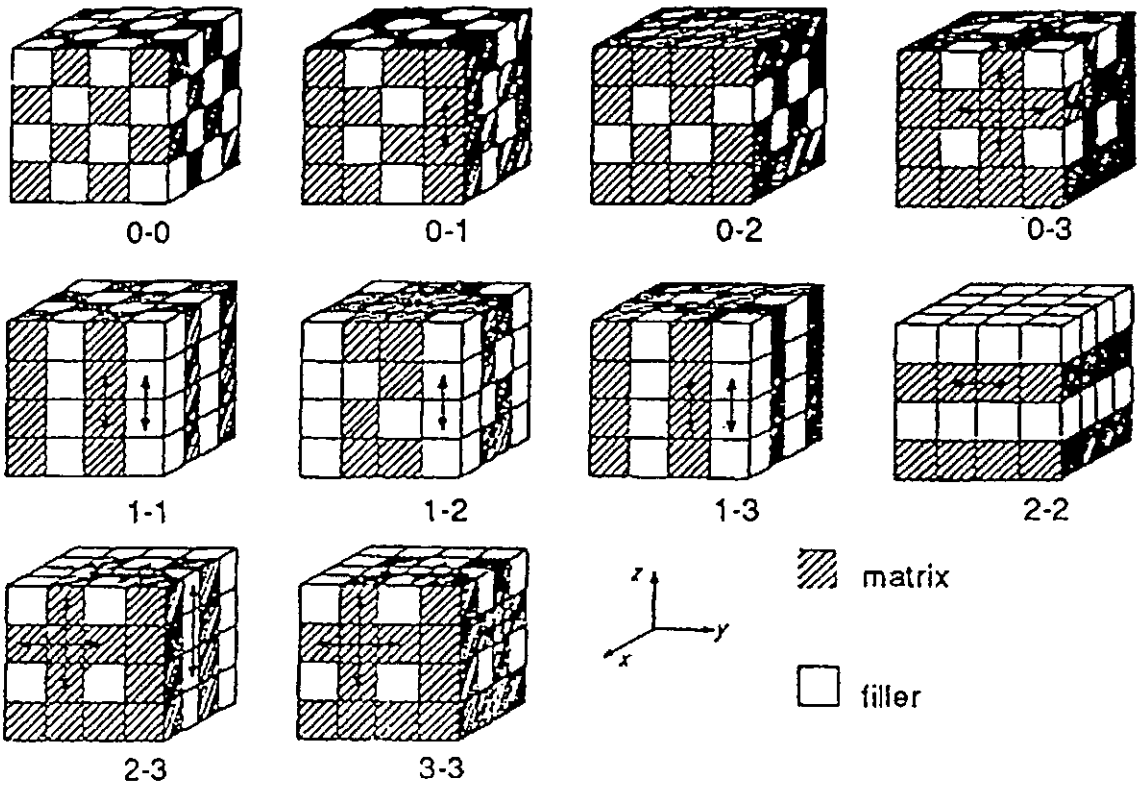

Figure 1.1 Ten different connectivity patterns of diphasic materials. [Newnham *et al.*, 1978]

Rather than using PZT as the inclusion, another ceramic PT was also employed. Banno and Ogura [1991] developed 0-3 composites consisting of chloroprene rubber and a mixture of two ceramics powder (PZT/ PT) with almost the same particle sizes (~ 3 μm). They had measured the piezoelectric d (d_{33}, d_h and d_{31}) coefficients of the composites with ceramic volume percent of 50 % as a function of ceramic powder mixture ratio. As shown in Figure 1.2, it was found that the d_{33} and d_h values of the composite increased with the fraction of the PT. Tandon and Singh [1994] used PZT/Chloroprene rubber and PT/Chloroprene rubber composites to fabricate hydrophones, and compared the performances between the composite and ceramic hydrophones (Figure 1.3). They found that the conventional PZT hydrophone had lower sensitivity than the PZT composite hydrophone, whereas the PT composite hydrophone showed the highest sensitivity. Besides, the composite hydrophones had nearly flat responses with no noticeable resonances.

Recently there has also been interest in studying composites using piezoelectrically active polymer PVDF and its copolymer P(VDF-TrFE) as matrix [Yamazaki and Kitayama, 1981; Abdullah and Das-Gupta, 1990; Dias and Das-Gupta, 1994]. For PVDF, after direct melt crystallization, it exists in non-polar α phase. To induce the piezoelectric and pyroelectric activities of the PVDF film, the film is first stretched at low temperature to produce polar β phase, and then an electric field is applied to the film to align the dipoles in the field direction (Figure 1.4) [Lovinger, 1983]. Hence, without stretching, the PVDF matrix of a 0-3 composite is not expected to contribute to the piezoelectric or pyroelectric properties of the composite

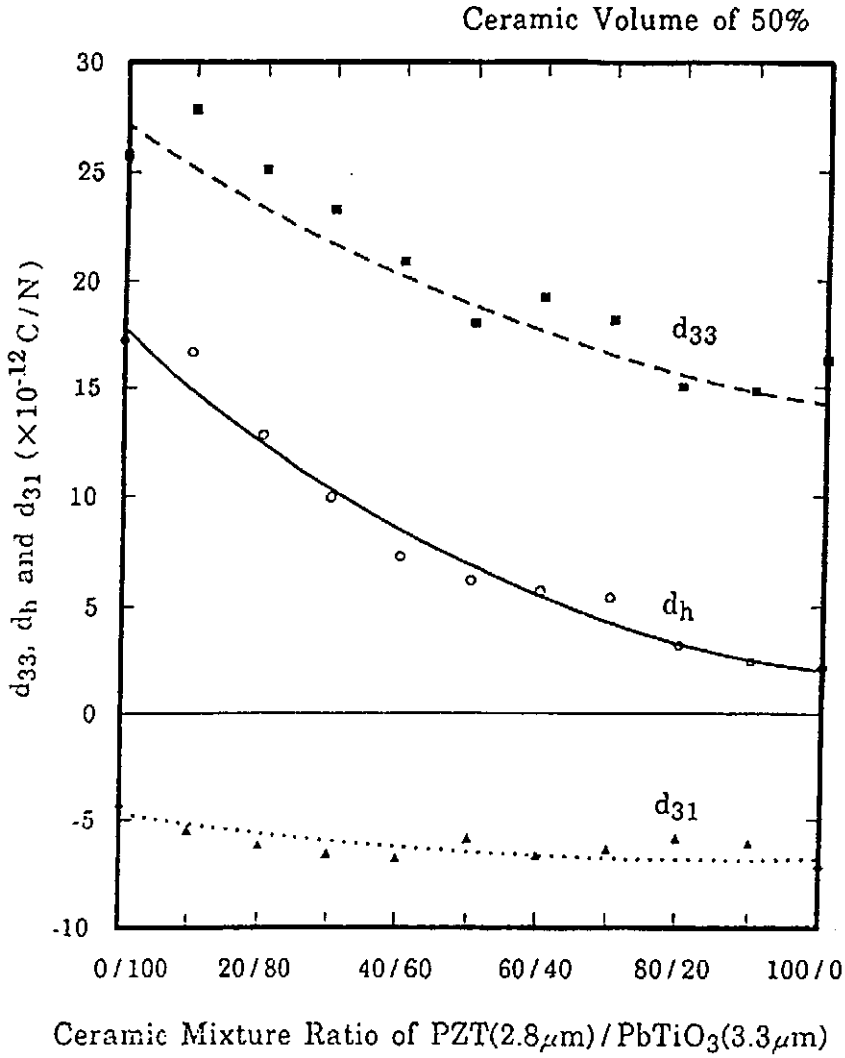

Figure 1.2 Piezoelectric d (d_{33}, d_h and d_{31}) coefficients of 0-3 composite consisting chloroprene rubber and ceramic powder mixture of PZT and PT with ceramic volume percent of 50 % as a function of ceramic powder mixture ratio. [Banno and Ogura, 1991]

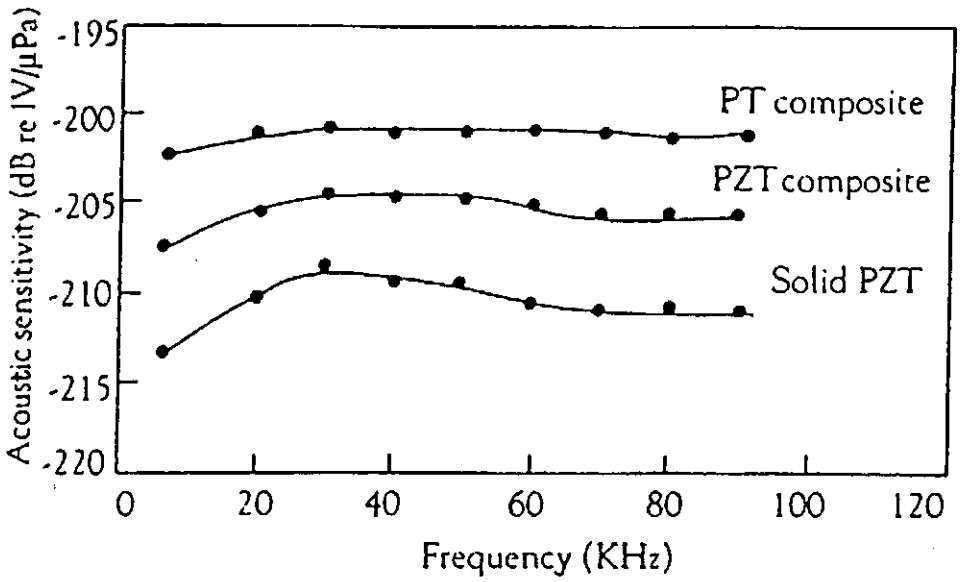

Figure 1.3 Variation of acoustic sensitivity as a function of frequency for three types of hydrophones. [Tandon and Singh, 1994]

[Yamazaki and Kitayama, 1981]. In the case of P(VDF-TrFE), when the VDF content is within the range of 0.6 to 0.82, the material forms into β phase directly from the melt [Davis *et al.*, 1984; Koga and Ohigashi, 1986]. So when the P(VDF-TrFE) is used as the matrix of a composite, its piezoelectric and pyroelectric properties, after induced by applying an electric field higher than its coercive field, can have contribution to the overall properties of the composites [Chan *et al.*, 1998].

In preparing the composite with the copolymer as matrix, it is important to select appropriate VDF/TrFE molar composition because most of the properties are strongly dependent on the composition. Higashihata *et al.* [1981] undertook the differential scanning calorimetry (DSC) measurement for the VDF-TrFE copolymers, PTrFE and

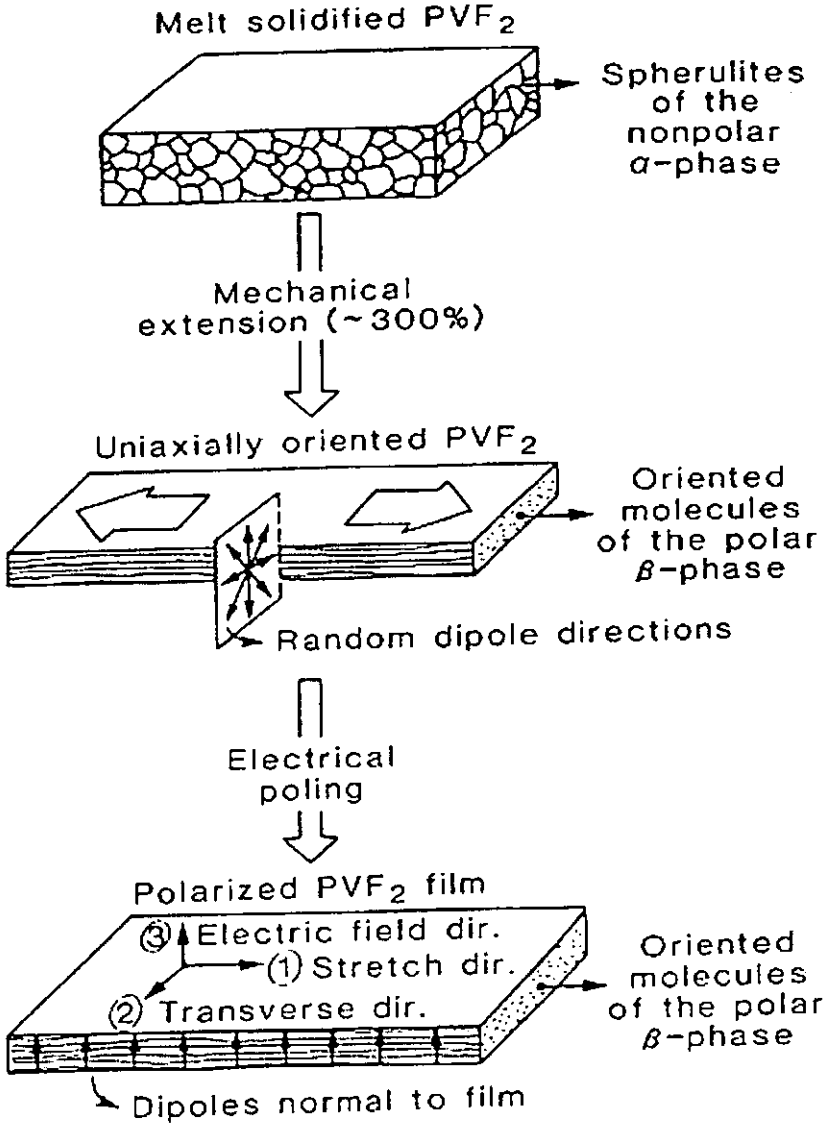

Figure 1.4 Schematic representation of the processes commonly employed to obtain piezoelectrically and pyroelectrically active PVDF film. [Lovinger, 1983]

PVDF, and found that the P(VDF-TrFE) copolymer exhibited a ferroelectric β-phase to a paraelectric phase transition when heated from 40 °C to its melting temperature T_m (Figure 1.5). The results showed that the transition temperature T_c of the copolymer increased with the VDF content. Koga and Ohigashi [1986] had studied the electromechanical coupling factor k_t (a measure of the transduction between the electrical and mechanical energy) of the copolymer as a function of VDF content and annealing temperature. They reported that, for the copolymer with the VDF content ranged from 0.65 to 0.82, a large k_t value of 0.27-0.3 had been found when the copolymer was annealed above the ferroelectric-to-paraelectric phase transition temperature. Therefore, to fabricate composite with high piezoelectric response, copolymers with VDF content between 70 and 80 mole % are more suitable as they provide good piezoelectric activity over a wide temperature range.

In the beginning, many researchers used the P(VDF-TrFE) copolymer as the matrix of the composites to improve the poling efficiency of the ceramic phase [Furukawa *et al.*, 1986; Ngoma *et al.*, 1990; Dias and Das-Gupta, 1994]. In poling the composite, the electric field acting on each phase can be estimated by the Maxwell-Wanger model [Coelho, 1979]. The ceramic inclusion and the polymer matrix of the 0-3 composite are modeled as a two-layer capacitor. After a dc field is applied to the composite for a time larger than the composite relaxation time (i.e. in long time poling), the ratio of the field acting on the ceramic phase to that on the polymer phase, E_c/E_p, is dependent on the ratio of the conductivity of the polymer to that of the ceramic σ_p/σ_c. Since the conductivity of the P(VDF-TrFE) copolymer increases significantly above its

ferroelectric-to-paraelectric phase transition temperature T_c, the ceramic phase of the composite can be poled effectively at a temperature above T_c under dc poling. However, poling of the copolymer phase in the composite has not been considered yet.

Chan *et al.* [1998] prepared PT/P(VDF-TrFE) 0-3 composites with different ceramic volume fractions up to 0.54, and the two phases of the composites were poled in the same direction. The piezoelectric and pyroelectric properties of the composites were investigated as a function of ceramic volume fraction (Figure 1.6). It was found that the piezoelectric coefficient of the composite decreased with the ceramic volume fraction while the pyroelectric coefficient increased. It is because the piezoelectric coefficients of the ceramic and the copolymer have opposite signs while the pyroelectric coefficients have the same sign. Therefore, when the two phases were poled in the same direction, the piezoelectric contributions from the two phases partially canceled each other while the pyroelectric contributions enhanced. Hence, it is of great interest to fabricate composite with two phases poled in opposite directions, such that the composite will have high piezoelectric but low pyroelectric activities, thereby reducing the electric noise due to temperature fluctuation. Such material will be valuable in fabricating ultrasonic hydrophone with good receiving sensitivity.

For fabrication of ultrasonic hydrophone, the thickness of the composite should be down to several micrometers, such that the thickness mode resonance of the composite occurs at very high frequency (> 100 MHz) which is far away from the operating frequency of the hydrophone. Most of the previous works of 0-3 composites

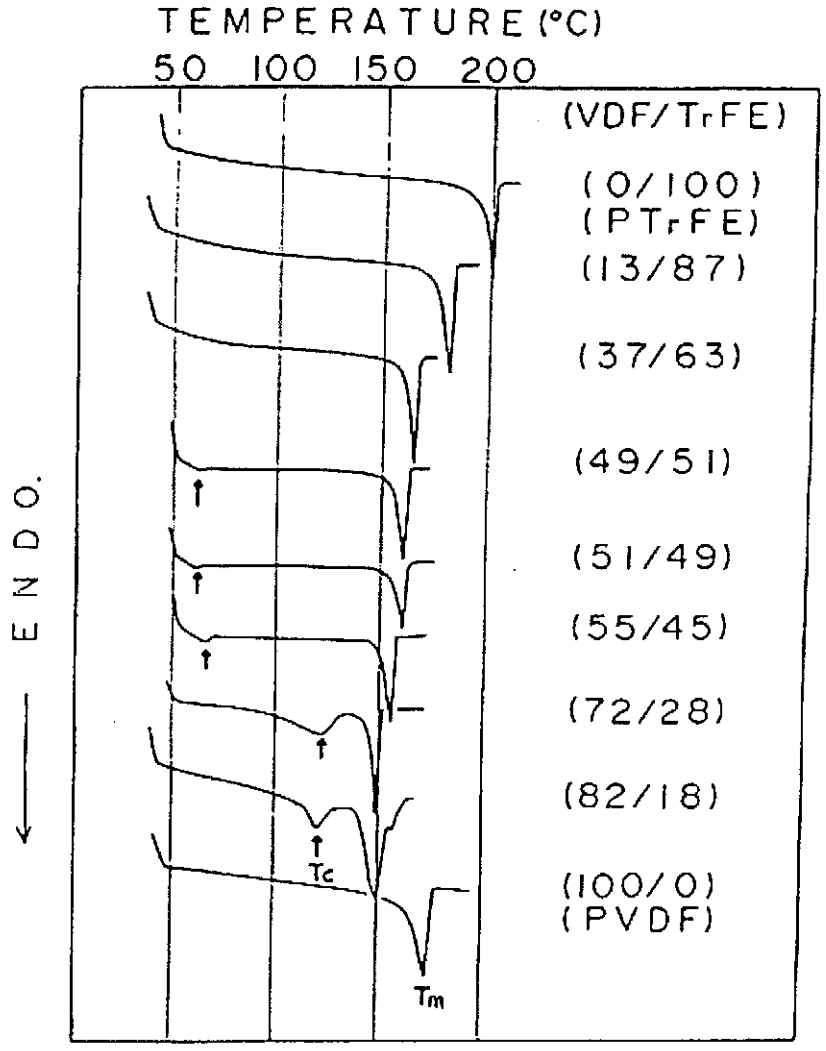

Figure 1.5 DSC thermodiagrams of VDF-TrFE copolymers, PTrFE and PVDF. [Higashihata *et al.*, 1981]

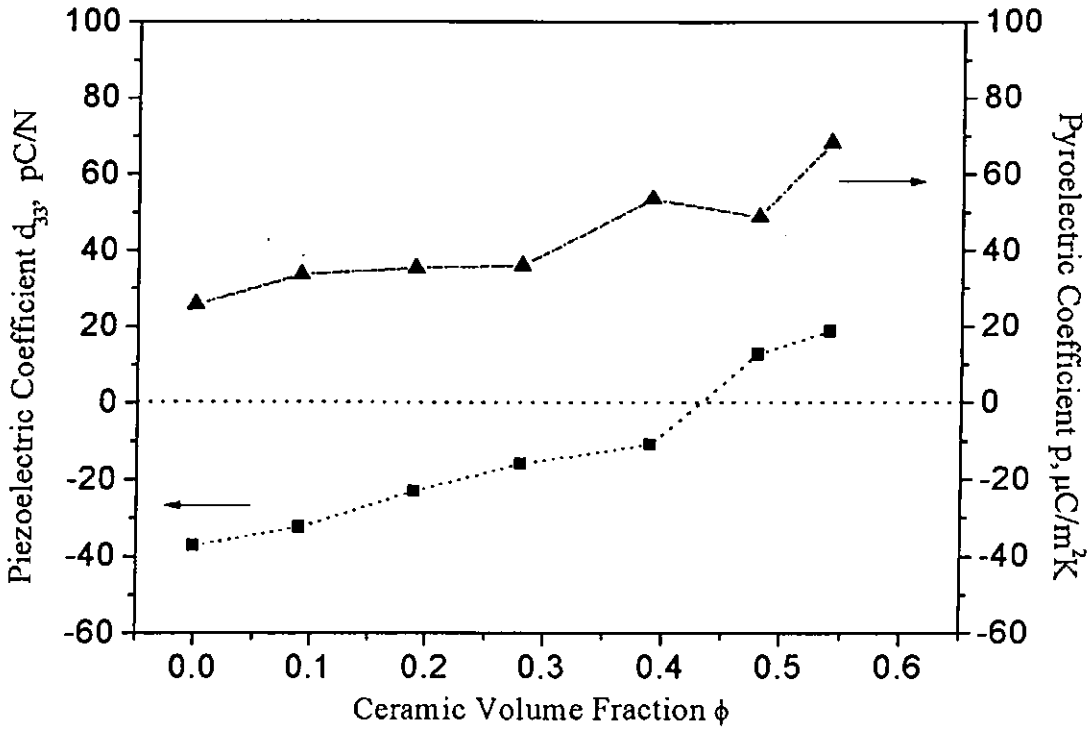

Figure 1.6 The piezoelectric and pyroelectric properties of the PT/P(VDF-TrFE) 0-3 composites with two phases poled in the same direction as a function of ceramic volume fraction [Chan *et al.*, 1998].

had used large ceramic powder, typically 1 to 5 μm, and the thickness of these composites were larger than 50 μm. This implied that, to fabricate homogeneous composite, the thickness of the sample should be at least ten times larger than the size of the ceramic powder. Hence, in preparing composite film with thickness of several micrometers, the ceramic particle should be in nanometer range. In recent years, there has been considerable interest in using the sol-gel technique to prepare ceramics, because high purity and ultrafine particles as small as several tens of nanometers can be prepared at relative low temperatures [Blum and Gurkovich, 1985; Ishikawa *et al.*,

1988; Calzada *et al.*, 1995]. By introducing such ceramic powder into copolymer solution, one can produce homogeneous 0-3 composite thin films with thickness down to several micrometers using the spin coating technique [Chen *et al.*, 1998a; Zhang *et al.*, 1999].

In the present work, we propose to fabricate ultrasonic hydrophones using poled 0-3 composite film as sensing element. Lead titanate (PT) is chosen as the ceramic phase because of its low permittivity, which leads to a large electrical response, and good piezoelectric response. And, the matrix material is vinylidene fluroide-trifluoroethylene copolymer (P(VDF-TrFE)) with a VDF/TrFE ratio of 70/30 mole % which provides good piezoelectric response and low acoustic impedance. The physical properties of these two materials are summarized in Table 1.1. Since there is little work of preparing 0-3 composites with both phases piezoelectrically active, especially on thin film sample, knowledge of poling such composite is limited. Therefore, we will establish the optimum conditions for poling 0-3 composite films and to evaluate such composites for ultrasonic hydrophone applications.

Table 1.1 Properties of PT and P(VDF-TrFE) (70/30 mole %) copolymer

Materials	PT	P(VDF-TrFE) 70/30 mole %
Transition temperature, T_c (°C)	490 [#]	102 (upon heating) [+] 62 (upon cooling) [+]
Density, ρ (kg/m^3)	6890 [*]	1800 [*]
Sound velocity (m/s)	4200 [*]	2400 [*]
Acoustic impedance, Z_o (MRayls)	29 [*]	4.51 [*]
Relative permittivity, ε_r	150 [#]	11 [+]
Piezoelectric coefficient, d_{33} (pC/N)	182 [#]	37 [+]
Electromechanical coupling factor, k_t (%)	0.6 [*]	0.3 [*]

[#] Wersing *et al.*, 1989; [*] Dias and Das-Gupta, 1993; [+] Chan *et al.*, 1998

1.3 Scope of the Work

The main objectives of this work are to fabricate PT/P(VDF-TrFE) 0-3 composite films with high piezoelectric but low pyroelectric activities, and to use the composite films for fabricating ultrasonic hydrophones.

The procedures for fabricating and poling PT/P(VDF-TrFE) 0-3 composite films have been established and described in Chapter Two. To investigate the effects of the poling procedure on the properties of the composite, composite films of four different polarization states were prepared: (a) only the ceramic phase poled, (b) only the copolymer phase poled, (c) two phases poled in opposite directions and (d) both phases

poled in the same direction. The degree of poling of the individual phase of the composite films was estimated and the electrical properties such as relative permittivity, piezoelectric and pyroelectric coefficients of the composite films were evaluated in Chapter Three. The composite films were then fabricated into needle-type hydrophones and an 8-element hydrophone array. The constructions of the needle-type hydrophone and hydrophone array were described in Chapter Four. The receiving sensitivity and angular response of the hydrophones were evaluated in Chapter Five. The observed angular responses of both the needle-type hydrophone and hydrophone array were compared with the theoretical values.

Chapter Two

Sample Preparation

2.1 Materials Used

2.1.1 Nanocrystallite Lead Titanate Powder

In the present study, nanocrystallite lead titanate (PT) powder prepared by the sol-gel process was used as the inclusion of the composite. The sol-gel process involved mixing the lead acetate trihydrate ($Pb(CH_3COO)_2 \cdot 3H_2O$) and titanium isoproxide ($Ti(OCH(CH_3)_2)_4$) in 2-methoxyethanol ($CH_3OCH_2CH_2OH$) to form a PT solution (known as "sol") [Chen *et al.*, 1998b]. By controlling the hydrolysis condition of the solution, a PT gel was obtained. The PT gel was dried at 100 °C for 24 hours and then annealed at 800 °C for 1 hour. The resulting ceramic block was ground to obtain PT ceramic powder of particle size smaller than 500 nm. The structure and crystallite size of the PT powder were studied using a X-ray diffractometer (XRD) with nickel-filtered Cu$K\alpha$ radiation (X'pert system, Philips Electronic Instruments), and the particle size distribution was measured using a particle-size analyzer (Horiba CAPA-700).

The XRD pattern of the PT ceramic powder is shown in Figure 2.1. Sharp diffraction peaks, which are well matched with the diffraction peaks of a polycrystallite PT film [Milne and Pyke, 1991], are observed indicating that the PT

powder was well crystallized. The average crystallite size of the PT powder was determined from the full width at half maximum (FWHM) of the (111) and (200) diffraction peaks using the Scherrer's equation [Birks and Friedman, 1946]:

$$L = \frac{K\lambda_x}{\sqrt{B^2 - b^2}\cos\theta} \tag{2.1}$$

where L is the crystallite diameter, K is Scherrer's constant (= 0.89), λ_x is the wavelength of the x-ray, θ is the diffraction angle, B is the FWHM of the observed diffraction peak and b is the width broadening due to instrumental effects. The value of b was estimated by the FWHM of the observed diffraction peak of a standard material (Si) with large grain size. It should be noted that the settings of the diffractometer for measuring the PT powder and the standard material are the same. The crystallite diameter of the PT powder, obtained by averaging the results for the (111) and (200) peaks, was 60 nm.

Figure 2.2 shows the particle size distribution of the PT powder. To ensure adequate dispersion of the powder in ethanol for the measurement, the sample was agitated thoroughly using an ultrasonic bath. It can be seen that the size of the PT powder is in the range of 100 to 500 nm, with the median diameter of about 200 nm. Using the resulting ceramic powder, homogeneous 0-3 composite thin films of thickness as small as 5 μm (~ 25 times of the particle size) can be fabricated. It is imperative to use films of such small thickness to fabricate ultrasonic hydrophones with flat frequency response up to several tens of MHz.

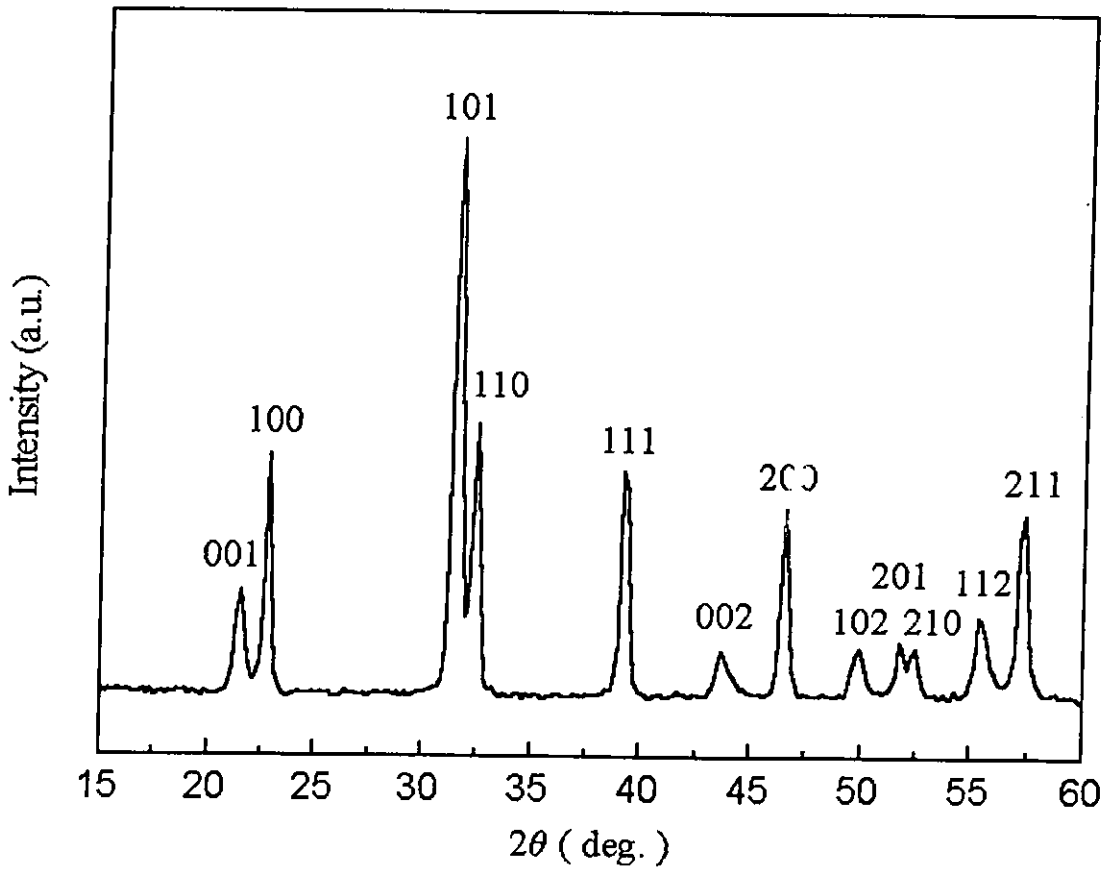

Figure 2.1 XRD pattern of the annealed PT powder.

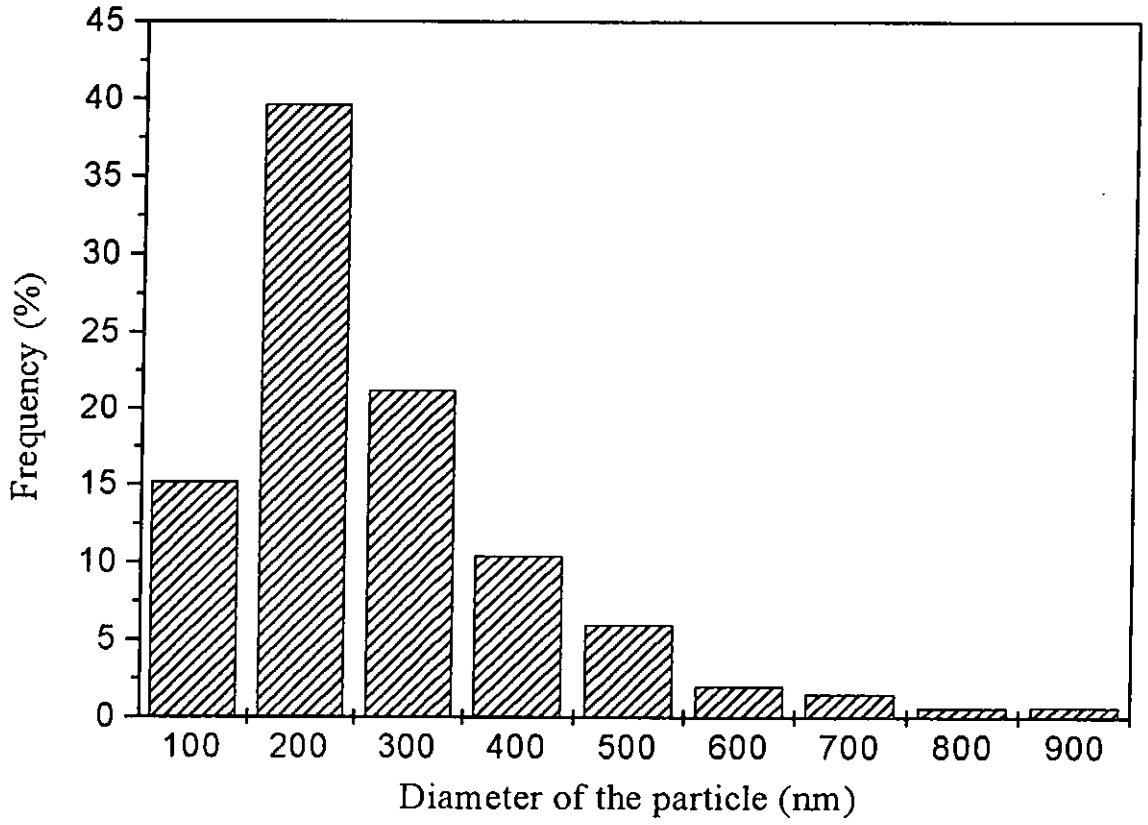

Figure 2.2 Particle size distribution of the PT powder.

2.1.2 P(VDF-TrFE) Copolymer

Copolymer of vinylidene fluoride and trifluoroethylene (P(VDF-TrFE)) with TrFE content of 30 mole% was used as the matrix. The copolymer was supplied in pellet form by Piezotch Co.. By using a differential scanning calorimeter (Perkin Elmer DSC7), the DSC thermograms of the copolymer upon first heating and cooling were measured at a rate of 10 °C/min. Upon heating, the ferroelectric-to-paraelectric phase transition temperature ($\uparrow T_c$) and melting temperature (T_m) were found to be 105 °C and 149 °C, respectively (Figure 2.3a). Upon cooling, the solidification temperature (T_s) and paraelectric-to-ferroelectric phase transition temperature ($\downarrow T_c$) were found to be 133 °C and 65 °C, respectively (Figure 2.3b). The plural peaks around $\downarrow T_c$ may correspond to the transition from the paraelectric phase to the β phase, γ phase and α phase [Koga and Ohigashi, 1986]. The observed values of $\uparrow T_c$, T_m, T_s and $\downarrow T_c$ were compared with the literature values for the composition 70/30 (= VDF/TrFE) [Bloomfield and Preis, 1986] and 73/27 mole% [Koizumi *et al.*, 1984] in Table 2.1. It can be seen that the TrFE content of the supplied copolymer should be very close to 30 mole%.

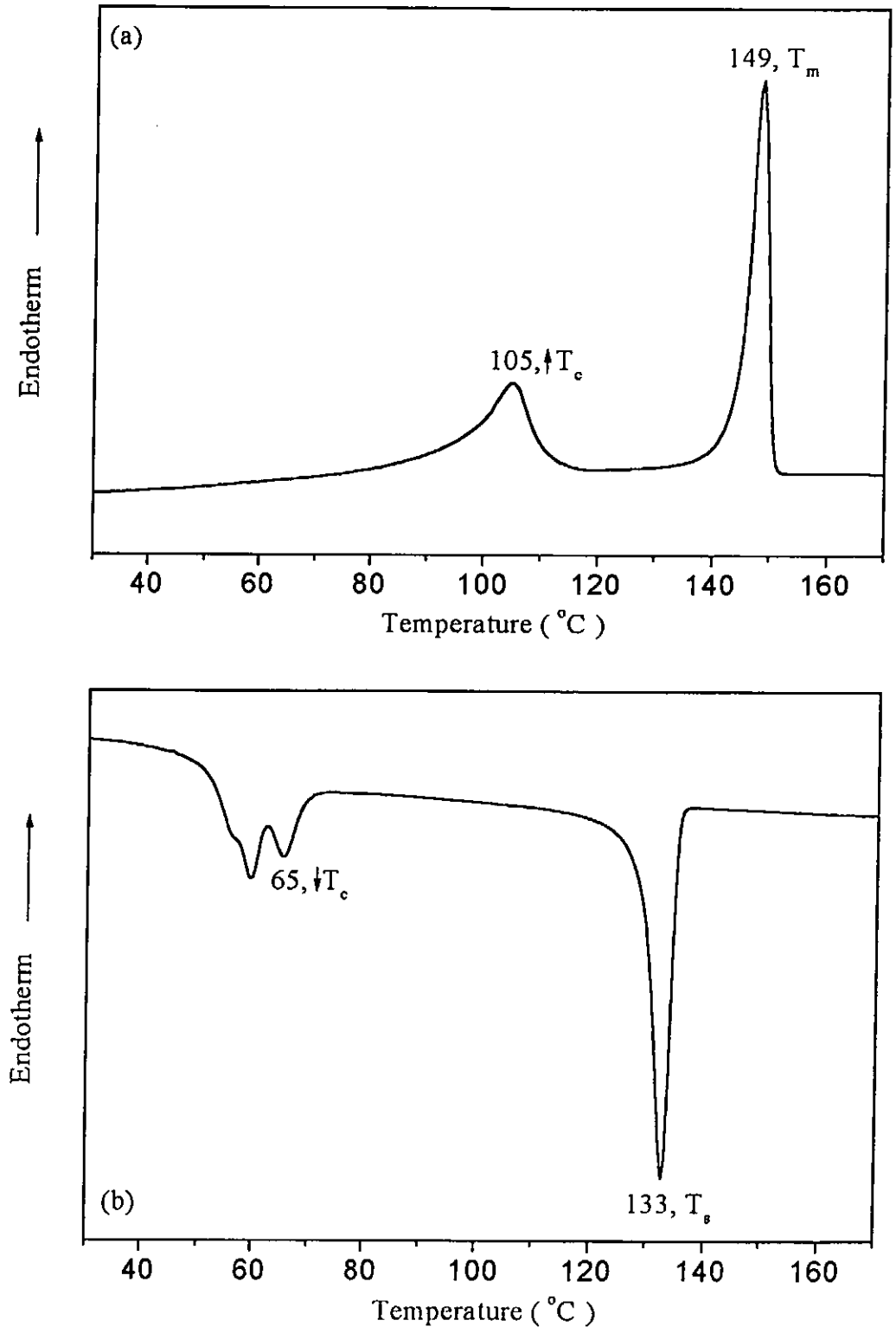

Figure 2.3 DSC thermograms of P(VDF-TrFE) (70/30 mole%) copolymer (a) for the first heating and (b) for the first cooling.

Table 2.1 Temperatures of melting T_m, solidification T_s and transition T_c.

mole% VDF	Heating		Cooling	
	T_m (°C)	$\uparrow T_c$ (°C)	T_s (°C)	$\downarrow T_c$ (°C)
70	149	105	133	65
70 #	147	108	....	....
73 ##	145	116	133	75

Bloomfield and Preis [1986]; ## Koizumi *et al.* [1984]

2.2 Fabrication of PT/P(VDF-TrFE) 0-3 Composites

PT/P(VDF-TrFE) 0-3 composite films were prepared by a spin-coating technique. The procedure for preparing the 0-3 composite films is shown in Figure 2.4. 3.75 g of the P(VDF-TrFE) pellet was dissolved in 25 ml of methyl-ethyl-ketone (MEK) to form a copolymer solution. To fabricate a composite film with the ceramic volume fraction of 0.26, 4.8 g of the PT powder was blended into the copolymer solution to form a suspension. The suspension was agitated using an ultrasonic bath for several hours to ensure good dispersion of the PT powder, and then filtered with a filter paper (0.5 μm) to remove the impurities and powder agglomerations. An aluminum (Al) bottom electrode of thickness 0.12 μm was thermally evaporated on a glass substrate. The composite film was fabricated by spinning the filtered suspension on the Al/glass substrate. To produce a composite film of thickness about 5 μm, a rotation speed of 2000 rpm and duration of 1 minute were used. The film was kept at 40 °C overnight and

then annealed at 120 °C for 2 hours to remove the solvent and to increase the crystallinity of the copolymer matrix. An Al top electrode was thermally evaporated on the film to form the desired capacitor structure (Figure 2.5). The thickness of the composite film was measured to be 4.8 μm, using a surface profiler (KLA-Tencor P-10).

2.3 Fabrication of P(VDF-TrFE) Copolymer

To fabricate P(VDF-TrFE) copolymer films of similar thickness to the composite film, a copolymer solution was prepared by adding 3.75 g of the copolymer pellet in 25 ml of MEK. The solution was stirred until the copolymer was completely dissolved, and then filtered with a filter paper (0.5 μm) to remove the impurities. The filtered solution was spin-coated on an Al/glass plate. The film was dried at 40 °C overnight and annealed at 120 °C for 2 hours to remove the solvent and to increase the crystallinity of the copolymer film. An Al top electrode was thermally evaporated on the film to form the same capacitor structure as the composite film. The thickness of the copolymer film was 4.4 μm, determined using a surface profiler.

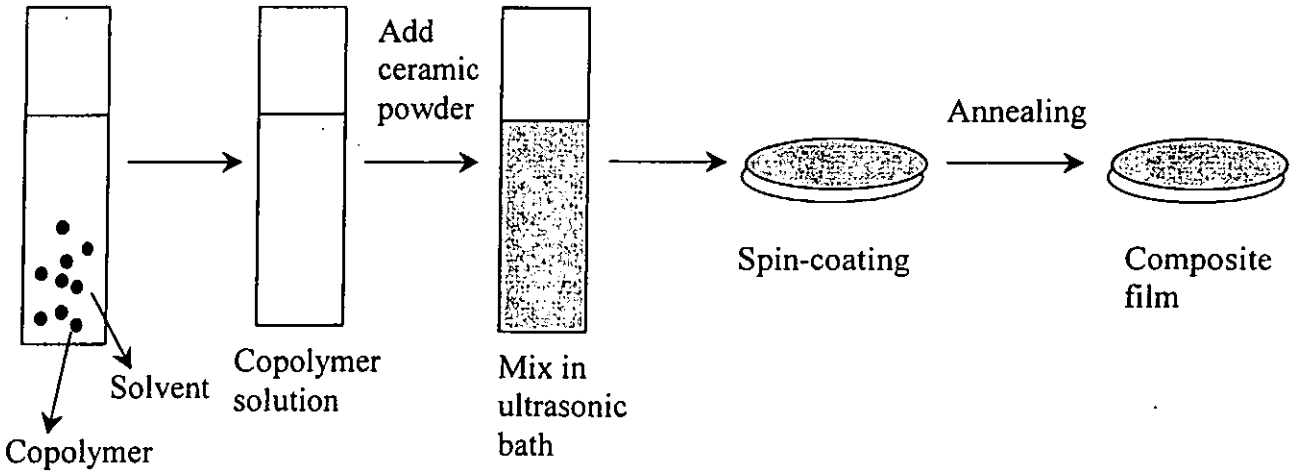

Figure 2.4 Procedure for preparing the PT/P(VDF-TrFE) 0-3 composite films.

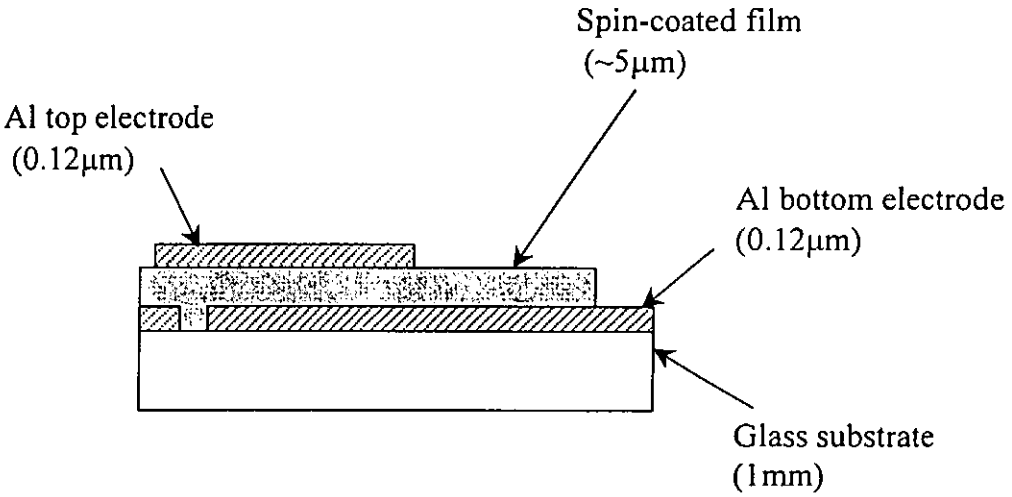

Figure 2.5 Structure of the thin film spin-coated on a glass substrate.

2.4 PT Volume Fraction of 0-3 Composites

The PT volume fraction of the composite film sample was calculated by using the relation:

$$\rho = \phi\rho_c + (1-\phi)\rho_p \qquad (2.2)$$

where ϕ is the PT volume fraction , ρ is the composite density, ρ_c is PT powder density and ρ_p is the P(VDF-TrFE) matrix density. The density of the PT powder was 7200 kg/m^3, determined using a density bottle technique; and those of the copolymer matrix and composite were 1900 $kg/m^3$and 3100 kg/m^3, respectively, determined by the hydrostatic weighing method.

The PT volume fraction of the composite obtained is about 0.22, which is lower than the targeted value 0.26. It is because the agglomerations of PT powder in the composite suspension have been filtered before the film is made.

2.5 Microstructure of PT/P(VDF-TrFE) 0-3 Composites

The microstructure of the PT/P(VDF-TrFE) 0-3 composite film was examined using a scanning electron microscope (SEM, Leica 440). In order to expose the PT ceramic powder inside the composite for the examination, the film sample was dipped into liquid nitrogen for 5 minutes, and then was fractured immediately in air. The SEM micrograph of the fracture surface of the composite film sample is shown in Figure 2.6.

It can be seen that the PT powder dispersed quite uniformly, without serious agglomeration, in the copolymer matrix.

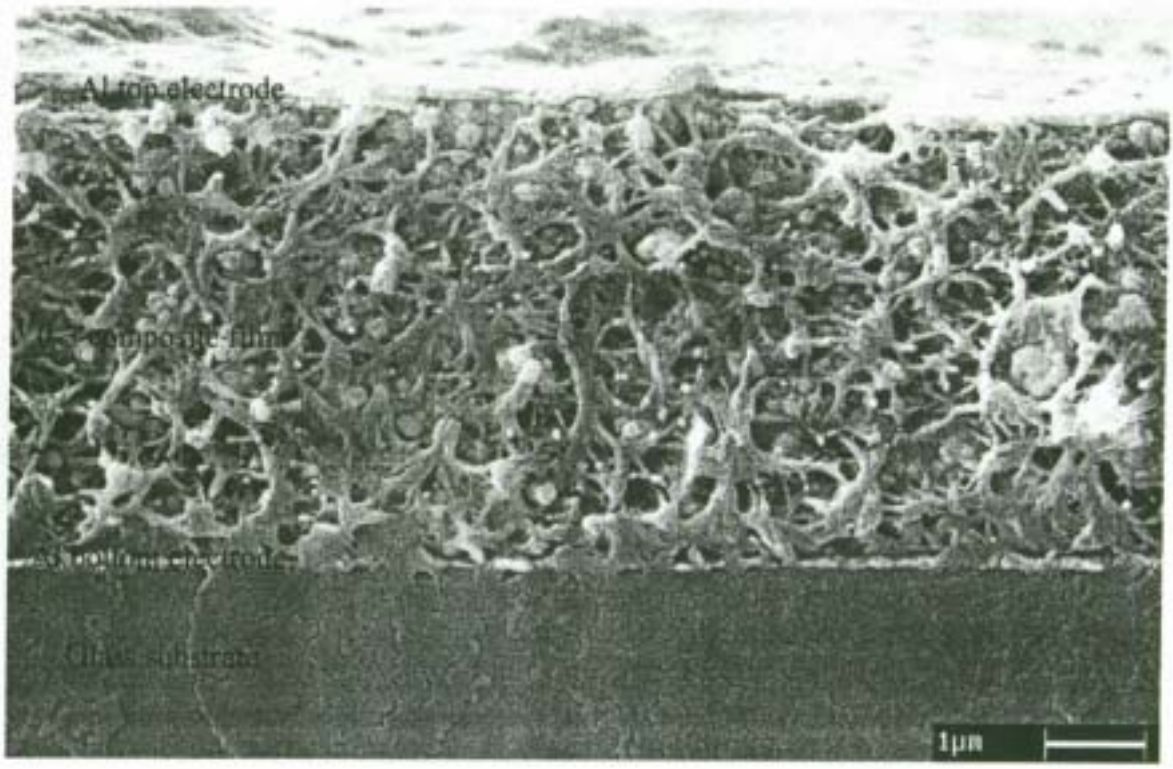

Figure 2.6 SEM micrograph of the fracture surface of the PT/P(VDF-TrFE) composite film sample.

2.6 Sample Poling

When the ferroelectric ceramic/polymer composites are formed, the ferroelectric dipoles are randomly orientated within the material and hence no net polarization is resulted. Therefore, they are not piezoelectirc or pyroelectric. To induce the piezoelectric and pyroelectric properties, a strong electric field is applied to the material to align the dipoles along the field direction, thus resulting in a net permanent polarization. This process is known as poling [ANSI/ IEEE std. 180, 1986].

One of the major considerations for poling the composite is the magnitude of the electric field applied to each phase, which can be estimated according to the Maxwell-Wagner model [Coelho, 1979]. In the model, the 0-3 composite with alternating ceramic particles and thin layers of polymer between two electrodes can be approximated to double-layer capacitor (Figure 2.7). Each layer represents a single phase and has it own relative permittivity ε_r and conductivity σ. When the poling time is longer than the interfacial relaxation time of the system, the ratio of the electric field across the ceramic phase to that across the polymer phase, E_c/E_p, is dependent on the ratio of the conductivity of the polymer to that of the ceramic σ_p/σ_c. Usually, σ_p is much smaller than σ_c, so the effective field across the ceramic phase is very small. One way to increase E_c/E_p is to increase the poling temperature [Chilton, 1991]. Since the conductivity of the copolymer increases abruptly at its ferroelectric-to-paraelectric phase transition temperature $\uparrow T_c$ [Chan *et al.*, 1997], the ceramic phase of the composite can be poled effectively at temperature higher than the $\uparrow T_c$ of the copolymer

under long time poling [Ploss *et al.*, 1998]. On the other hand, when the poling time is short, E_c/E_p is governed by the ratio of the relative permittivity of the polymer to that of the ceramic $\varepsilon_{rp}/\varepsilon_{rc}$. In general, ε_{rc} is much larger than ε_{rp}, so E_c/E_p is very small and the polymer phase of the composite can be poled without changing the polarization state of the ceramic phase under short time poling [Ploss *et al.*, 1998].

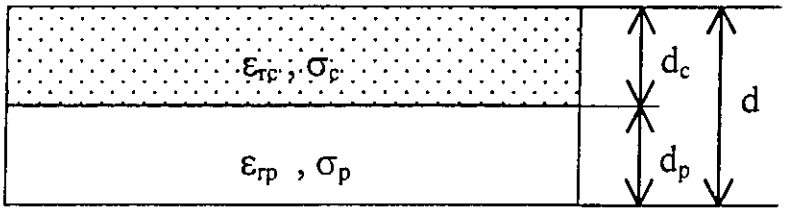

Figure 2.7 Maxwell-Wagner model for a diphasic composite.

Based on the above considerations, the ceramic and the copolymer phases of the composites were poled separately, with the ceramic phase poled under a dc electric field at temperature higher than $\uparrow T_c$ of the copolymer and the copolymer phase poled under an ac field at a lower temperature. In the present study, PT/P(VDF-TrFE) composite film samples of four different polarization states were prepared: sample A (only the ceramic phase poled), sample B (only the copolymer phase poled), sample C (two phases poled in opposite directions) and sample D (both phases poled in the same direction). A poled P(VDF-TrFE) copolymer film (sample E) was also prepared.

To prepare sample A, the composite film was heated to 120 °C and then a dc field was applied across the thickness of the sample. The experimental setup for the dc

poling is schematically shown in Figure 2.8. Due to the capacitance charging effect, the initial current flow may be large, leading to electrical breakdown across the sample. To prevent the excessive current flow, the poling field E was increased by a step-wise process (Figure 2.9) until a maximum poling field E_{max} (~ 65 MV/m) was reached. After the application of E_{max} for 1 hour, the field was switched off and the sample was cooled to room temperature. As the electric field was applied only at temperature higher than the ferroelectric-to-paraelectric phase transition temperature of the copolymer $\uparrow T_c$ (105 °C, Figure 2.3a), only the ceramic phase of the composite was poled.

To prepare sample B, the composite film was heated to 70 °C and then several cycles of an ac field of frequency 10 Hz was applied across the sample. A Sawyer-Tower circuit, which was designed for the measurement of polarization hysteresis loop [Saywer and Tower, 1930], was used to carry out the ac poling of the sample (Figure 2.10). Similarly, the poling field was increased progressively to a maximum value of 70 MV/m in a step of 2.5 MV/m. The polarization direction of the copolymer phase was determined by the direction of the ac field in the last half cycle.

Samples C and D were prepared by ac poling the copolymer phase of sample A following the poling procedure for sample B. Sample C was re-poled such that the copolymer phase was poled in a direction opposite to that of the ceramic phase, while the polarization of the copolymer phase of sample D was parallel to that of the ceramic phase.

Sample E (pure copolymer film) was poled following the poling procedure for sample B. The maximum poling field E_{max} was about 70 MV/m. The poling conditions for all the samples are summarized in Table 2.2.

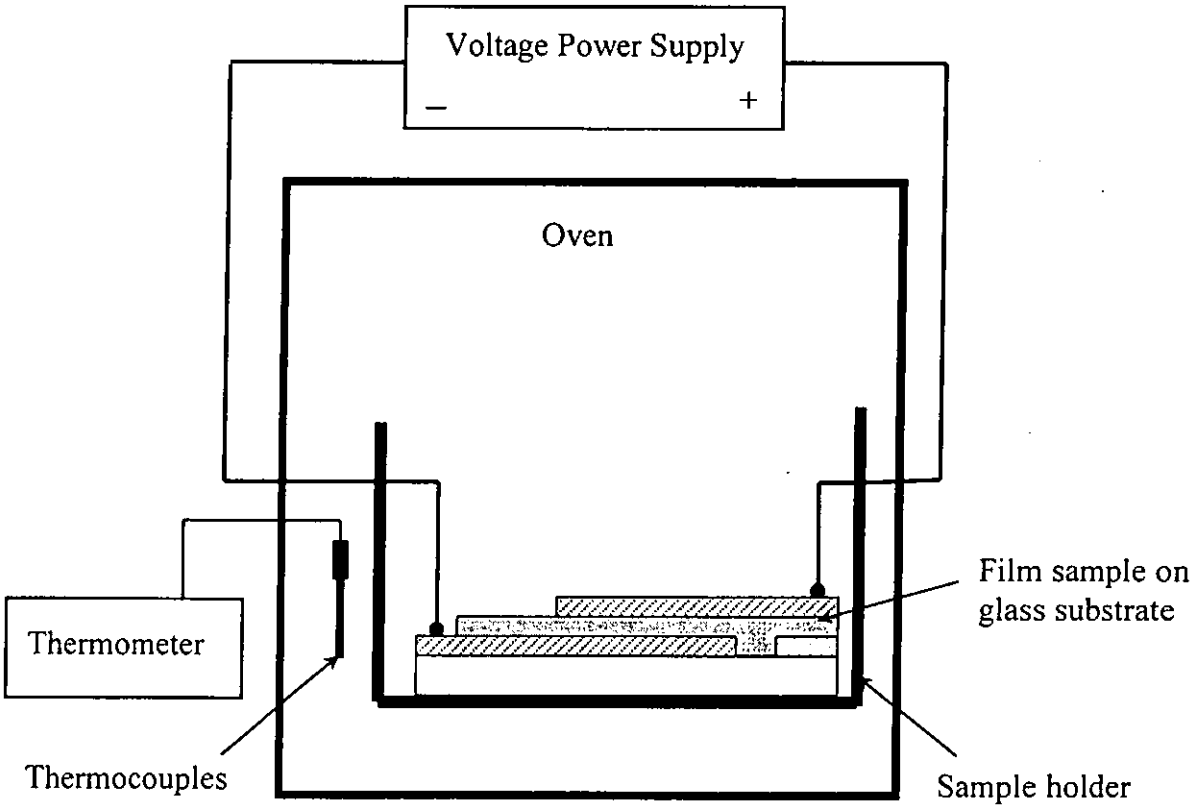

Figure 2.8 Schematic diagram of the setup for dc poling.

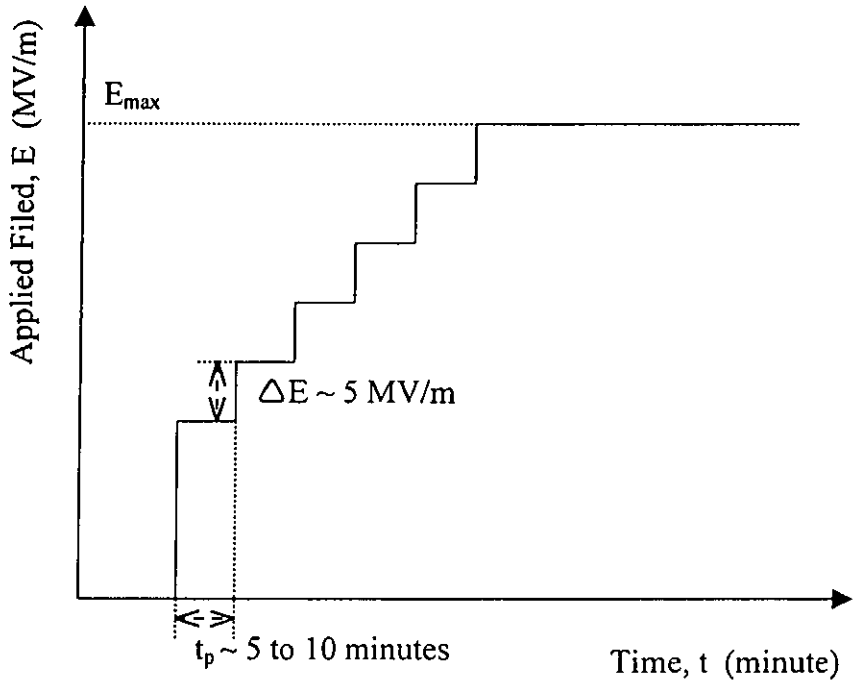

Figure 2.9 Step-wise process for dc poling of 0-3 composites.

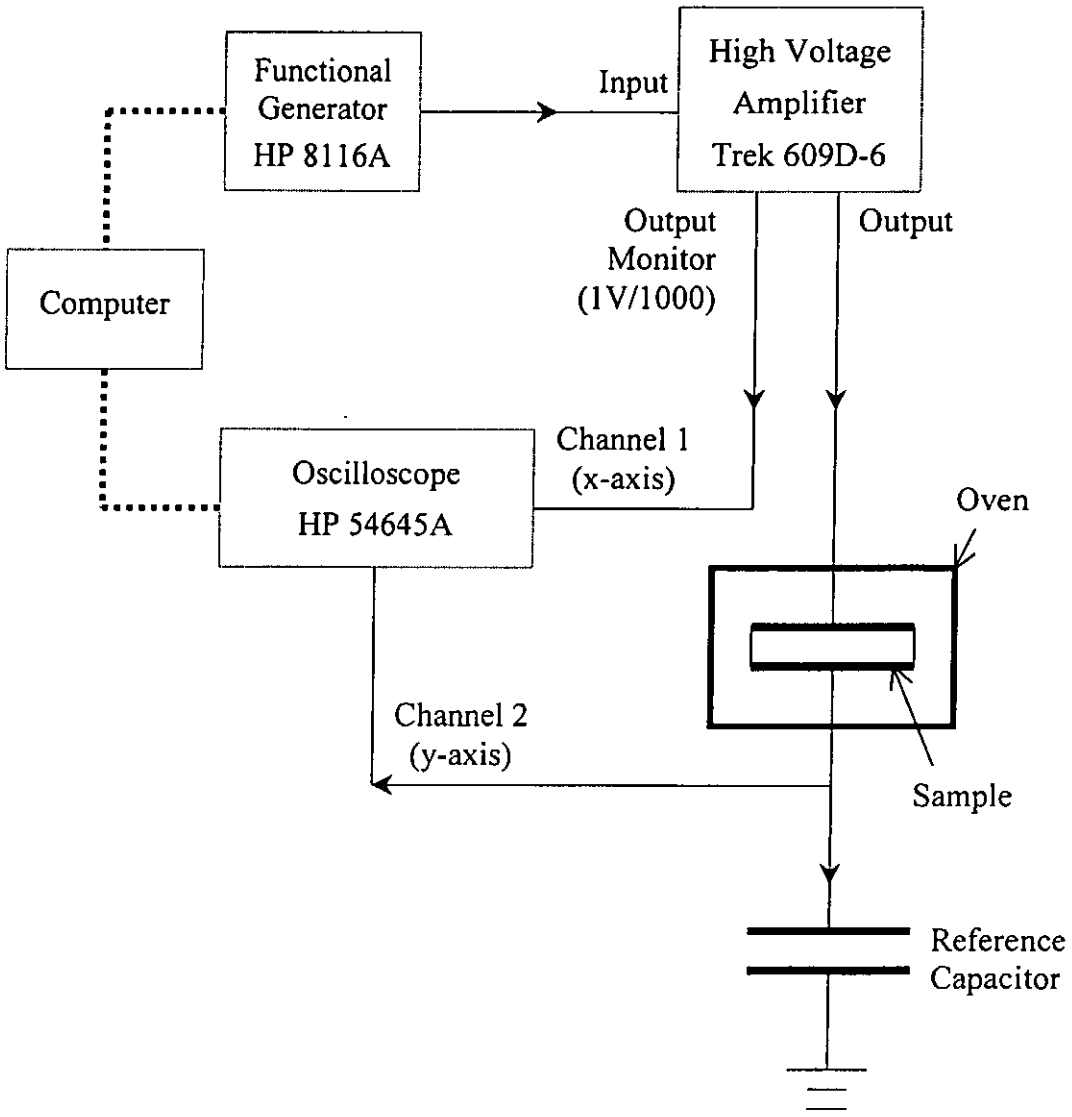

Figure 2.10 Schematic diagram of the setup for ac poling.

Table 2.2 Poling conditions of the composite and copolymer samples.

Sample	Poling Conditions	Polarization States
A	dc 65 MV/m at 120 °C for 1h, ↑	Only the ceramic phase poled
B	ac 70 MV/m at 10 Hz and 70 °C, ↑	Only the copolymer phase poled
C	1) dc 65 MV/m at 120 °C for 1h, ↑ 2) ac 70 MV/m at 10 Hz and 70 °C, ↓	Two phases poled in opposite directions
D	1) dc 65 MV/m at 120 °C for 1h, ↑ 2) ac 70 MV/m at 10 Hz and 70 °C, ↑	Both phases poled in the same direction
E pure P(VDF-TrFE)	ac 70 MV/m at 10 Hz and 70 °C, ↑	The copolymer phase poled

* The arrows indicate the polarization direction after poling

Chapter Three

Characterization of PT/P(VDF-TrFE) 0-3 Composites

3.1 Introduction

In Chapter two, PT/P(VDF-TrFE) 0-3 composite films of different polarization states were prepared using various poling procedures. The effectiveness of the poling procedures was studies in this chapter. The degree of poling of the ceramic phase of the composite was estimated from the X-ray diffraction pattern, while that of the copolymer phase was estimated from the remanent polarization measured in the ac poling. Besides, the relative permittivity, piezoelectric coefficient and pyroelectric coefficient of the composite films were studied.

3.2 Estimation of the Degree of Poling in the 0-3 Composites

3.2.1 X-ray Diffraction Method

The degree of poling of the ceramic phase of the 0-3 composite is estimated from the XRD pattern [Yamazaki and Kitayama, 1981]. In tetragonal crystals such as lead titanate and lead zirconate titanate, 180° and 90° domain switching usually occurs

under the influence of a strong electric field [Berlincourt and Krueger, 1959]. For the 180° domain switching, the domain is switched from an anti-parallel direction to a parallel direction with the applied field, so the dimension of the ceramic unit cell and then the XRD pattern do not change (Figure 3.1 (a)). However, for the 90° domain switching, the domain is switched from a perpendicular direction to a parallel direction with the applied field. The length of the unit cell along the field direction increases while that normal to the field direction decrease (Figure 3.1 (b)). This will result in a change of the XRD pattern: the diffraction peaks associated with the (00h) planes become larger and those associated with (h00) planes become smaller. Therefore, the degree of poling of the ceramic phase of the composite can be estimated from the change of the intensities of the (00h) and (h00) diffraction peaks. In the present study, the degree of poling of the ceramic phase α_c is calculated from the expression [Yamazaki and Kitayama, 1981]:

$$\alpha_c = 1 - \left(\frac{I_{(002)}}{I_{(200)}} \right) \left(\frac{I'_{(200)}}{I'_{(002)}} \right) \tag{3.1}$$

where $I'_{(002)}$ and $I'_{(200)}$ are the intensities of the X-ray diffraction peaks associated with the (002) and (200) planes respectively of the poled ceramics, and $I_{(002)}$ and $I_{(200)}$ are those of the unpoled ceramics. Since the X-ray diffraction pattern does not reflect the 180° domain switching, the calculated α_c is only the estimation and used for comparison.

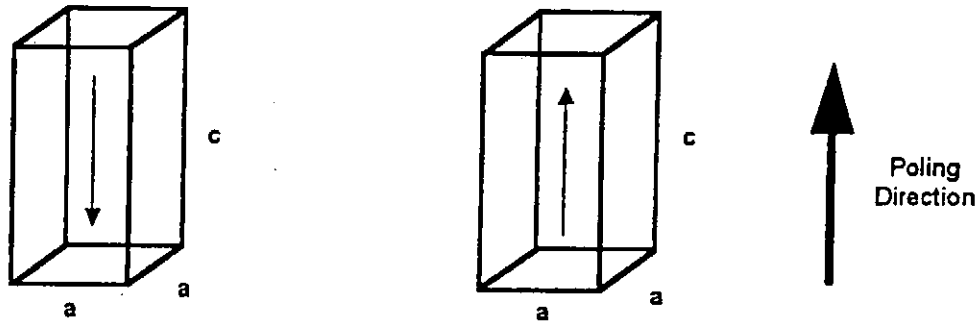

(a) Switching of 180° Domain

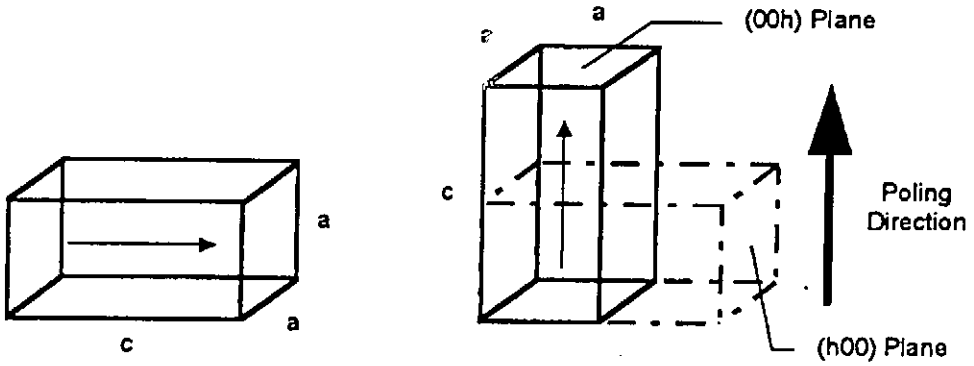

(b) Switching of 90° Domain

Figure 3.1 Schematic diagram of 180° and 90° domain switching.

3.2.2 Hysteresis Measurement

As mentioned in section 2.6, a Sawyer-Tower circuit was applied to pole the copolymer phase of the composite by an ac field. The degree of poling of the copolymer phase can then be estimated from the simultaneously obtained polarization hysteresis loop. When a high ac field E is applied across the sample, the polarization charge Q generated on the sample is transferred to a reference capacitor (Figure 2.10). By measuring the voltage V_c across the reference capacitor, the amount of the polarization charge Q and then the electric displacement D of the sample can be calculated:

$$Q = V_c C \tag{3.2}$$

$$D = \frac{Q}{A} \tag{3.3}$$

where C is the capacitance of the reference capacitor and A is area of the electroded surface of the sample. To ensure the full application of E across the sample, the capacitance of the reference capacitor should be much larger than that of the sample. Since the relative permittivity of the composite (at 70 °C) is usually large, the polarization of the sample is equal to the observed electric displacement. As discussed in section 2.6, the electric field applied on the ceramic phase is so small that its dipoles will not switch under the ac field, so the observed polarization mainly arise from the switching of the dipoles in the copolymer phase. Therefore, in the present study, the degree of poling of the copolymer phase of the composite, α_p, is estimated from the observed remanent polarization P_r (the resulting polarization after the application of an ac field, i.e. P at E = 0):

$$\alpha_p = \frac{P_r}{P_r^\circ} \tag{3.4}$$

where P_r° is the remanent polarization of a fully poled copolymer sample.

3.3 Measurement of Relative Permittivity

In evaluating the materials for hydrophone applications, its relative permittivity ε_r should be considered [Troilo *et al.*, 1994 and Cui *et al.*, 1997]. The capacitances of the composite and copolymer samples were measured as functions of temperature and frequency using an impedance analyzer (HP4194A). The relative permittivity ε_r of the sample is determined using the following equation:

$$\varepsilon_r = \frac{Cd}{\varepsilon_0 A} \tag{3.5}$$

where C is the capacitance of the sample, ε_o is the permittivity of the free space (= 8.85 $\times$ 10^{-12} F/m), A is the area of the electroded surface of the sample, and d is the thickness of the sample.

3.4 Measurement of Piezoelectric Coefficient

The piezoelectric coefficient d_{ip} is one of the important material parameters for characterizing the piezoelectric activity of a ferroelectric material. It is defined as, for the direct piezoelectric effect

$$d_{ip} = \left(\frac{\partial D_i}{\partial T_p}\right)_E \qquad (i = 1,2,3;\ p = 1,2,.....5,6) \qquad (3.6)$$

or , for the converse piezoelectric effect

$$d_{ip} = \left(\frac{\partial S_p}{\partial E_i}\right)_T \qquad (i = 1,2,3;\ p = 1,2,.....5,6) \qquad (3.7)$$

where D is the electric displacement, E is the electric field, T is the stress and S is the elastic strain. The piezoelectric coefficient d for both effects are thermodynamically identical, with units of coulomb/newton (C/N) in the direct effect and meter/volt (m/V) in the converse effect. Among the piezoelectric coefficients d_{ip}, d_{33}, where 3 represents the thickness direction of the sample (i.e. the poling direction), is the most useful material parameter for the hydrophone applications.

In the present study, the d_{33} value for the converse piezoelectric effect was determined. An electric field was applied across the sample and the induced surface displacement of the sample along the thickness direction was measured. For ferroelectric thin films, due to the small thickness, the surface displacement lies in the Ångström range. Therefore, a Mach-Zehnder type heterodyne interferometer (SH-120, B.M. Industries, France) [Royer and Dieulesaint,1986; Zhang *et al.*,1988;

Karasik *et al.*, 1995] was used to measure the surface displacement of the thin films (Figure 3.2). A linearly polarized laser beam L (frequency f_L, wavelength λ_L = 632.8 nm) from a He-Ne laser is split into a reference beam R and a probe beam M by a beam splitter. The complex amplitude of the laser beam can be written as:

$$L = le^{i2\pi f_L t} \tag{3.8}$$

where l is the amplitude of the laser beam L and t is the time.

The reference beam R is directed through a Dove prism and a polarizing beam splitter into a photodetector. Its complex amplitude is expressed as:

$$R = re^{i2\pi f_L t} \tag{3.9}$$

where r is the amplitude of the reference beam R.

The frequency of the probe beam M is shifted by a frequency f_B (70 MHz) in a Bragg cell, and then this beam (now labeled S) is phase modulated by the surface displacement of the film sample, $\phi(t) = 2k_L u\sin(2\pi f_u t)$ (wave number $k_L = 2\pi/\lambda_L$, vibration frequency f_u, displacement amplitude u).

$$S = se^{i(2\pi f_L + 2\pi f_B)t + \phi(t)}$$

$$= se^{i(2\pi f_L t + 2\pi f_B t + \frac{4\pi}{\lambda_L} u\sin(2\pi f_u t))} \tag{3.10}$$

where s is the amplitude of the phase modulated beam S.

The interference of the beams R and S on the photodetector delivers a current I at the Bragg cell frequency:

$$I \quad \alpha \quad \cos\left[2\pi f_B t + \frac{2\pi}{\lambda_L} 2u\sin(2\pi f_u t)\right] \tag{3.11}$$

The current can be expanded into a Bessel development:

$$I \quad \alpha \quad Re\left\{e^{i2\pi f_B t}\left[J_0\left(\frac{4\pi u}{\lambda_L}\right)+2iJ_1\left(\frac{4\pi u}{\lambda_L}\right)\sin(2\pi f_u t)+2iJ_2\left(\frac{4\pi u}{\lambda_L}\right)\sin(4\pi f_u t)+.....\right]\right\} \quad (3.12)$$

For small amplitude displacement u, the ratio of the amplitudes of the current components at f_B and $f_B \pm f_u$ can be approximated as:

$$\frac{J_0\left(\frac{4\pi u}{\lambda_L}\right)}{J_1\left(\frac{4\pi u}{\lambda_L}\right)} \cong \frac{\lambda_L}{2\pi u} \quad (3.13)$$

where J_0 and J_1 are the Bessel function of the zeroth and the first order, respectively. In this work, the amplitudes of the current components (in dBm) at f_B (A_0) and $f_B \pm f_u$ (A_1) were measured using a spectrum analyzer (HP 3589A) (Figure 3.3); and the displacement amplitude u is calculated by:

$$u = \frac{\lambda_L}{2\pi 10^{\frac{(A_0 - A_1)}{20}}} \quad (3.14)$$

The piezoelectric coefficient d_{33} of the film can then be calculated as:

$$d_{33} = \frac{\left(\frac{u}{d}\right)}{\left(\frac{V}{d}\right)} = \frac{u}{V} \quad (3.15)$$

where d is the thickness of the film and V is the voltage applied across the film.

The sign of d_{33} is determined by measuring the phase angle between the driving voltage and the output signal of the interferometer using a lock-in amplifier. The driving voltage is applied to the top electrode of the sample. When the observed phase angle is close to zero, it indicates that the piezoelectric response of the sample is in phase with the

driving voltage, then the piezoelectric coefficient of the sample is taken as positive in sign. When the observed phase angle is close to 180°, the piezoelectric coefficient of the sample is taken as negative in sign.

Figure 3.2 Schematic diagram of the setup for piezoelectric coefficient measurement.

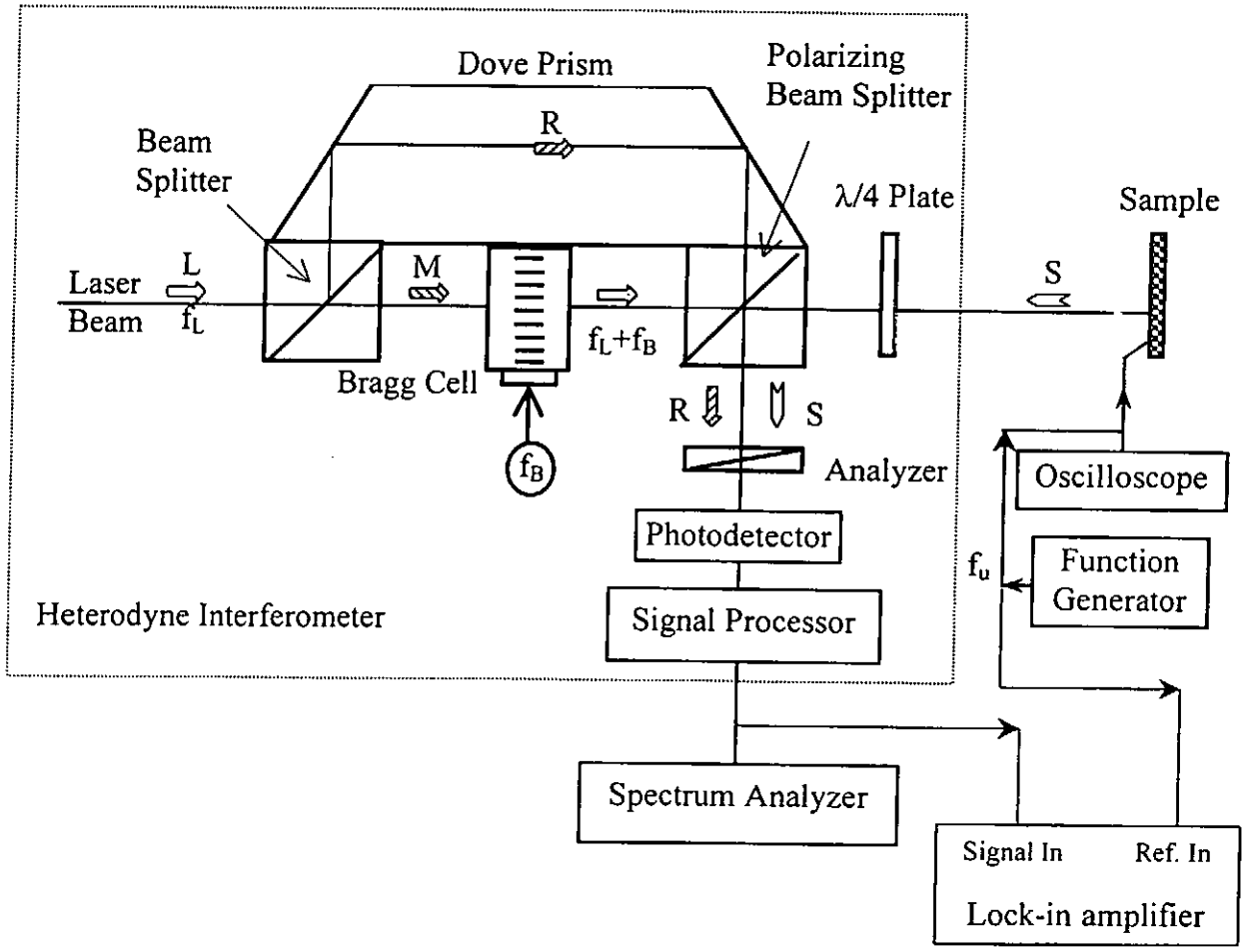

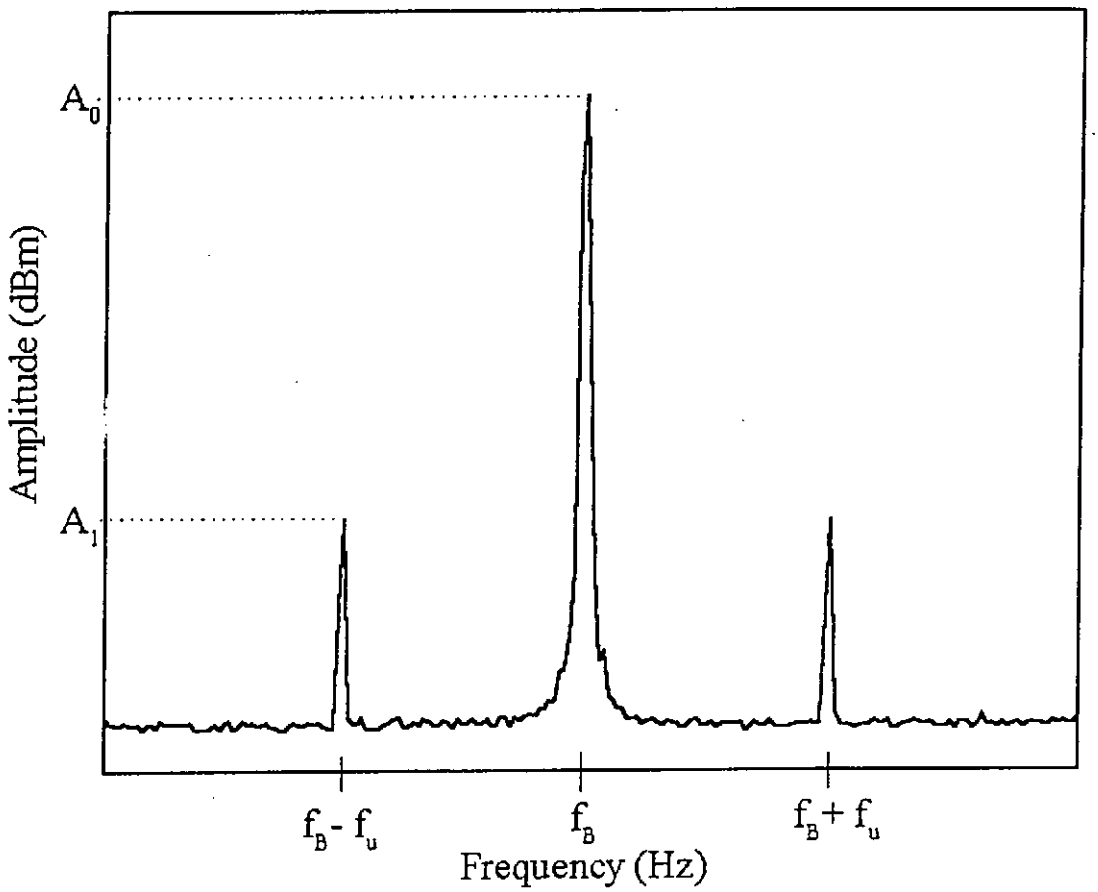

Figure 3.3 Frequency spectrum recorded by a spectrum analyzer.

3.5 Measurement of Pyroelectric Coefficient

The pyroelectric effect is defined as the change of the spontaneous polarization P_s with temperature Θ:

$$p_i = -\frac{\partial P_i}{\partial \Theta} \tag{3.16}$$

where p (C/m^2K) is the pyroelectric coefficient, i = 1, 2, 3. Usually, the pyroelectric coefficient p_3 (or simply p) is determined by measuring the polarization charge Q or the rate of change of Q (i.e. pyroelectric current) induced on the sample surface normal to the spontaneous polarization:

$$p_3 = \frac{\partial D}{\partial \Theta} = -\frac{1}{A}\frac{\partial Q}{\partial \Theta} \tag{3.17}$$

where D is the electric displacement and A is the area of the electroded surface of the sample.

Quasi-static direct method [Byer and Roundy, 1972] is the simplest way to measure the pyroelectric coefficient. In this method, the sample is heated at a constant rate and the short-circuit pyroelectric current is recorded. However, especially for polymeric materials, the pyroelectric current consists of not only the true reversible pyroelectric current but also the irreversible depolarization current due to space charge relaxation [Das-Gupta and Abdullah, 1988]. To separate the true pyroelectric current from the depolarization current, a dynamic method [Garn and Sharp, 1982; Sharp and Garn, 1982; Dias *et al.*, 1993] was used in the present work. The sample is heated

sinusoidally about a certain temperature Θ_I with frequency f and amplitude Θ_o using a Peltier element (Figure 3.4):

$$\Theta_s(t) = \Theta_I + \Theta_o e^{i(2\pi ft)} \tag{3.18}$$

For low frequency heating, the depolarization current I_d is in phase with the temperature while the true pyroelectric current I_p is in phase with the heating rate $d\Theta_s/dt$ (i.e. 90° out of phase with the temperature). To ensure the sample is heated uniformly, a frequency of 5 mHz and an amplitude of 1 K are used. The short-circuit current induced on the sample is amplified by an electrometer and measured by a digital lock-in amplifier. The pyroelectric coefficient p is then calculated using the component of the observed current 90° out of phase with the temperature variation, I_p:

$$p = \frac{1}{A}\left(\frac{\partial Q}{\partial \Theta}\right)$$

$$= \frac{1}{A}\left(\frac{\frac{dQ}{dt}}{\frac{d\Theta_s}{dt}}\right)$$

$$= \frac{1}{A}\left(\frac{I_p}{i2\pi f\Theta_o}\right) \tag{3.19}$$

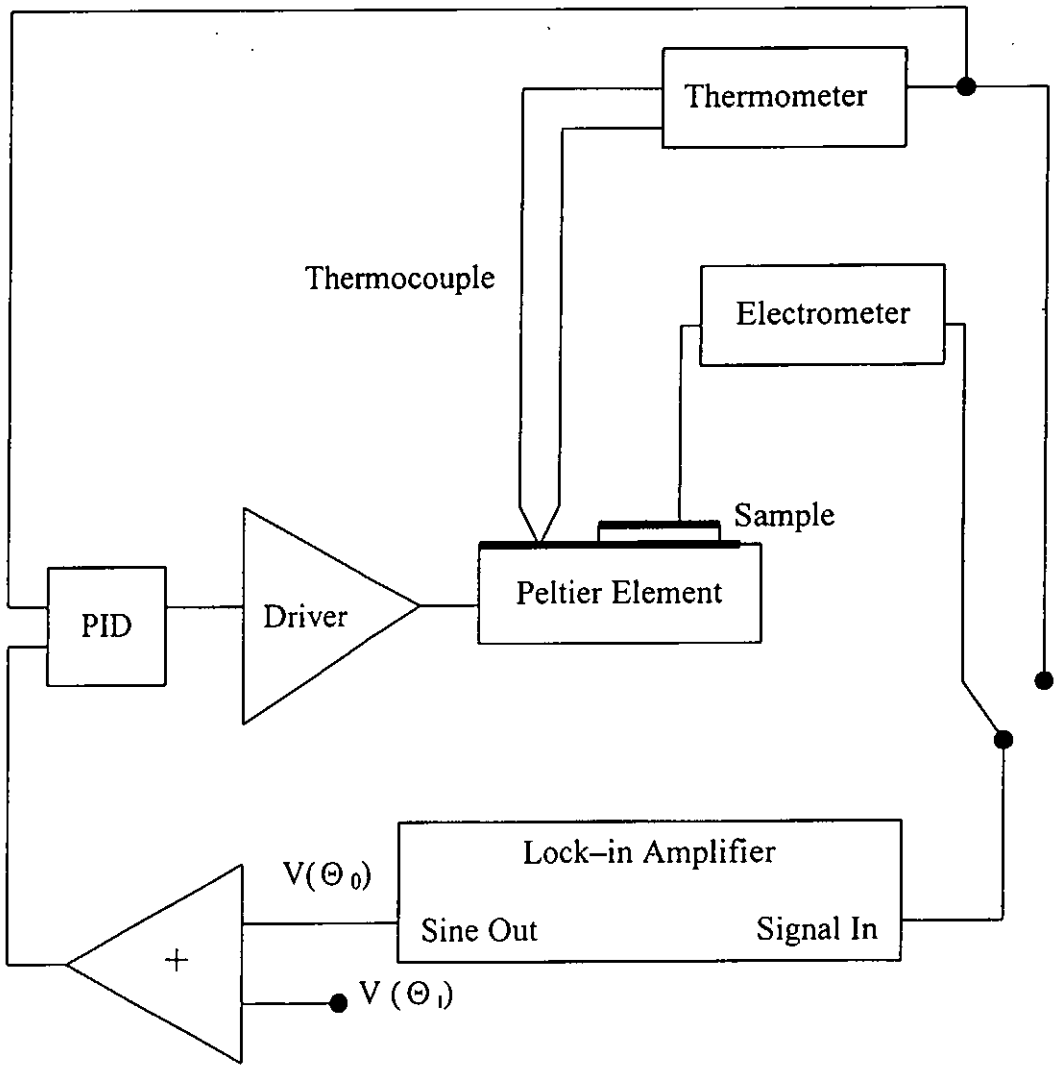

Figure 3.4 Schematic diagram of the setup for pyroelectric coefficient measurement.

3.6 Results and Discussion

3.6.1 Degree of Poling of the Composites

The intensities of the diffracted x rays from the surfaces of the composite samples A, C and D were measured as a function of diffraction angle 2θ. Figure 3.5 shows the XRD patterns of the composite (sample A) before and after poling. Similar XRD patterns were observed for the other composites. It can be seen that the intensity of the (200) diffraction peak decreases and that of the (002) diffraction peak increases after poling. The degrees of poling of the ceramic phase α_c for samples A, C and D are determined using equation 3.1 and tabulated in Table 3.1. The α_c values for the three samples are quite high (about 0.73), indicating that the ceramic phase of the composite can be poled effectively under the dc field at 120 °C. This is probably due to the high dc conductivity of the copolymer at high temperature (above its ferroelectric-to-paraelectric phase transition temperature). This leads to a substantial transport of charge through the copolymer matrix to the boundaries of the ceramic particles, and hence the particles can be poled.

Table 3.1 The poling ratio of the ceramic phase α_c for the composites of different polarization states

Composite sample	Polarization states	Poling ratio (α_c)
A	Only the ceramic phase poled	0.75
C	Two phases poled in opposite directions	0.73
D	Both phases poled in the same direction	0.72

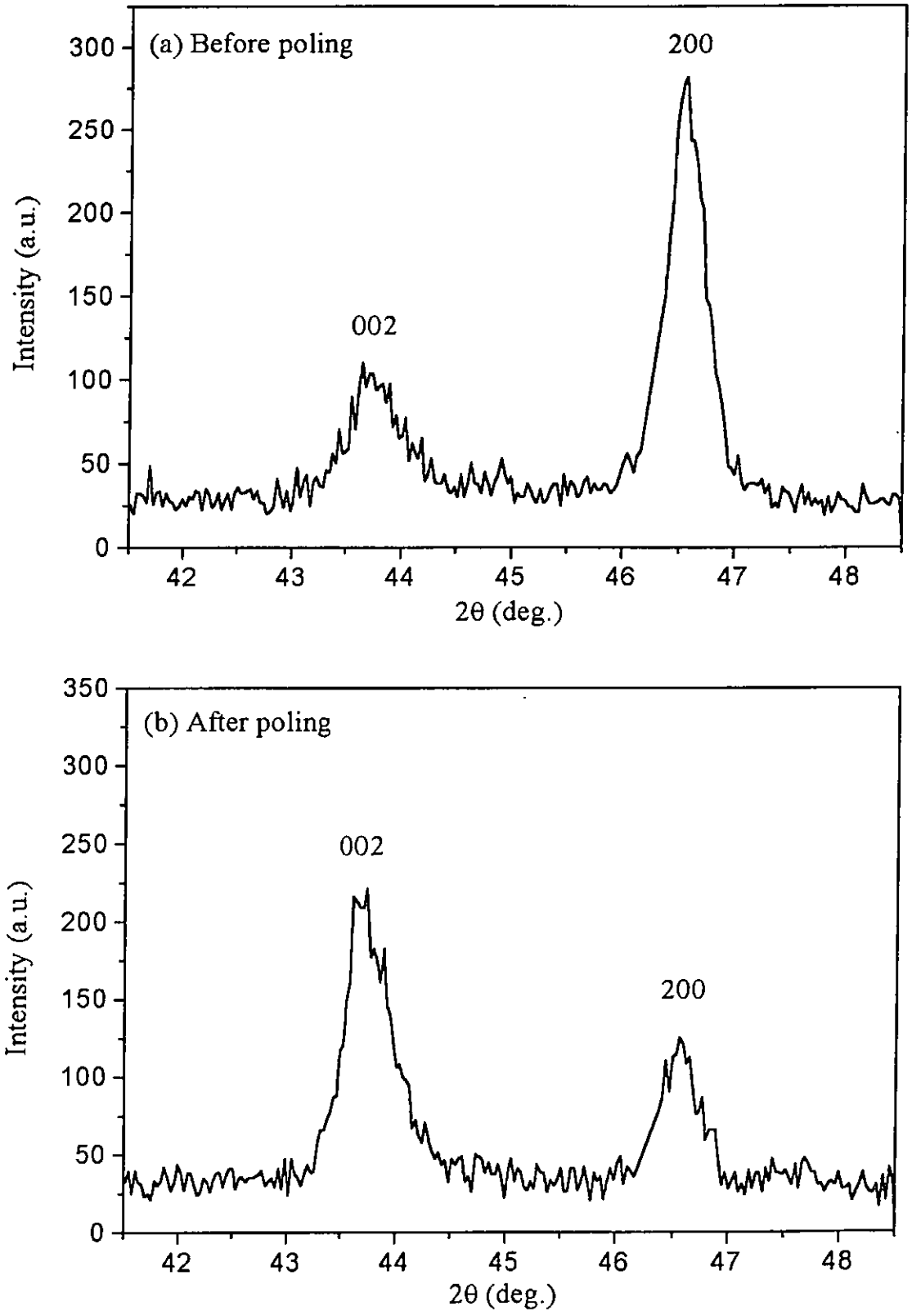

Figure 3.5 XRD patterns of the composite (sample A) before and after poling.

The P-E hysteresis loops of the composites and the copolymer were measured during the ac poling. As shown in Figure 3.6, the hysteresis loops for the composite with only the copolymer phase poled (sample B) are similar to those for the copolymer (sample E). When a small electric field is applied to the composite sample, the polarization increases linearly with the electric field. It is because the electric field is not large enough to switch the dipoles and the sample behaves as a normal dielectric material. When the electric field is sufficiently high, a number of dipoles in the copolymer phase can be switched along the field direction and a hysteresis loop is observed. When the electric field continues to increase, the hysteresis loop grows and the remanent polarization increases. The variation of the remanent polarization with the electric field for the composite (sample B) and the copolymer (sample E) is shown in Figure 3.7. It can be seen that the values of P_r for the composite and the copolymer increase rapidly when the electric field is larger than 50 MV/m, reflecting that the electric field is high enough to switch the dipoles. For the composite, when the electric field increases to ~ 72 MV/m, electrical breakdown occurs. The highest value of P_r is ~ 3.3 $\mu C/cm^2$. For the copolymer poled under the same electric field, the value of P_r is ~ 3.4 $\mu C/cm^2$ which is very close to that of the composite. This indicates that the observed polarization of the composite mainly arises from the switching of the dipoles in the copolymer phase. Besides, when the copolymer is fully poled under an ac field of 100 MV/m, the remanent polarization (i.e. P_r^o) is 5 $\mu C/cm^2$. Using equation 3.4, the degrees of poling of the copolymer phase α_p for samples B, C, D and E are determined and tabulated in Table 3.2. The values of α_p for all samples are very close (about 0.65).

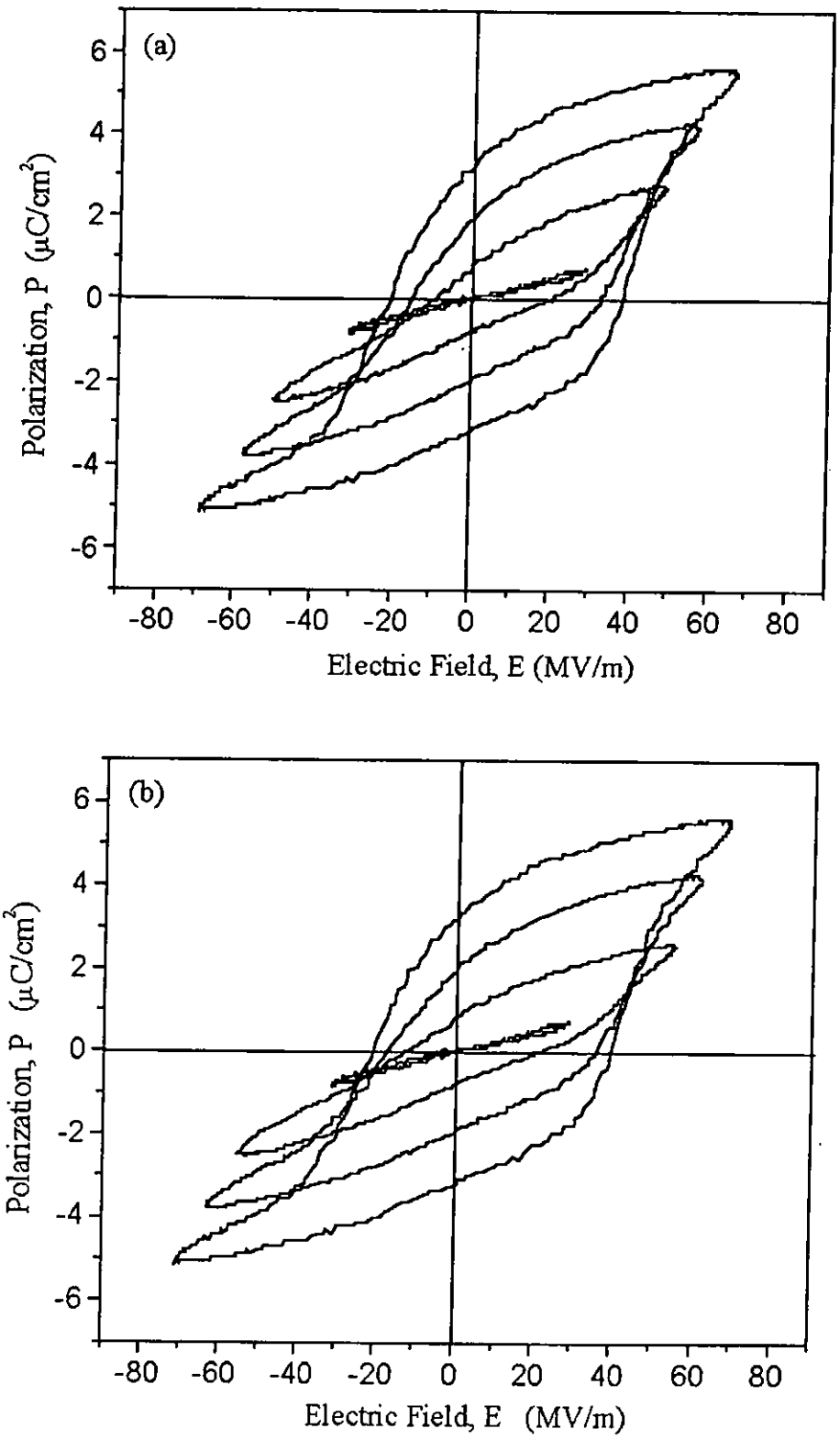

Figure 3.6 Hysteresis loops of (a) PT/P(VDF-TrFE) composite (sample B) and (b) P(VDF-TrFE) copolymer (sample E) measured at 10 Hz and 70 °C.

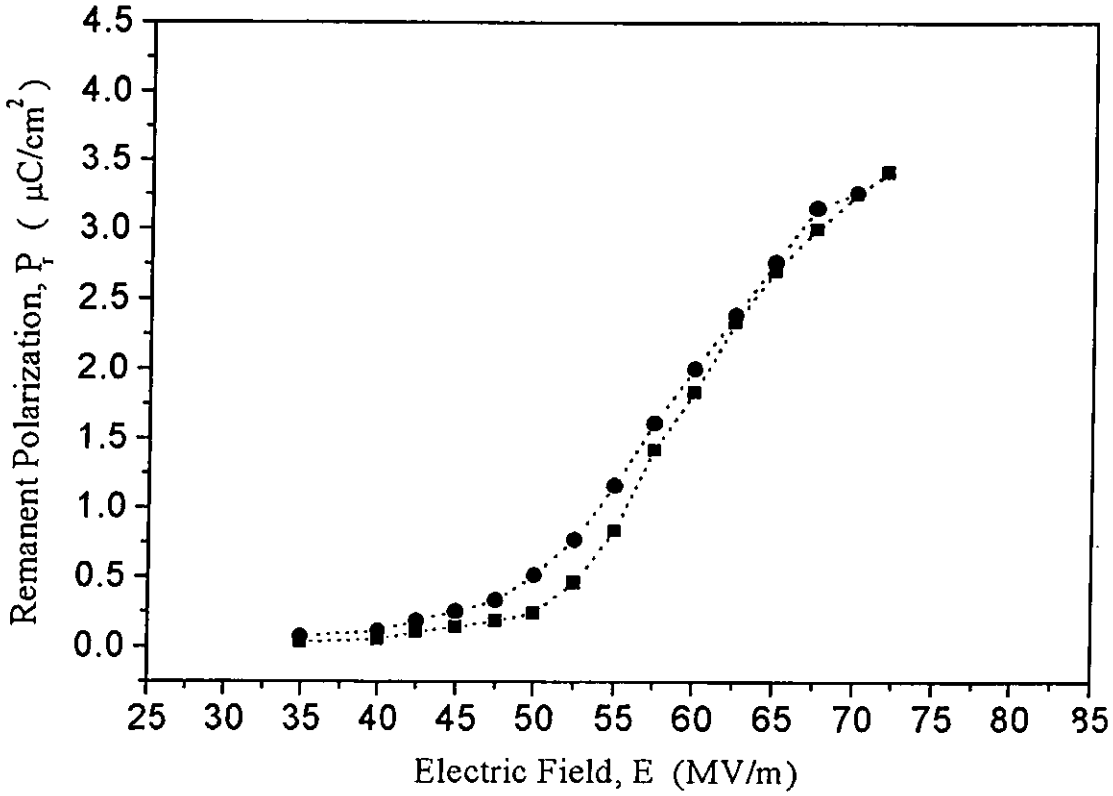

Figure 3.7 Variation of the remanent polarization P_r with the electric field E for the composite (sample B), ---●---; and copolymer (sample E), ---■---.

Table 3.2 The poling ratio of the copolymer phase α_p for the composites of different polarization states.

Sample	Polarization states	Poling ratio (α_p)
B	Only the copolymer phase poled	0.65
C	Two phases poled in opposite directions	0.63
D	Both phases poled in the same direction	0.66
E (pure P(VDF-TrFE))	The copolymer phase poled	0.68

3.6.2 Relative Permittivity of the Composites

The relative permittivity at 1 kHz of the unpoled 0-3 composite and copolymer was measured as a function of temperature upon heating and cooling. As shown in Figure 3.8, thermal hysteresis is observed for both the composite and copolymer upon heating and cooling. The phase transition of the copolymer can be indicated by a maximum in the relative permittivity ε_r [Furukawa *et al.*, 1981]. For the composite upon heating, ε_r reaches a maximum value at about 110 °C which corresponds to the ferroelectric-to-paraelectric phase transition of the copolymer matrix (i.e. $\uparrow T_c \approx 110$ °C). Upon cooling, ε_r reaches a maximum value at about 75 °C, which is the paraelectric-to-ferroelectric phase transition of the copolymer matrix (i.e. $\downarrow T_c \approx 75$ °C). Similar result is observed for the pure copolymer, indicating that the PT powder does not affect the transition of the copolymer matrix upon heating and cooling. As discussed in section 2.6, only the ceramic phase of the composite can be poled at a temperature higher than the $\uparrow T_c$ of the copolymer phase, while the copolymer phase can be poled at a temperature below its $\uparrow T_c$. By determining the $\uparrow T_c$ of the copolymer phase, we can decide the poling temperature for the ceramic and the copolymer phase. In the present work, the ceramic particles and the copolymer matrix were poled at 120 °C and 70°C, respectively.

Besides, the room temperature relative permittivity of the composite and the copolymer was measured as a function of frequency. As shown in Figure 3.9, ε_r of all

the poled samples decreases due to dipole alignment. For sample A, the decrease in ε_r is very small. As the ceramic volume fraction of the composite is low (about 0.2), the decrease in the permittivity of the ceramic phase due to dipole alignment is not significant, so the overall ε_r of the composite does not change too much. When the copolymer phase of samples B, C and D is poled, the ε_r decreases by 10-15 % in the frequency range of 1 kHz to 10 MHz. Such decrease is similar to that observed in the poled copolymer (sample E).

As compared with the copolymer, the ε_r of the composite is about 60 % larger. In general, small value of ε_r is required for a good sensing material in order to attain high voltage piezoelectric coefficient g_{33} ($\sim d_{33}/ \varepsilon_r\varepsilon_o$). However, from a device viewpoint, too small value of the ε_r is not preferred. In practice, the capacitance of the sensing element should be large enough to prevent interference from the stay capacitance associated with the connecting cable. Fabrication of 0-3 composite can increase the ε_r of the copolymer by simply adding ceramic powder in the copolymer matrix. And the ε_r of the composite can be adjusted by changing the ceramic volume fraction.

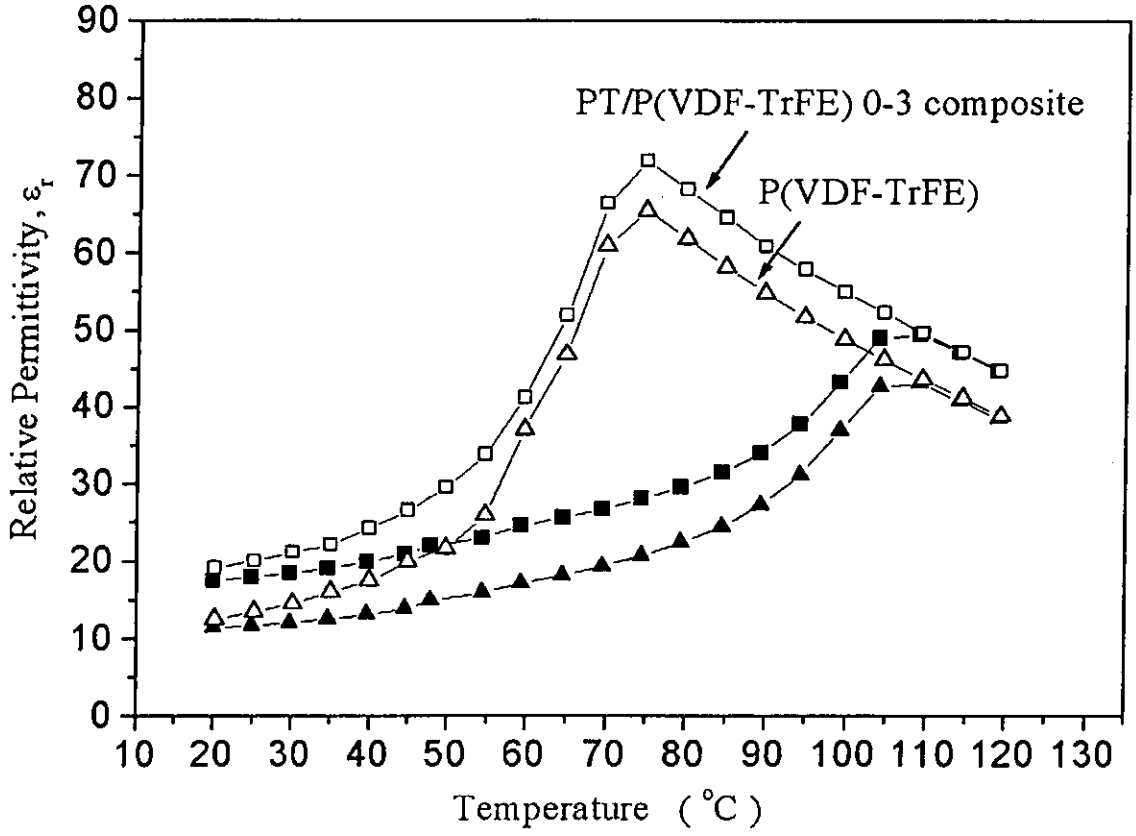

Figure 3.8 Relative permittivity against temperature of unpoled composite and P(VDF-TrFE) copolymer upon heating and cooling (solid: heating; open: cooling).

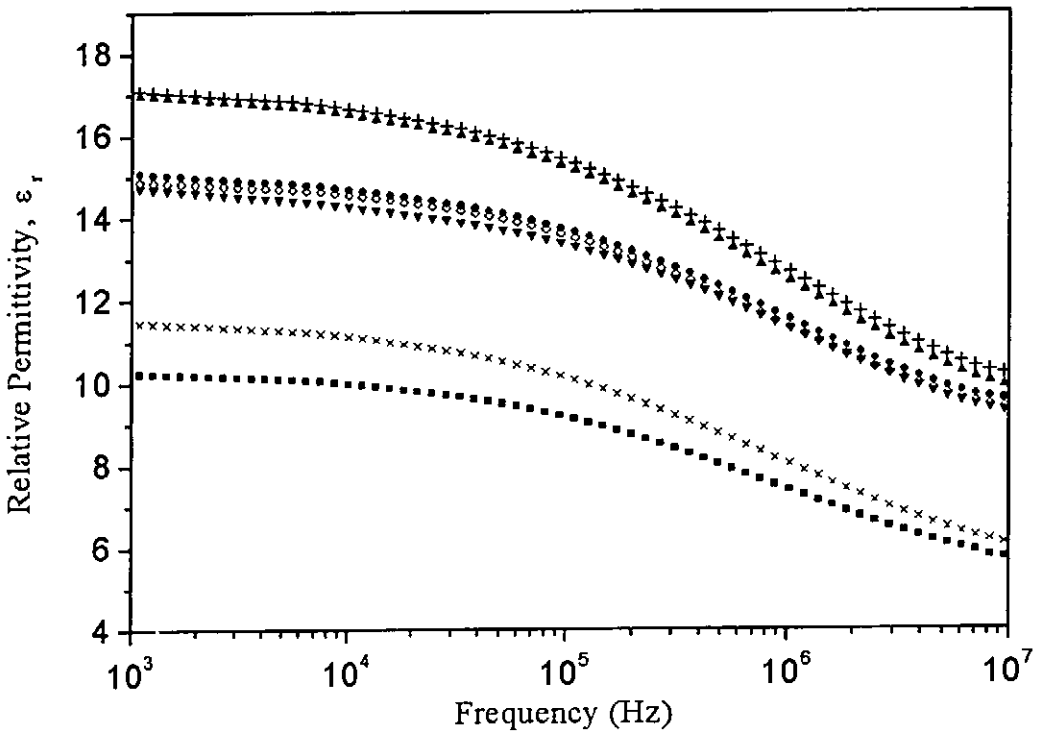

Figure 3.9 Relative permittivity against frequency for the composites and the copolymer before and after poling.

+ : Unpoled composite
× : Unpoled copolymer
▲ : Composite with only the ceramic phase poled (sample A)
◇ : Composite with only the copolymer phase poled (sample B)
▼ : Composite with two phases poled in opposite directions (sample C)
● : Composite with both phases poled in the same direction (sample D)
■ : Poled copolymer (sample E)

3.6.3 Piezoelectric Coefficient of the Composites

To fabricate a piezoelectric sensor working in the thickness mode, the thickness piezoelectric coefficient d_{33} is a useful material parameter for selecting appropriate sensing material. Using a single beam laser interferometer, the piezoelectric coefficient d_{33} of all the samples (A to E) was determined. As reported by previous workers [Li *et al.*, 1995; Kholkin *et al.*, 1996], to measure the actual displacement induced in the piezoelectric sample, the sample should be mounted tightly to a rigid holder to prevent bending vibration. Besides, the measuring frequency should be far below the mechanical resonances of the sample. As the film was spin-coated on the glass substrate, the substrate was glued rigidly on a large aluminum block to ensure that only the desired thickness mode vibration was excited in the measurement. Figure 3.10 shows the variation of the displacement with the position along the sample length direction. It can be seen that the vibrational displacement is almost constant in the poled region of the sample while it becomes zero in the unpoled region. This indicates that the bending vibration is not present. The displacement of the sample at different measuring frequencies is plotted in Figure 3.11. It can be seen that the displacement is approximately constant in the frequency range of 5 to 2000 kHz, indicating that the mechanical resonance has not been excited in this frequency range. The piezoelectric coefficient of all the samples were then measured at 15 kHz in this work. Figure 3.12 shows the variation of the displacement with the driving voltage at 15 kHz for the sample E and a linear piezoelectric response is observed. Similar results were obtained for the other samples and the piezoelectric coefficient of the samples was then determined from the slope of the curve.

As mentioned before, all the film samples were spin-coated on the glass substrates. The films are laterally clamped by the substrate and thus can not vibrate freely. Hence, the measured value of d_{33} for these samples becomes smaller. For a film completely clamped by the substrate, the lateral strain is zero, and the effective piezoelectric coefficient d_{33}' subjected to the clamping is related to the true coefficient d_{33} by [Royer and Kmetik, 1992]:

$$d_{33}' = d_{33} - 2\left(\frac{d_{31}s_{13}^{E}}{s_{11}^{E} + s_{12}^{E}}\right) \tag{3.20}$$

where s_{11}^{E}, s_{12}^{E} and s_{13}^{E} are the elastic compliances at constant electric field of the film, and d_{31} is the transverse piezoelectric coefficient of the film. In order to determine the true coefficient, the values of s_{11}^{E}, s_{12}^{E}, s_{13}^{E} and d_{31} of the sample are required. For a fully poled copolymer film, the effective piezoelectric coefficient is 15 pm/V. By using the literature values of s_{11}^{E}, s_{12}^{E}, s_{13}^{E} and d_{31} [Wang *et al.*, 1993] and equation 3.20, the d_{33} value of the copolymer film is determined to be about 25.1 pm/V. It can be seen that the value of d_{33}' is about 60 % of the d_{33} value, indicating that the clamping effect is quite significant. However, the values of s_{11}^{E}, s_{12}^{E}, s_{13}^{E} and d_{31} of the composite samples are not available. Therefore, in the present work, we have only determined the effective piezoelectric coefficient for all the samples. Since the elastic compliances of the composite samples should not change significantly after the poling process, the value of d_{33}' is used for comparing the piezoelectric properties of the samples.

The values of d_{33}' of all the samples are tabulated in Table 3.3. Sample A has a d_{33}' value smaller than that of sample B. When the copolymer phase of the composite is poled in a direction opposite to that of the ceramic phase (sample C), the value of d_{33}' of

the composite is higher than those of samples A and B, indicating that the piezoelectric responses of the two phases reinforce each other. It is because the piezoelectric coefficients of the ceramic and the copolymer phase are opposite in sign. The d_{33}' value of sample C is found to be 30 % larger than that of the pure copolymer (sample E). When the copolymer phase is poled in a direction parallel to that of the ceramic phase (sample D), the composite has a d_{33}' value smaller than those of samples A and B, indicating that the piezoelectric responses of the two phases partially cancel each other. Among the five samples, sample C has the highest piezoelectric activity, so it can be used to fabricate piezoelectric sensors with good receiving sensitivity.

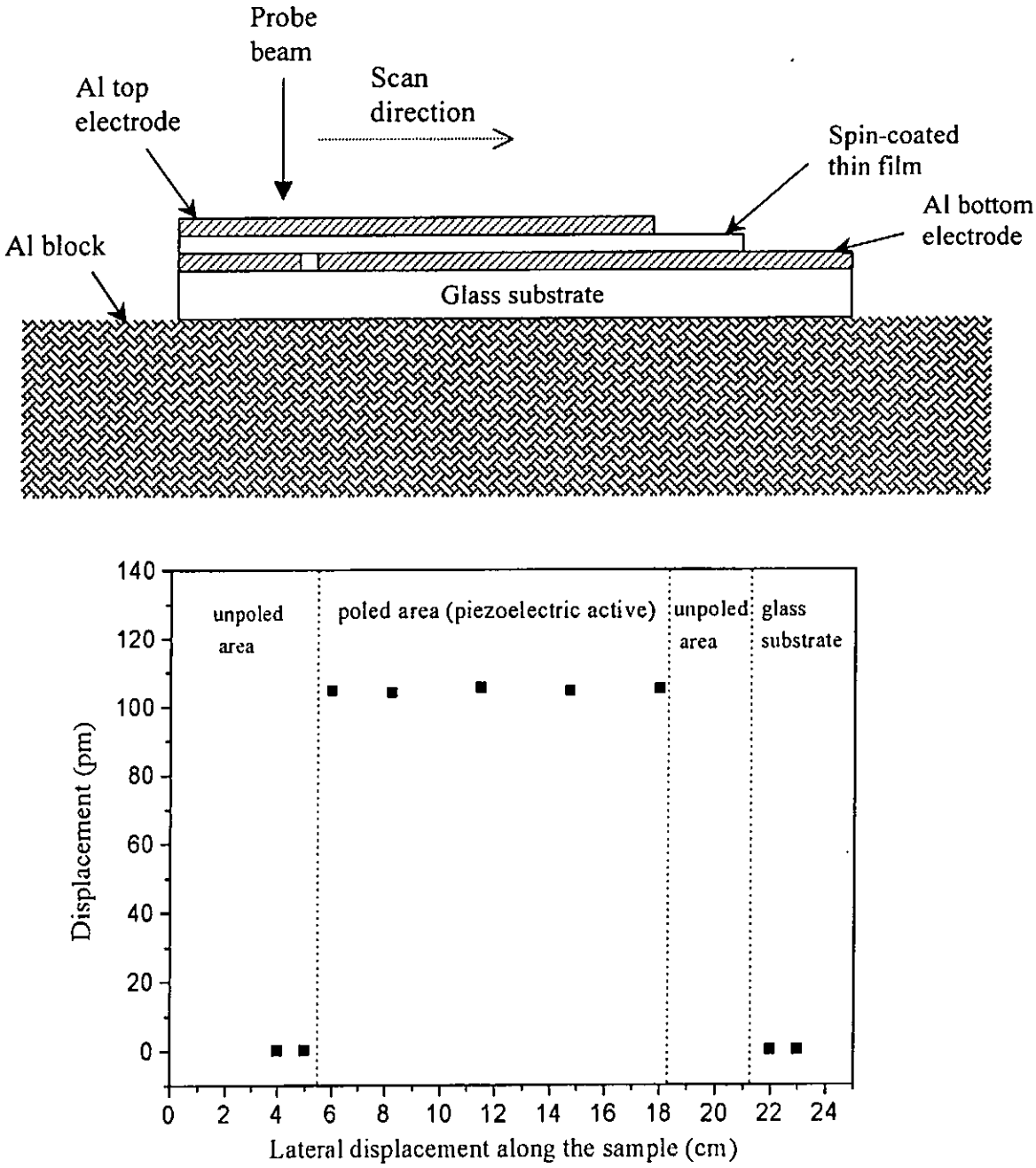

Figure 3.10 Variation of the amplitude of vibration across the sample surface measured at 15 kHz.

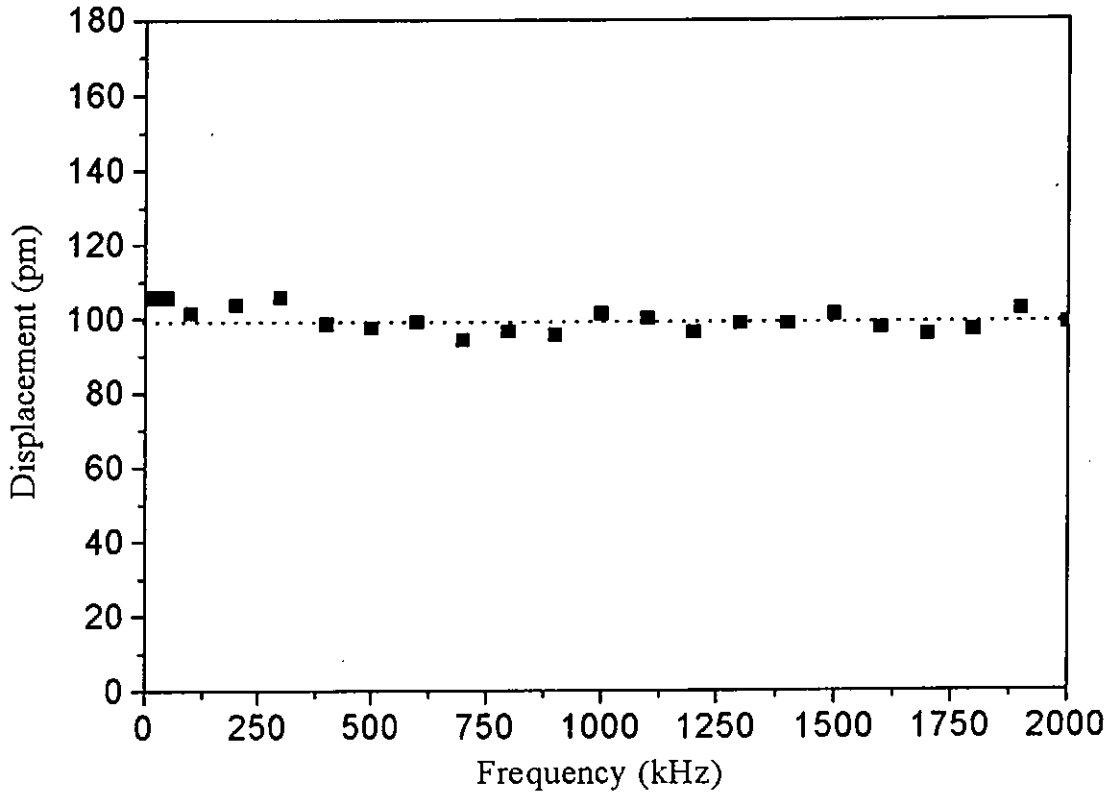

Figure 3.11 The displacement of the film sample at different measuring frequencies.

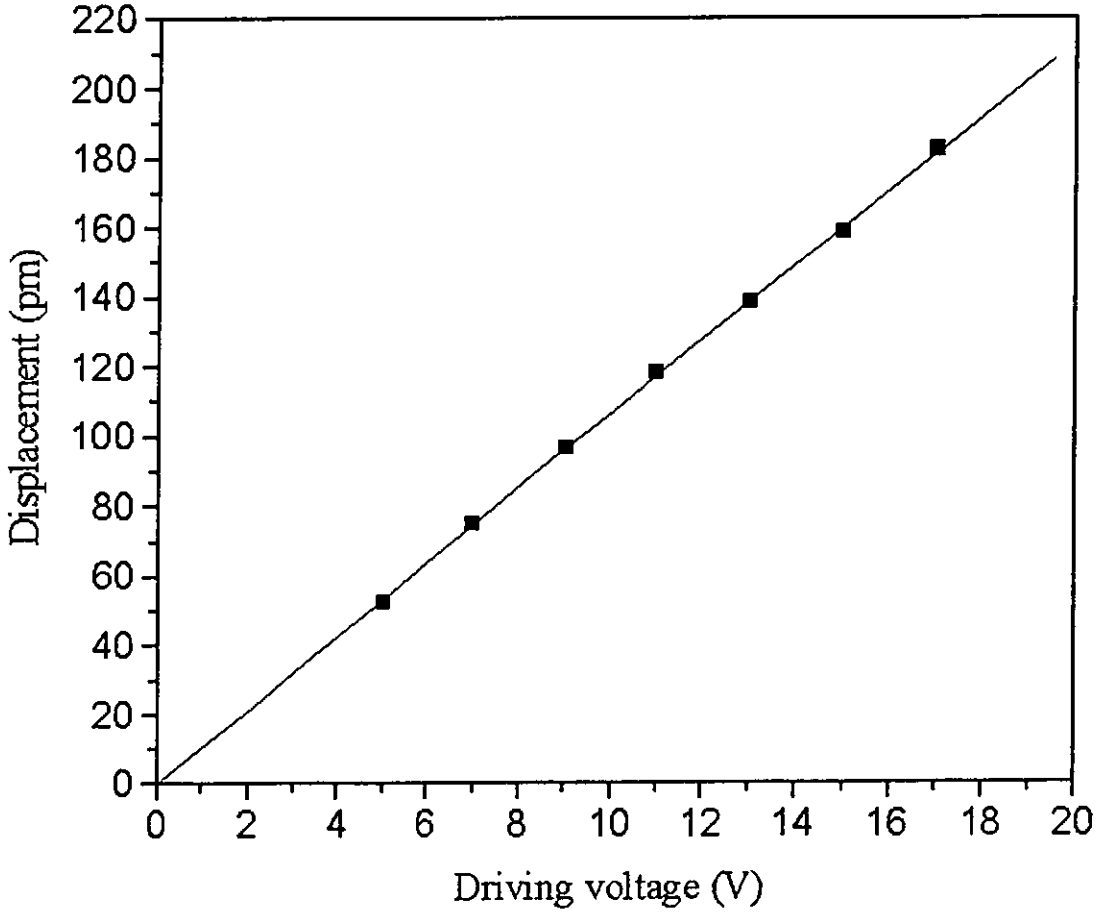

Figure 3.12 Variation of the displacement with driving voltage at 15 kHz for sample E

Table 3.3 Effective piezoelectric coefficients of the composite and copolymer samples measured at room temperature.

Samples	Polarization direction		Phase angle (deg.)	Effective d_{33}' (pm/V)
	Ceramic phase	Copolymer phase		
A	↑	Unpoled	-6.1	+ 7.4
B	Unpoled	↑	+174.1	- 8.2
C	↑	↓	- 6.8	+ 14
D	↑	↑	+173.6	- 4.0
E (pure P(VDF-TrFE))		↑	+174.6	- 10.5

3.6.4 Pyroelectric Coefficient of the Composites

The pyroelectric coefficient of all the samples was measured and tabulated in Table 3.4. It should be noted that the top electrode of the sample is always connected to the input of the electrometer in the pyroelectric measurement. The p value of sample A is 50 % less than that of sample B. For sample C, it has a p value in between those of samples A and B, but in opposite sign. Since the pyroelectric coefficients of the ceramic and the copolymer phase have the same sign, the pyroelectric activities of the two phases poled in opposite directions partially cancel each other. As compared with sample E, the pyroelectric response of sample C is 40 % smaller. Therefore, another advantage of using sample C as the sensing element of the piezoelectric sensors is to eliminate the noise signal due to temperature fluctuation. When the two phases of a

composite are poled in the same direction (sample D), the pyroelectric responses of the phases reinforce each other and higher pyroelectric response is obtained. It can be seen that the p value of sample D is about 30 % larger than that of sample E. Thus, sample D can be a good candidate for the pyroelectric sensors applications.

To investigate the effect on the polarization of the ceramic phase by the ac poling process, samples A, B and C were heated at 120 °C for 45 minutes and their pyroelectric coefficients were re-measured. It is expected that, by annealing at 120°C ($>\uparrow T_c$ of the copolymer) for 45 minutes, the polarization of the copolymer phase can be removed. For sample A, the re-measured value of p is - 8.5, indicating that the additional annealing process does not affect the existing polarization state of the PT phase. The re-measured value of p of samples B and C are - 0.1 and - 9.0, respectively. This shows that the application of an ac field to the composite pole the copolymer phase only and has no effect on the ceramic phase.

Table 3.4 Pyroelectric coefficients of the composite and copolymer samples measured at room temperature.

Samples	**Polarization direction**		**p, ($\mu C/m^2K$)**
	Ceramic phase	Copolymer phase	
A	↑	Unpoled	- 8.9
B	Unpoled	↑	- 17.0
C	↑	↓	+ 14.0
D	↑	↑	- 28.3
E (pure P(VDF-TrFE))		↑	- 22.4

3.7 Summary

A procedure for poling the ceramic and the copolymer phases of 0-3 composite separately has been developed, which allows the two phases to be poled either in opposite directions or in the same direction. The ceramic phase was poled under a dc electric field at a temperature above the ferroelectric-to-paraelectric phase transition of the copolymer while the copolymer phase was poled under an ac field at lower temperature. Composites of four different polarization states were prepared and characterized: (a) only the ceramic phase poled, (b) only the copolymer phase poled, (c) two phases poled in opposite directions and (d) both phases poled in the same direction. The degrees of poling of the two phases of the composites are quite high, showing that the ceramic and the copolymer phases can be poled effectively. Composite with two phases poled in opposite directions has improved piezoelectric activity and reduced sensitivity to temperature fluctuation. It is found that its piezoelectric response is about 30 % larger than that of the copolymer, so it is of great interest in using such composite for the piezoelectric sensor applications. For the composite with both phases poled in the same direction, its pyroelectric activity is improved, about 30 % larger than that of the copolymer. Besides, its piezoelectric activity is reduced, thereby minimizing the noise signal induced by the vibration. Therefore, it can be used as a sensing element for pyroelectric sensors.

Chapter Four

Fabrication of Hydrophones

4.1 Introduction

As shown in Chapter three, the piezoelectric and pyroelectric properties of the PT/P(VDF-TrFE) 0-3 composites can be adjusted by using different poling procedures. Composite film with two phases poled in opposite directions has improved piezoelectric response and reduced sensitivity to temperature fluctuation. In addition, with thickness of several micrometers, the thickness mode resonance of the film occurs at very high frequency (> 100 MHz). Therefore, it is possible to use this material to construct ultrasonic hydrophones with good receiving sensitivity and flat frequency response.

In the present study, three samples are used as sensing elements for fabricating needle-type hydrophones: sample A (PT/P(VDF-TrFE) 0-3 composite film with only the ceramic phase poled), sample C (PT/P(VDF-TrFE) 0-3 composite film with two phases poled in opposite directions), and sample E (poled P(VDF-TrFE) copolymer film). Sample C is also used to fabricate a hydrophone array with eight sensing elements. The construction of the needle-type hydrophone and the 8-element hydrophone array are described in the following sections.

4.2 Construction of Needle-type Hydrophone

The film samples were peeled off from the glass substrate and the Al electrodes were etched away in potassium hydroxide solution (KOH). A chromium-gold (Cr/Au) layer of thickness 0.15 μm was thermally evaporated on one of the film surfaces as bottom electrode. Circular elements of diameter about 0.6 mm were cut out from the films for subsequent hydrophone fabrication.

The construction of a needle-type hydrophone is shown schematically in Figure 4.1. A copper wire of diameter 0.7 mm was held in the center of the stainless steel tubing by epoxy (Araldite, produced by Ciba-Geiby). After the epoxy had set, the tip of the needle was polished to expose the tip of the wire. The circular element, with the electroded surface facing the tip, was carefully glued to the tip of the exposed wire using silver-paint. The edge of the circular element was then insulated by epoxy. A Cr/Au layer of thickness 0.15 μm was evaporated on the surface of the element to make contact with the steel tubing and served as the ground electrode. The needle was connected to a 50 Ω coaxial cable of length 0.3 m, which was the shortest practical length required to connect the hydrophone output signal to an amplifier. As the hydrophone was tested in water, the junction between the needle and the coaxial cable was covered with epoxy to prevent leakage of water. The photograph of the needle-type hydrophone is shown in Figure 4.2.

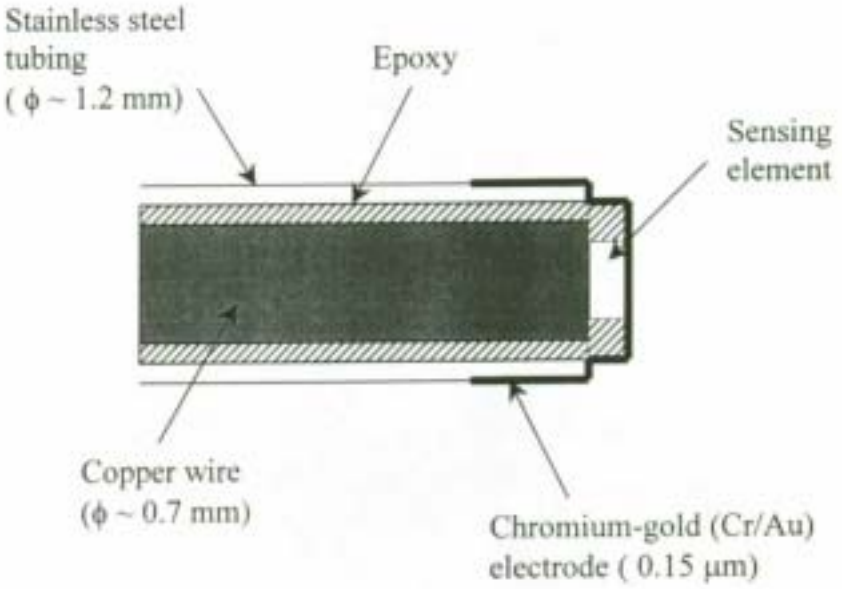

Figure 4.1 Schematic diagram of the needle head of the needle-type hydrophone.

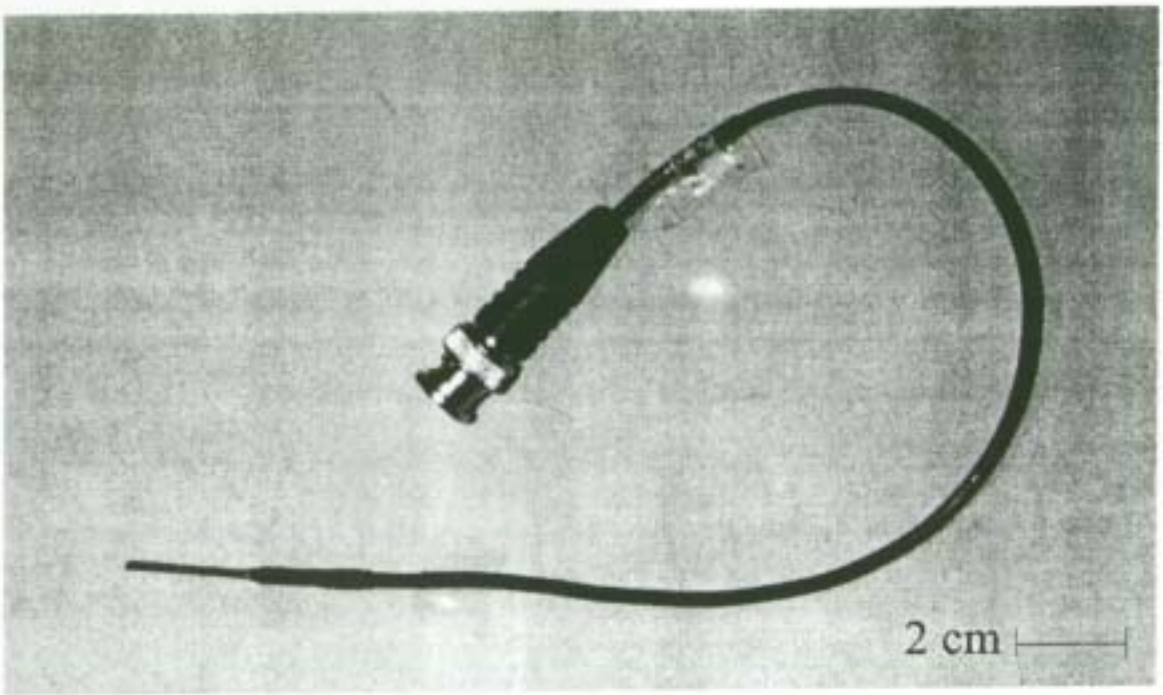

Figure 4.2 Photograph of the needle-type hydrophone.

4.3 Construction of 8-element Hydrophone Array

The construction of the 8-element hydrophone array is shown schematically in Figure 4.3. Similar to the construction of the needle-type hydrophone, the copper wires of diameter 1.0 mm were held by epoxy in the center of the holes of the polyacetal (POM) housing which was fixed in a stainless steel tubing of diameter 4 mm and length 160 mm. After the epoxy had set, the tips of the copper wires were polished to obtain flat surfaces. The circular elements, with the electroded surface facing the tip, were carefully glued to the tip of exposed wire using silver-paint and the edge of the elements was insulated by epoxy. A Cr/Au layer of thickness 0.15 μm was evaporated on the top surfaces of elements to make contact with the steel tubing and serve as the ground electrode. The center-to-center separation between the elements was 2.5 mm. The photograph of the 8-element hydrophone array is shown in Figure 4.4.

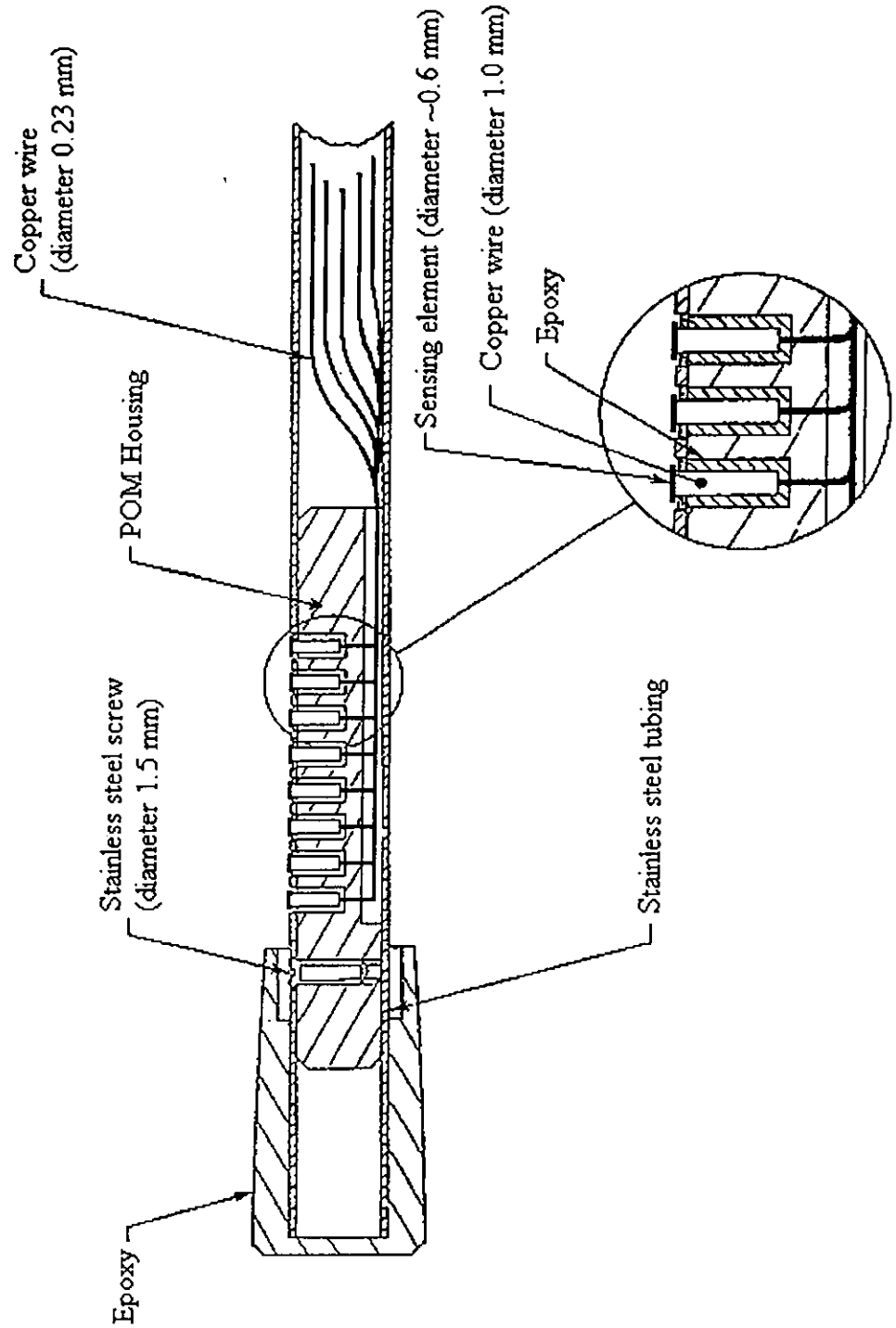

Figure 4.3 Schematic diagram of the 8-element hydrophone array.

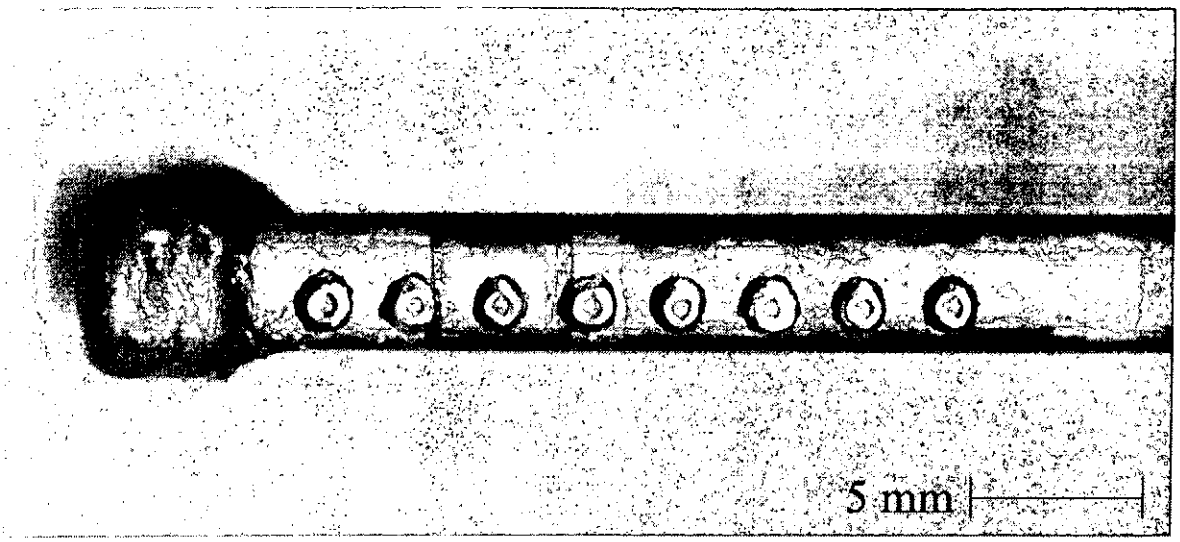

Figure 4.4 Photograph of the 8-element hydrophone array.

Chapter Five

Evaluation of Hydrophones

5.1 Introduction

A hydrophone is an electroacoustic device designed for measuring the spatial and temporal characteristics of an acoustic field in water. It should provide an undistorted voltage waveform replica of the acoustic pressure at each point in the field, and the output voltage should be proportional to the acoustic pressure. The receiving sensitivity of the hydrophone is given by the output voltage to the acoustic pressure, and expressed in V/MPa or in dB rel 1 V/μPa.

Ideally, the receiving sensitivity of the hydrophone is independent of the angle at which the acoustic wave is incident. To achieve this, the size of the sensing element must be small as compared with the acoustic wavelength in the propagation medium. For the biomedical applications, the operating frequency is normally up to 15 MHz and the minimum acoustic wavelength is about 0.1 mm. With the existing piezoelectric materials and hydrophone designs, the receiving sensitivity of a sensor with such small sensing area would be too low for the applications. Therefore, the practical hydrophones have sensing element greater than the acoustic wavelength. Consequently, averaging of the acoustic pressure over the sensing element occurs

leading to angular variation in the hydrophone output and underestimation of the spatial peak pressure. Knowledge of this angular dependence is important in order to assess the error introduced by it in a given measurement and to correct for the error when necessary [Chivers *et al.*, 1980 and Smith, 1989].

The angular response of a hydrophone can be compared with three theoretical models: (a) the circular piston in a rigid planar baffle, (b) the circular piston in a soft (pressure-release) baffle and (c) the unbaffled circular piston. In the first case, the plane surface of a circular transducer is assumed as a circular piston in a rigid planar baffle. Based on the diffraction theory, the angular dependence of the pressure U generated by the transducer in the far field region is given by [Morse and Ingard, 1968]:

$$U(r,\delta) = U(r)\left(\frac{2J_1(km\sin\delta)}{km\sin\delta}\right) \tag{5.1}$$

where J_1 is the Bessel function of the first order, k (= $2\pi/\lambda$) is the wave number, m is the radius of the piston, r is the distance from the center of the piston to the field point, and δ is the angle between r and the piston axis. The angular response of a hydrophone in the receive mode is then expressed as [Shombert *et al.*, 1982]:

$$V(\delta) = V_o\left(\frac{2J_1(ka\sin\delta)}{ka\sin\delta}\right) \tag{5.2}$$

where V_o is the output voltage when the pressure wave is normally incident on the hydrophone, a is the radius of the sensing element of the hydrophone and δ is the angle of incidence of the pressure wave. Selfridge *et al.* [1980] suggested that the

rigid baffle model is inappropriate for small array elements. Hence, they proposed the use of the soft baffle model, in which the angular dependence is modified by an additional cos θ term. And the theoretical hydrophone response is given by:

$$V(\delta) = V_o\left(\frac{2J_1(ka\sin\delta)}{ka\sin\delta}\right)\cos\delta \tag{5.3}$$

The additional term can narrow the main lobe and cause the response to be zero at the incident angle equal to 90°. The third model based on an unbaffled piston (i.e. piston in free space) has been suggested by Delannoy *el al.* [1979] and the predicted hydrophone response is expressed as:

$$V(\delta) = V_o\left(\frac{2J_1(ka\sin\delta)}{ka\sin\delta}\right)\left(\frac{1+\cos\delta}{2}\right) \tag{5.4}$$

As shown in Chapter four, three samples were used as sensing elements for fabricating needle-type hydrophones: sample A (PT/P(VDF-TrFE) composite film with only the ceramic phase poled), sample C (PT/P(VDF-TrFE) composite film with two phases poled in opposite directions) and sample E (poled (P(VDF-TrFE) copolymer film). Besides, an 8-element hydrophone array was fabricated using sample C as the sensing element. The performances of the needle-type hydrophones and hydrophone array were evaluated in water. At first, the receiving sensitivities of the needle-type hydrophones and hydrophone array were examined as a function of frequency. The angular response of the hydrophone was measured and compared with the three theoretical models.

5.2 Experimental Techniques

5.2.1 Receiving Sensitivity Measurement

The receiving sensitivity of the sample hydrophone is determined by a comparison method in which the received signal from the sample hydrophone is compared with that of a reference hydrophone with known sensitivity. It should be noted that all the hydrophones were soaked in water for at least 10 minutes before the measurement.

The experimental setup is shown in Figure 5.1. A function generator (HP 8116A) was used to generate tone bursts of 15 cycles at a single frequency with a repetition rate of 1 kHz. The signal was amplified by a power amplifier (Research Amplifier 25A100) to about 15 V peak and then was used to drive a plane transducer (6.35 mm diameter, 10 MHz centre frequency, Panametrics) to generate a short burst of ultrasonic waves. The driving voltage (peak) was monitored by a digitizing oscilloscope with 1 MΩ input impedance in parallel with 8 pF capacitance (HP infinium).

A PVDF bilaminar shielded membrane hydrophone with an active element of diameter 0.5 mm (GEC-Marconi, Type Y-34-3598 calibrated by National Physical Laboratory, UK) was used as a reference hydrophone to characterize the acoustic waves at a distance in the far field region of the acoustic waves (distance > n^2/λ_a, where n is the transducer radius and λ_a is the wavelength of the acoustic wave). The voltage signal from the membrane hydrophone was amplified five times

by a matched amplifier (National Physical Laboratory, UK) and then measured by the oscilloscope with 1 MΩ input impedance (1MΩ // 8 pF). The hydrophone was aligned for maximum output voltage by translating it normal to the acoustical axis of the transducer. Without changing the driving conditions for the transducer, the sample hydrophone was substituted at the same test point, and the output voltage was maximized and measured following the same procedure. The end-of-cable loaded sensitivity M_a at the output of the amplifier connected to the sample hydrophone is then calculated from:

$$M_a = \left(\frac{V_L}{V_s} \right) M_s \tag{5.5}$$

where V_L and V_s are the maximum output voltages of the sample hydrophone and membrane hydrophone, respectively, and M_s is the end-of-cable loaded sensitivity of the membrane hydrophone (with the amplifier). The calibration curve for the end-of-cable loaded sensitivity (gain = 5) of the membrane hydrophone is shown in Figure 5.2. The uncertainty in the sensitivity is about ± 7 % in the frequency range of 1 to 10 MHz. The end-of-cable loaded sensitivity of the sample hydrophone M_L (without the amplifier) is given by:

$$M_L = \frac{M_a}{G} \tag{5.6}$$

where G is the gain of the amplifier.

In practice, an end-of-cable open-circuit sensitivity M_o which is independent of the loading conditions is usually used. If the hydrophone has output impedance Z

and is connected to an electrical load Z_{load} (i.e. oscilloscope), the two sensitivities are related by [AIUM/NEMA, 1998]:

$$M_L = M_o \sqrt{\frac{\{\mathrm{Re}(Z_{load})\}^2 + \{\mathrm{Im}(Z_{load})\}^2}{\{\mathrm{Re}(Z_{load}) + \mathrm{Re}(Z)\}^2 + \{\mathrm{Im}(Z_{load}) + \mathrm{Im}(Z)\}^2}} \qquad (5.7)$$

where Re and Im denote the real and imaginary parts of a complex impedance, respectively. In general, the impedances of the hydrophone and the load can be assumed to be capacitive, and equation 5.7 can be simplified as:

$$M_L = \left(\frac{C_h}{C_h + C_{load}}\right) M_o \qquad (5.8)$$

where C_h is the end-of-cable capacitance of the hydrophone (i.e. Im(Z)), and C_{load} is the capacitance of the load.

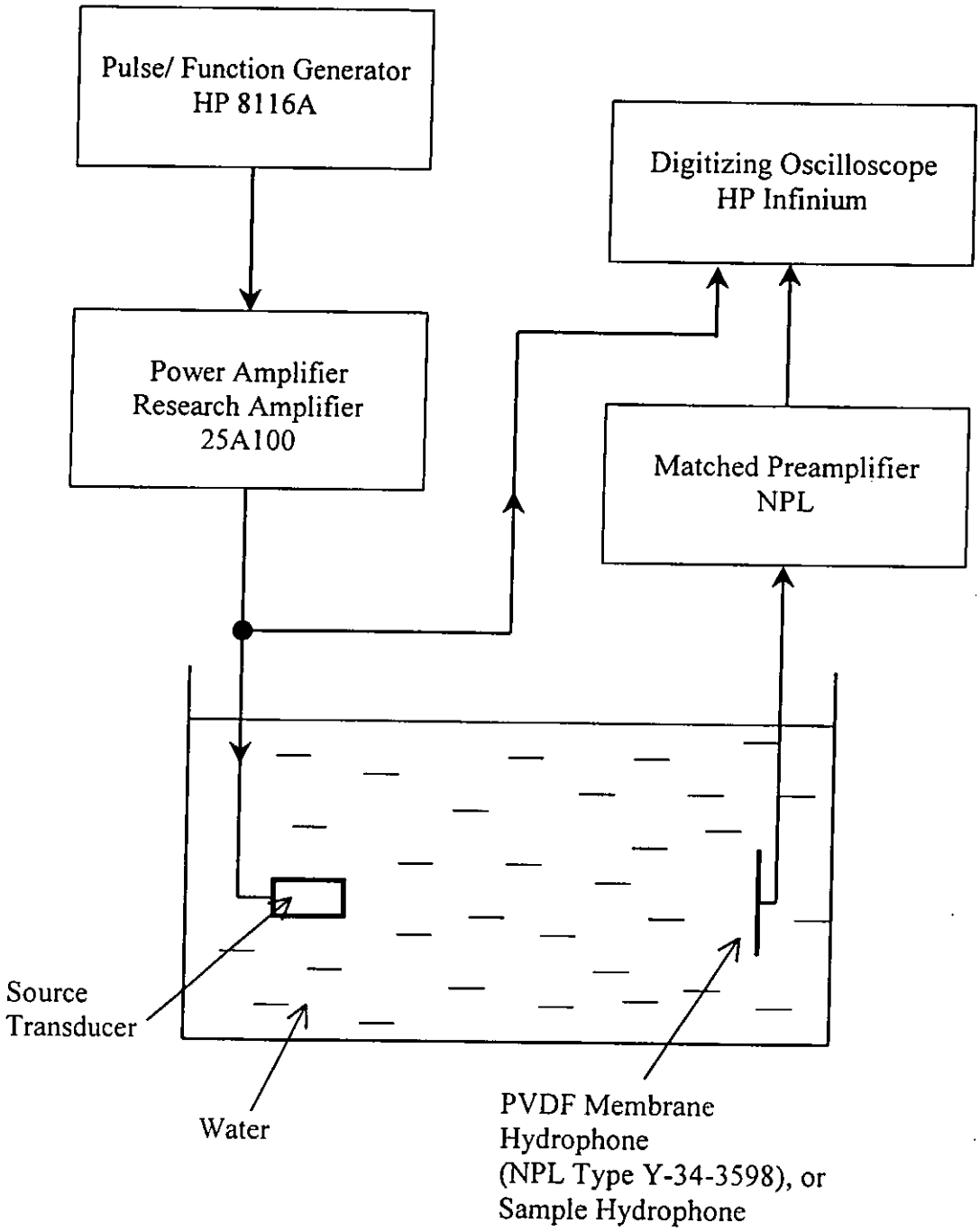

Figure 5.1 Schematic diagram of the setup for measuring receiving sensitivity of a hydrophone.

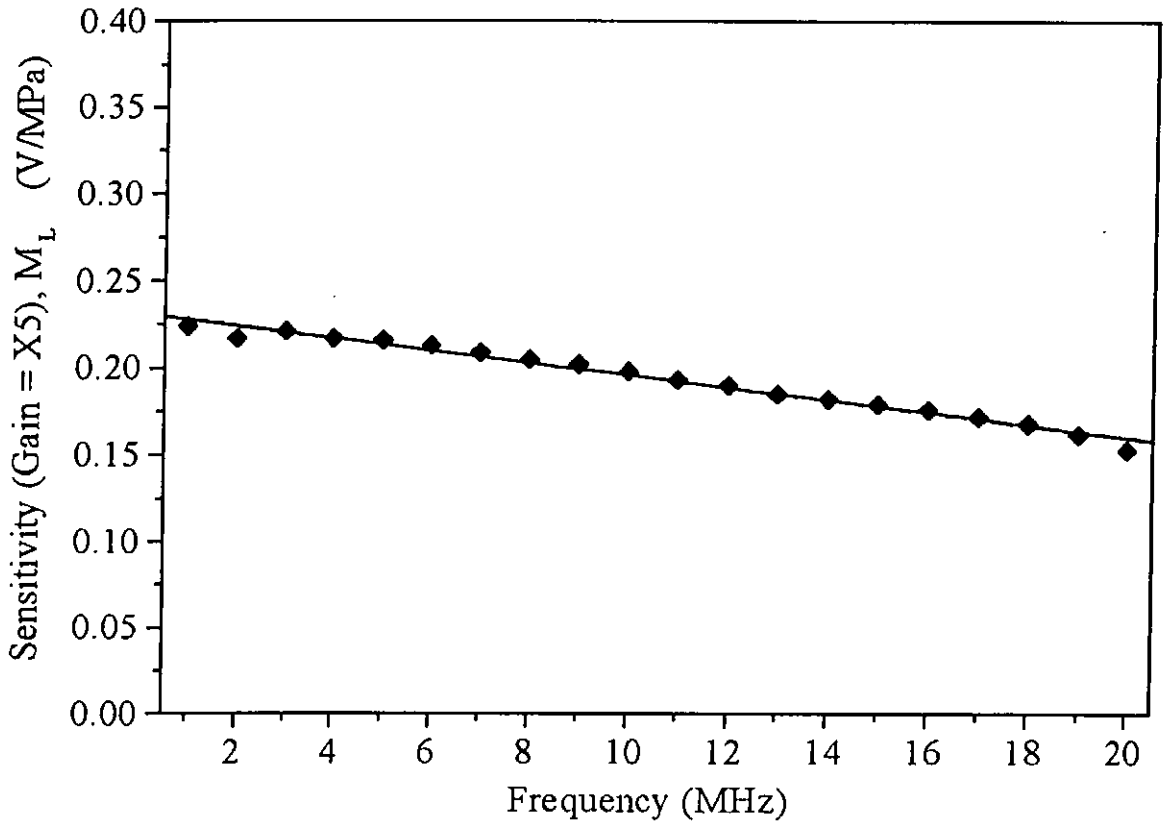

Figure 5.2 The calibration curve for the end-of-cable loaded sensitivity with gain = 5 of the PVDF membrane hydrophone (National Physical Laboratory, UK)

5.2.2 Angular Response Measurement

The experimental setup is similar to the setup for measuring the receiving sensitivity (Figure 5.1). The plane transducer was driven to generate a short burst of ultrasonic wave at the center frequency of the transducer. Four plane transducers (Panametrics) of frequencies 2.25, 5, 7.5 and 10 MHz were used. The hydrophone was located in the far field region of the acoustic waves and aligned for maximum output voltage by translating it normal to the acoustical axis. To measure the angular response, the hydrophone was rotated about a diametrical axis of the sensing element of the hydrophone (Figure 5.3). The output voltage of the hydrophone was measured as a function of angular position of the hydrophone (i.e. incident angle of the acoustic wave).

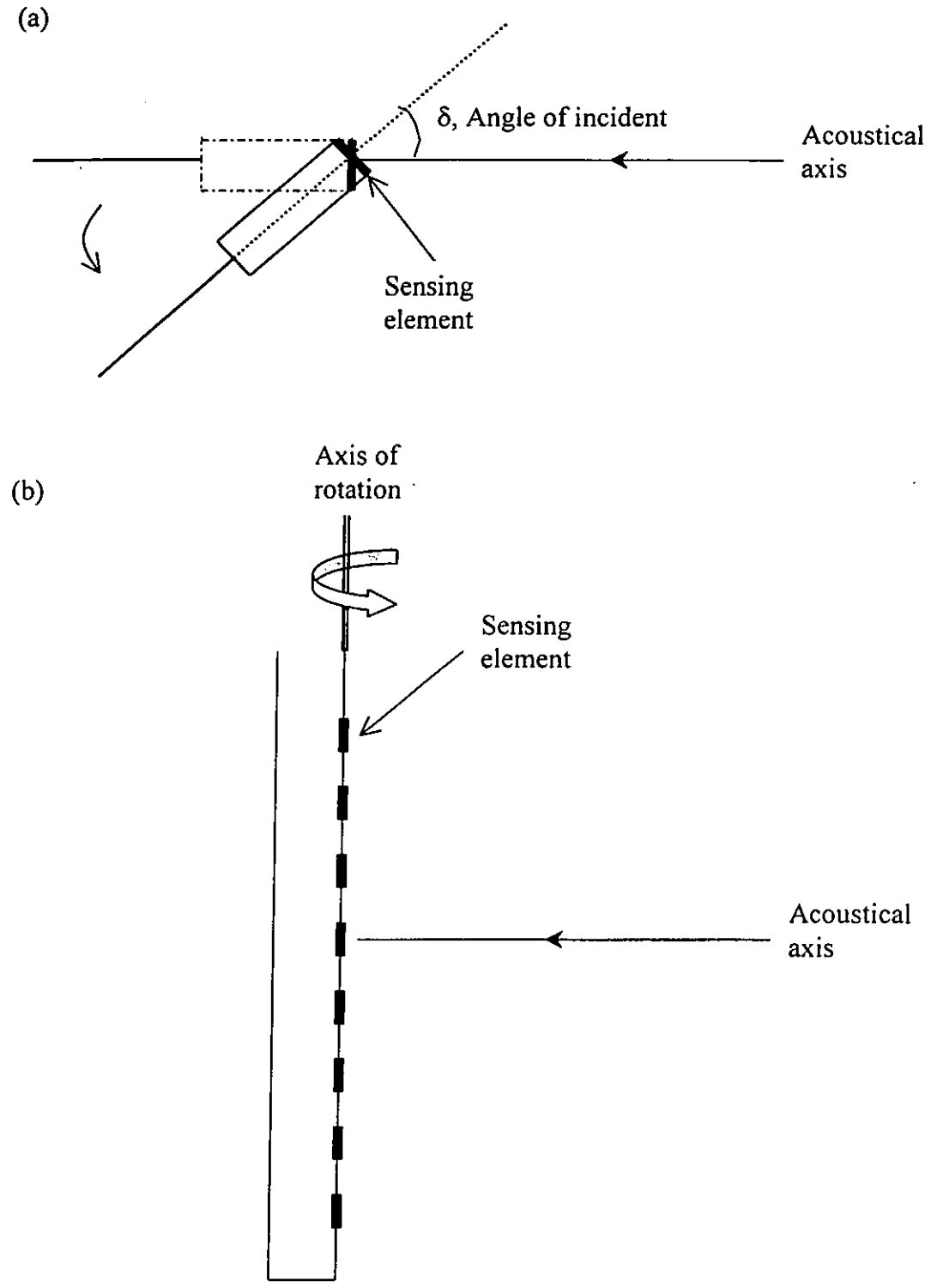

Figure 5.3 Schematic diagrams for measuring the angular response of (a) needle-type hydrophone and (b) hydrophone array.

5.3 Results and Discussion

5.3.1 Receiving Sensitivity of Hydrophones

The end-of-cable capacitance of the three needle-type hydrophones C_h was measured at room temperature in the frequency range of 2 to 8 MHz using an impedance analyzer (HP 4194A). As shown in Figure 5.4, the capacitances of the three hydrophones decrease slightly with the frequency. The composite hydrophone with only the ceramic phase poled (sample A) has the highest capacitance. After two phases poled in opposite directions, the capacitance of the composite hydrophone (sample C) decreases. It is because the permittivity of the copolymer phase decreases after dipole alignment.

The receiving waveforms of the needle-type hydrophones to a tone burst at 5 MHz are shown in Figure 5.5. The three hydrophones provide undistorted voltage waveform, indicating good temporal resolution of the hydrophone. Since the acoustic impedance of the copper wire is much larger than that of the sensing materials, ringdowns are observed in the waveforms. As compared with the copolymer hydrophone (sample E), the two composite hydrophones (sample A and C) have slightly shorter ringdown, reflecting that the composite is stiffer than the copolymer.

The end-of-cable loaded sensitivity (with the amplifier) of the needle-type hydrophones M_a was measured using the comparison method. Using equations 5.6

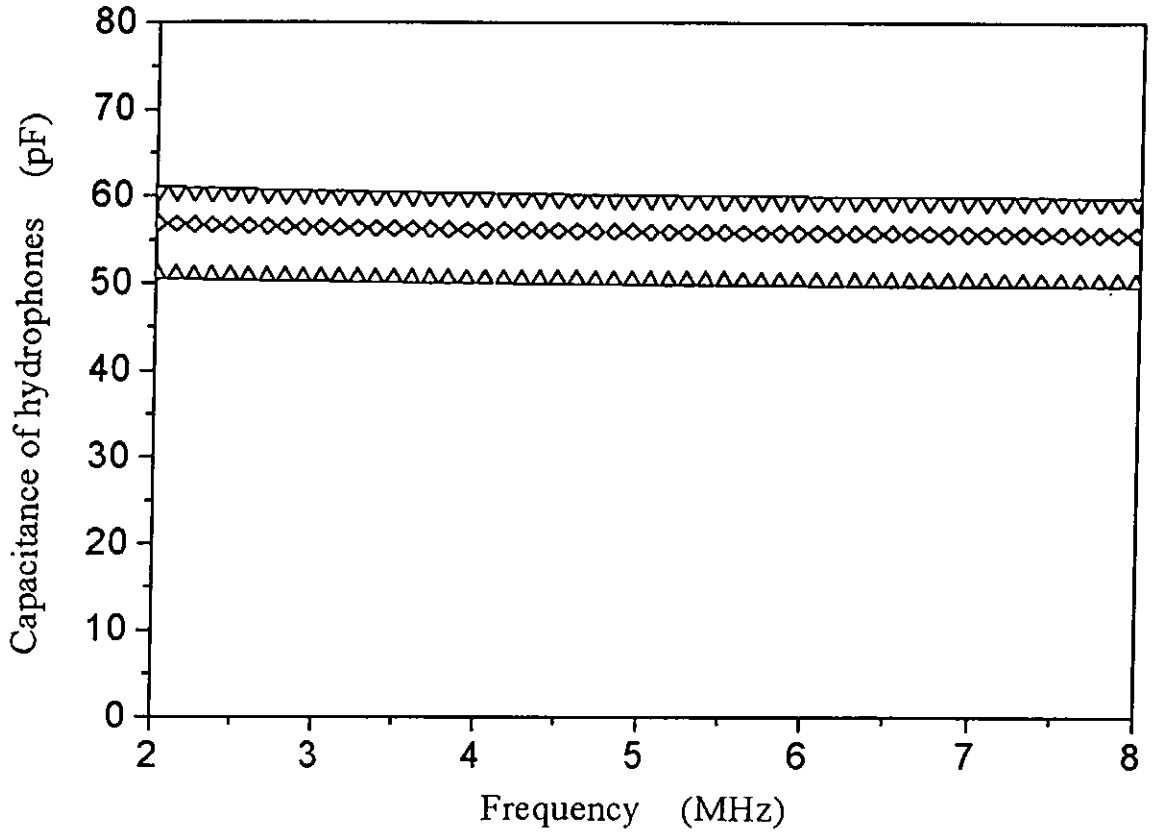

Figure 5.4 End-of-cable capacitance of the needle-type hydrophones with different sensing elements as a function of frequency: PT/P(VDF-TrFE) composite with only the ceramic phase poled, ▽; PT/P(VDF-TrFE) composite with two phases poled in opposite directions, ◇; and P(VDF-TrFE), △.

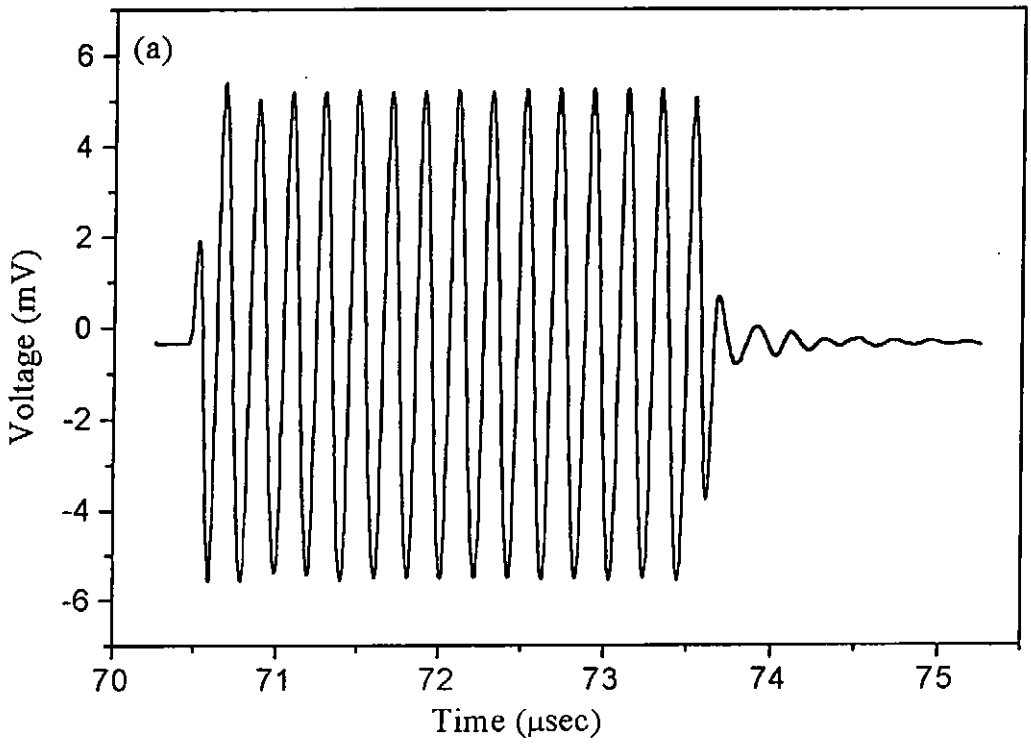

Figure 5.5 Receiving waveforms of the needle-type hyrophones with different sensing elements to a tone burst at 5 MHz: (a) PT/P(VDF-TrFE) composite with only the ceramic phase poled, (b) PT/P(VDF-TrFE) composite with two phases poled in opposite directions; and (c) P(VDF-TrFE).

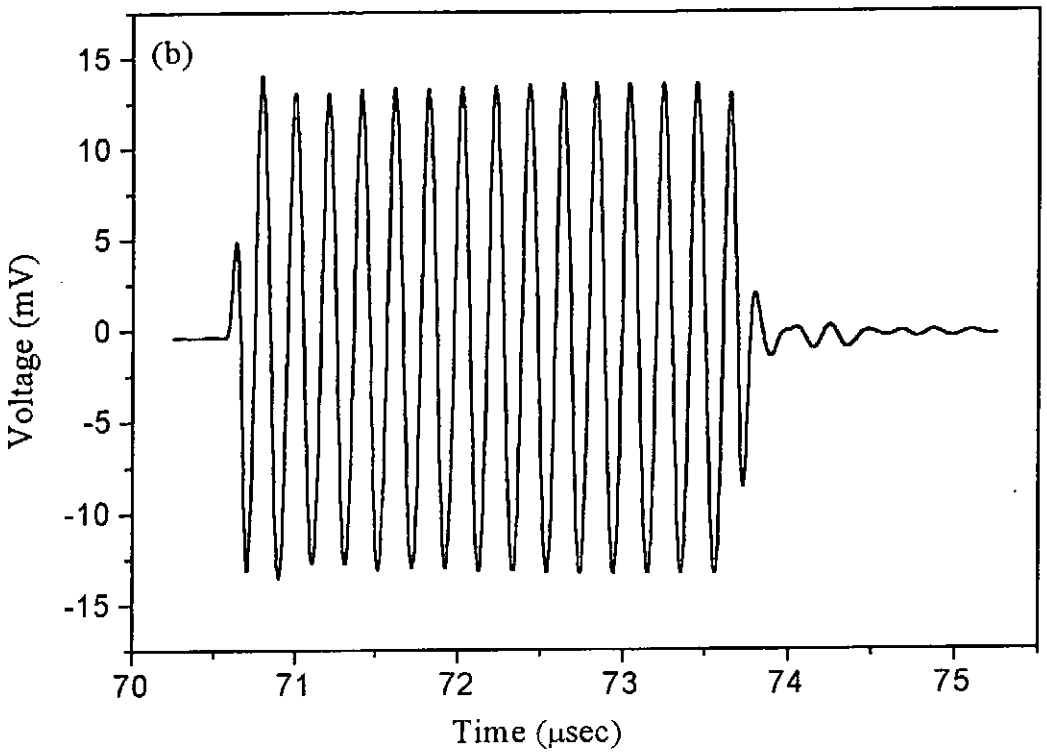

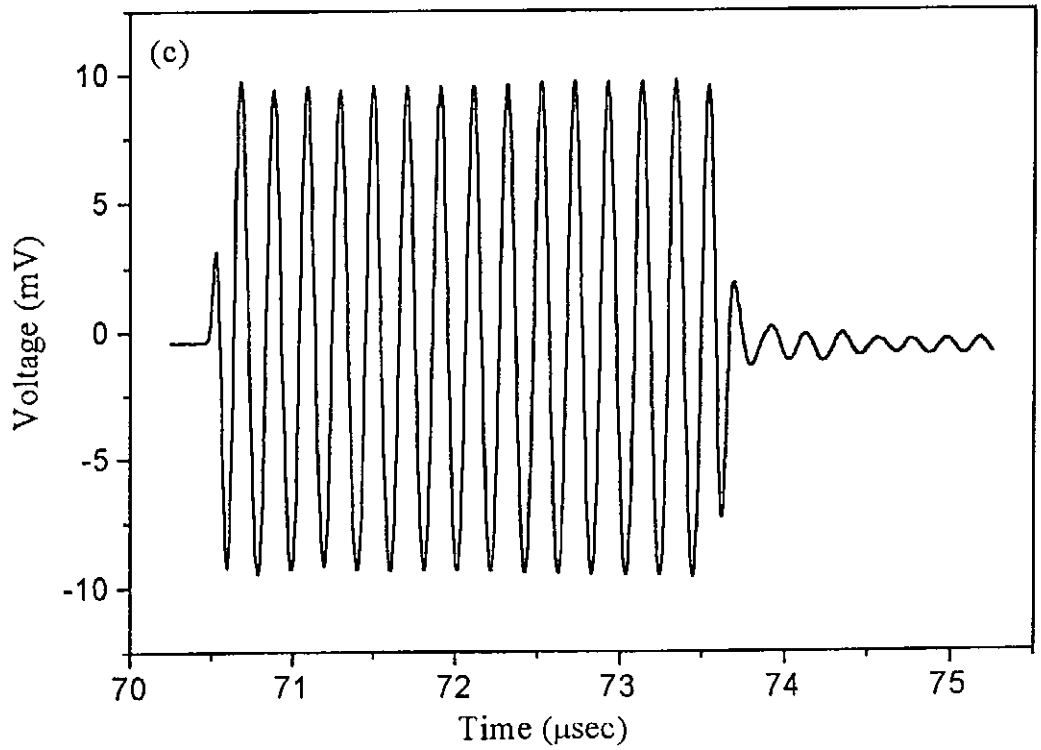

Figure 5.5 (Continued)

and 5.8, the end-of-cable open-circuit sensitivity of the needle-type hydrophones M_o was determined. As shown in Figure 5.6, the frequency response of the three hydrophones is varied within ± 1.4 dB in the frequency range of 2 to 8 MHz, which satisfy the requirement established by the AIUM/NEMA (i.e. ± 1.5 dB in the same frequency range). Among the three hydrophones, the composite with only the ceramic phase poled has the lowest sensitivity. It is because its longitudinal piezoelectric coefficient d_{33} is low. For the composite with two phases poled in opposite directions, its d_{33} value is about 1.9 times larger than that of the composite with only the ceramic phase poled. Referring to Figure 5.6, the sensitivity of the composite hydrophone with two phases poled in opposite directions is about 2.2 times larger than that of the composite hydrophone with only the ceramic phase poled. As compared with the copolymer, the d_{33} value of the composite with two phases poled in opposite directions is 30 % larger. The sensitivity of the corresponding hydrophone is 40 % larger than that of the copolymer hydrophone. It can be seen that the sensitivity of the hydrophone is approximately proportional to the piezoelectric coefficient d_{33} of the sensing element. In principle, for a piezoelectric sensor working in thickness mode, the open-circuit voltage sensitivity of the sensor M_{oc} is given by [Dario *et al.*, 1984]:

$$|M_{oc}| = \frac{d_{33}t}{\varepsilon_{33}^{T}} \tag{5.9}$$

where d_{33} is the longitudinal piezoelectric coefficient of the sensing element , ε^{T}_{33} is the dielectric permittivity (measured at constant stress) of the element, and t is the

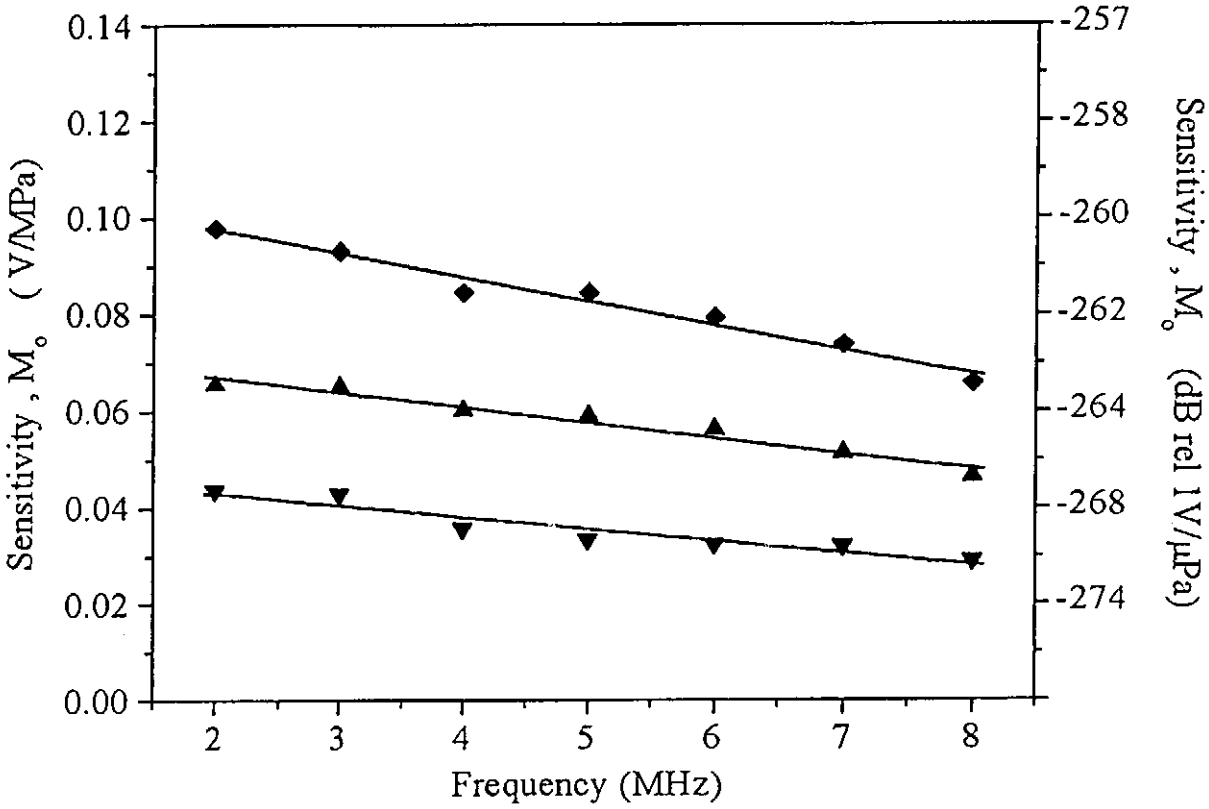

Figure 5.6 End-of-cable open-circuit sensitivities M_o of the hydrophones with different sensing elements as a function of frequency: PT/P(VDF-TrFE) composite with only the ceramic phase poled, ▼; PT/P(VDF-TrFE) composite with two phases poled in opposite directions, ◆; and (c) P(VDF-TrFE), ▲.

thickness of the element. The sensitivity of the sensor is linearly dependent on the piezoelectric coefficient d_{33} of the sensing element. The experimental results agree quite well with the theoretical expectation.

In practice, the sensing element is fabricated into a hydrophone containing a mounting (stainless steel tube with epoxy) and a coaxial cable (Figure 5.7). The simplified equivalent electrical circuit for the hydrophone is shown in Figure 5.8. The capacitance of the element C_f is loaded by the capacitance of the mounting C_e and the capacitance of the coaxial cable C_c. The end-of-cable open-circuit sensitivity of the hydrophone M_o is related to the open-circuit sensitivity of the element M_{oc} as [Chivers and Lewin, 1982]:

$$M_o = \frac{C_f}{C_h} M_{oc} \tag{5.10}$$

where $C_h = C_f + C_e + C_c$ is the end-of-cable capacitance of the hydrophone. Since the area of the sensing element is quite small, the capacitance of the element C_f is much smaller than that of the loading ($C_e + C_c$), so the sensitivity of the hydrophone M_o is greatly affected by the capacitance of the loading. Therefore, in comparing the sensitivity of the hydrophone, the loading of the hydrophone should be considered. Table 5.1 shows the capacitances at 5 MHz of the hydrophones, the sensing elements and the loading. The capacitances of the loading of the three hydrophones are very close (about 50 pF), so the reduction of the voltage at the end-of-cable for the three hydrophones are similar.

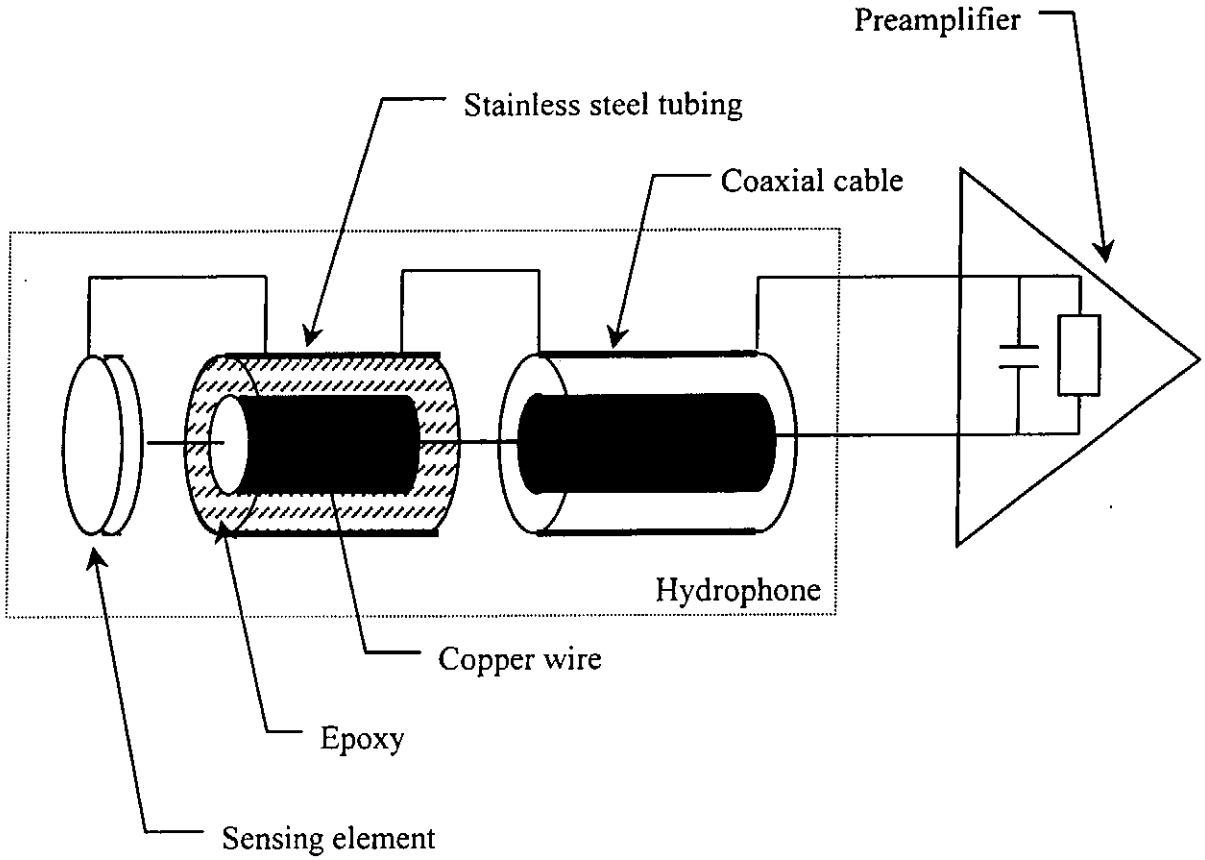

Figure 5.7 Schematic diagram of a needle-type hydrophone.

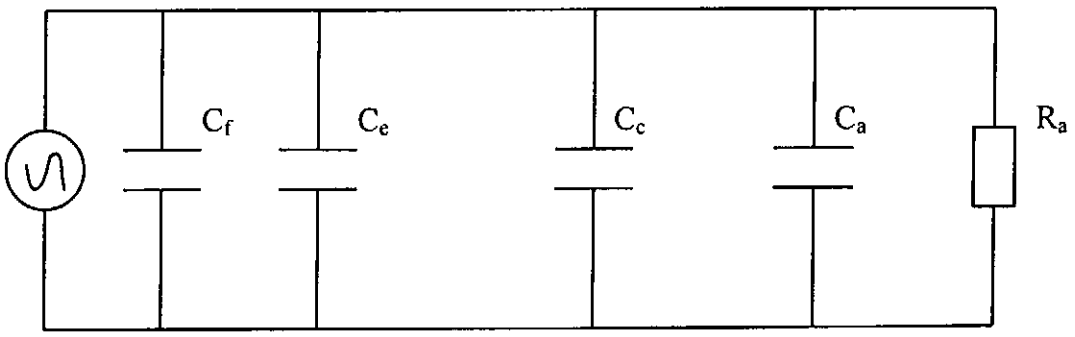

Figure 5.8 Simplified equivalent electrical circuit of a needle-type hydrophone.

Table 5.1 The capacitances at 5 MHz of the hydrophones, the sensing elements and the loading.

Hydrophone	Capacitance of the hydrophone (pF)	Capacitance of the sensing element (pF)	Capacitance of the loading (pF)
PT/P(VDF-TrFE) 0-3 composite with only the ceramic phase poled	59.9	5.6	54.3
PT/P(VDF-TrFE) 0-3 composite with two phases poled in opposite directions	56.3	4.5	51.8
P(VDF-TrFE) copolymer	51.3	3.0	48.3

For the hydrophone array, the end-of-cable capacitance of the array elements as a function of frequency is shown in Figure 5.9. The end-of-cable capacitances of the eight elements are almost the same (about 20 pF). Figure 5.10 shows the receiving waveforms of the array element 4 to a tone burst at 5 MHz. Similar waveforms are observed for the other elements. The undistorted waveform indicates good temporal resolution of the array. Due to the acoustic impedance mismatch between the copper wire and the sensing element, ringdowns are observed in the waveform.

In the hydrophone array, it is important to investigate the effect of the inter-element coupling. At first, the receiving sensitivity of the individual element was

measured with short-circuit of the other elements, so the electrical pick-up from the adjacent array elements was eliminated. Secondly, the receiving sensitivity of the individual element was re-measured without short-circuit of the other elements. Figure 5.11 shows the end-of-cable open-circuit sensitivity of the array element 4 with and without short-circuit of the other elements. The sensitivities of the element differ slightly in two cases, indicating that the inter-element coupling is not significant. Similar results are observed for the other elements. The end-of-cable open- circuit sensitivity of the eight elements (measured with short-circuit of the other elements) is shown in Figure 5.12. The frequency responses of all the elements are flat within ± 1.5 dB in the frequency range of 2 to 8 MHz. Besides, the difference in the sensitivities amongst the eight elements is about 7 %. As compared with the needle-type hydrophone with the same sensing material, the sensitivity of the array is 2.7 times larger. According to equation 5.10, the sensitivity of the hydrophone is inversely proportional to its end-of-cable capacitance. Comparing the end-of-cable capacitances of the array and the needle-type hydrophone, the array is 2.6 times smaller (Figure 5.4 and 5.9). This indicates that the difference in the sensitivity between the array and the needle-type hydrophone mainly arises from the difference in their end-of-cable capacitances.

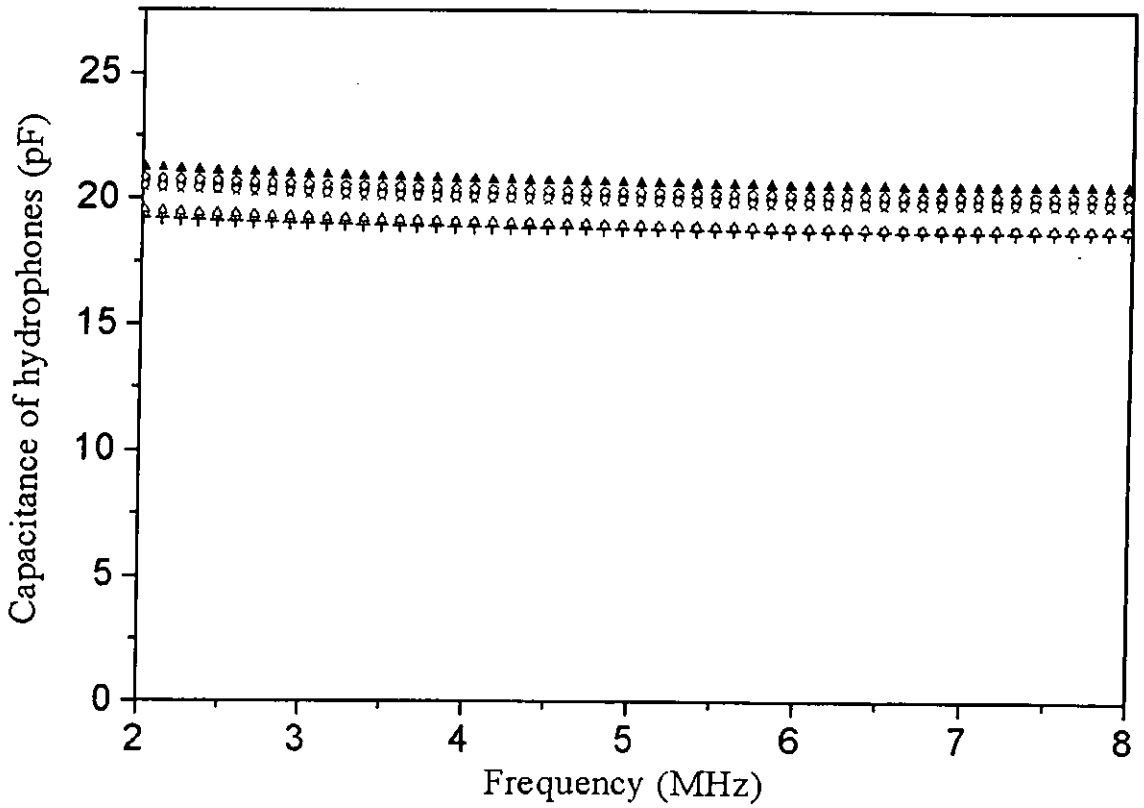

Figure 5.9 End-of-cable capacitance of the array elements as a function of frequency (element 1, □; element 2, ×; element 3,+; element 4,▽; element 5,○; element 6,▲; element 7,△ and element 8, ◇).

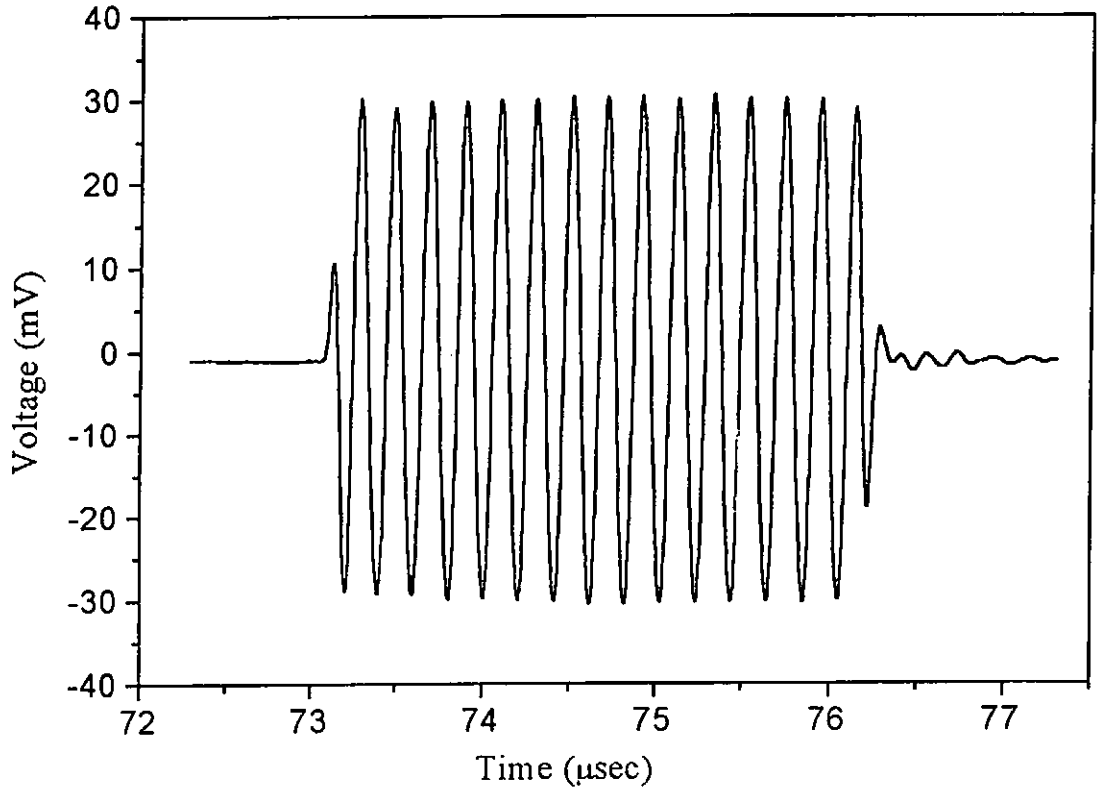

Figure 5.10 Receiving waveform of the array element 4 to a tone burst at 5 MHz.

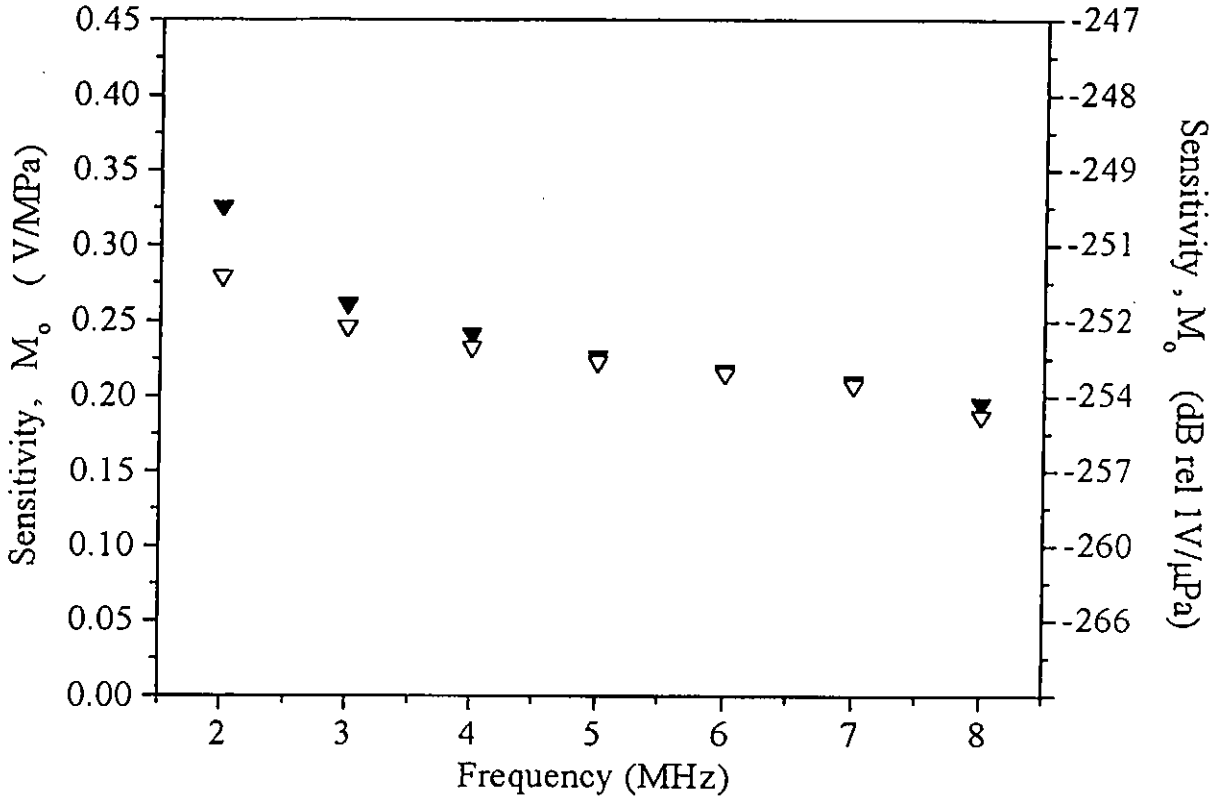

Figure 5.11 End-of-cable open-circuit sensitivity M_o of the array element 4 as a function of frequency (open: with short-circuit of other elements; solid: without short-circuit of other elements).

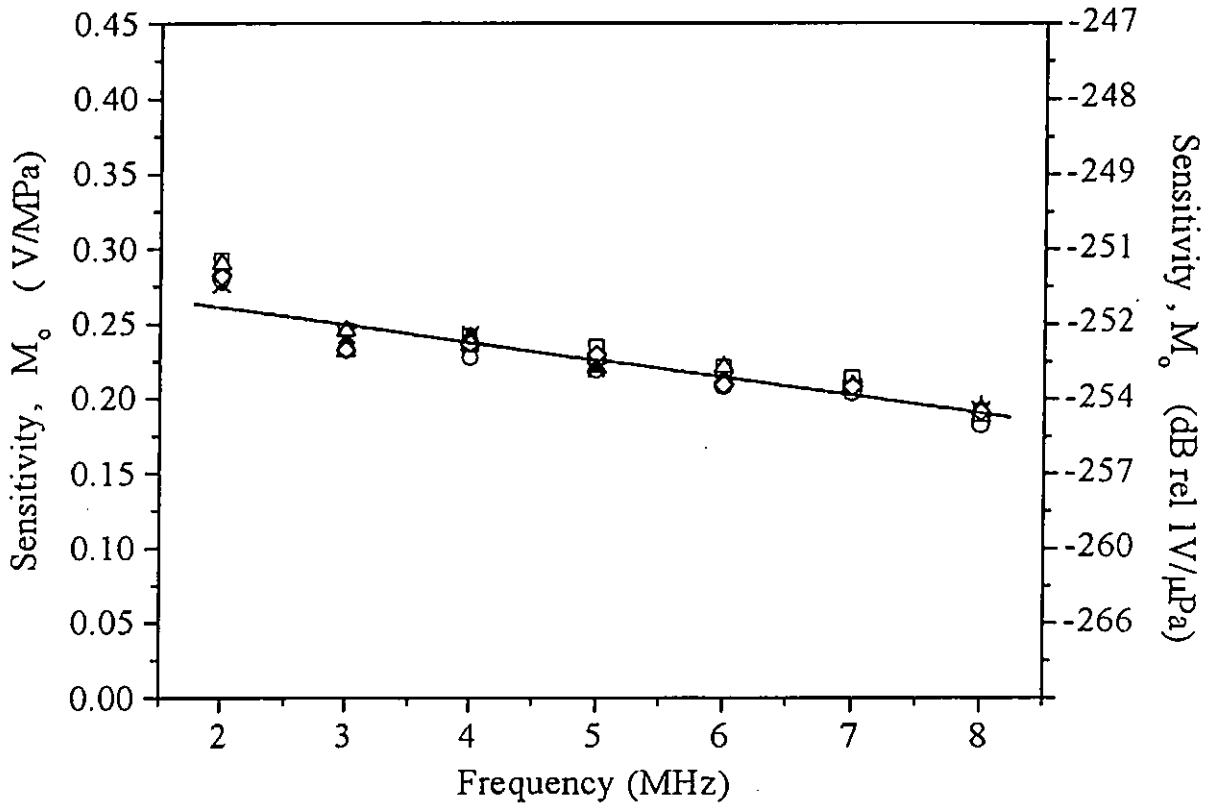

Figure 5.12 End-of-cable open-circuit sensitivities M_o of the eight elements as a function of frequency (element 1, □; element 2, ×; element 3,+; element 4,▽; element 5,○; element 6,▲; element 7,△ and element 8, ◇).

5.3.2 Angular Response of Hydrophones

The angular response of three different types of the needle-type hydrophones at 5 MHz was measured. As shown in Figure 5.13, the response curves for the three hydrophones consist of a main lobe and symmetrical side lobes. The widths of the main lobe of the three hydrophones are similar but the amplitudes of the side lobe are slightly different. In the fabrication process, the whole sensing element may be not tightly attached on the copper, so the receiving response of the sensing element is not uniform over its surface. As a result, when the incident angle of the acoustic pressure wave is large, the receiving response of different hydrophones may vary from each other. The measured responses of the three hydrophones agree well with the theoretical predictions. Since the predicted values from the three models are very close, it is difficult to decide which model is appropriate for the hydrophone.

The variation of the angular response of the needle-type hydrophone with the frequency was investigated. Figure 5.14 shows the angular response of the composite hydrophone with two phases poled in opposite directions at different frequencies. It can be seen that the main lobe becomes narrower and the number of the side lobe increases as the frequency increases. At 2.25 MHz, there is significant different between the predictions from the three models. The measured response of the hydrophone agrees well with the predicted values from the unbaffled piston model, reflecting that the hydrophone behaves more likely as a piston in a free space. As the frequency increases, the predicted values from the three models get closer. The

measured responses of the hydrophone also have good agreement with the predicted angular responses at higher frequencies.

The angular response of the hydrophone array at frequencies of 2.25, 5 and 10 MHz was measured. The response curves of the array element 4 at different frequencies are shown in Figure 5.15, which are similar to those of the needle type hydrophone with the same sensing material. At 2.25 and 5 MHz, the angular responses of the array agree closely to the predicted values from the unbaffled piston model. The -3 dB and -6 dB angular response angles at which the received voltage decreased to 71 % (-3 dB) and 50 % (-6 dB) of the maximum received voltage, respectively, were measured for the eight elements and given in Table 5.2. It can be seen that the measured angles for the eight elements are almost the same, confirming that the angular responses of all the elements are similar.

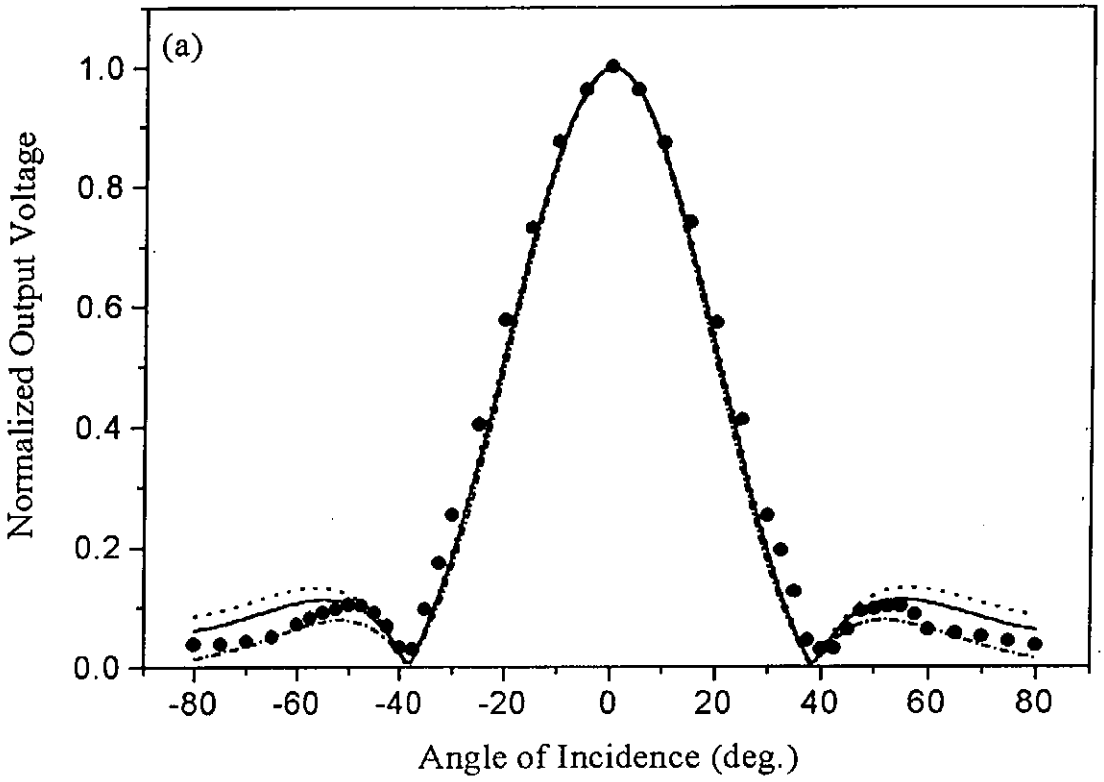

Figure 5.13 Angular response of the needle-type hydrophones with different sensing elements at 5 MHz: (a) PT/P(VDF-TrFE) composite with only the ceramic phase poled, (b) PT/P(VDF-TrFE) composite with two phases poled in opposite directions and (c) P(VDF-TrFE).

Theoretical values:

- - - - - : Rigid baffle model

——— : Unbaffled piston model

—.— : Soft baffle model

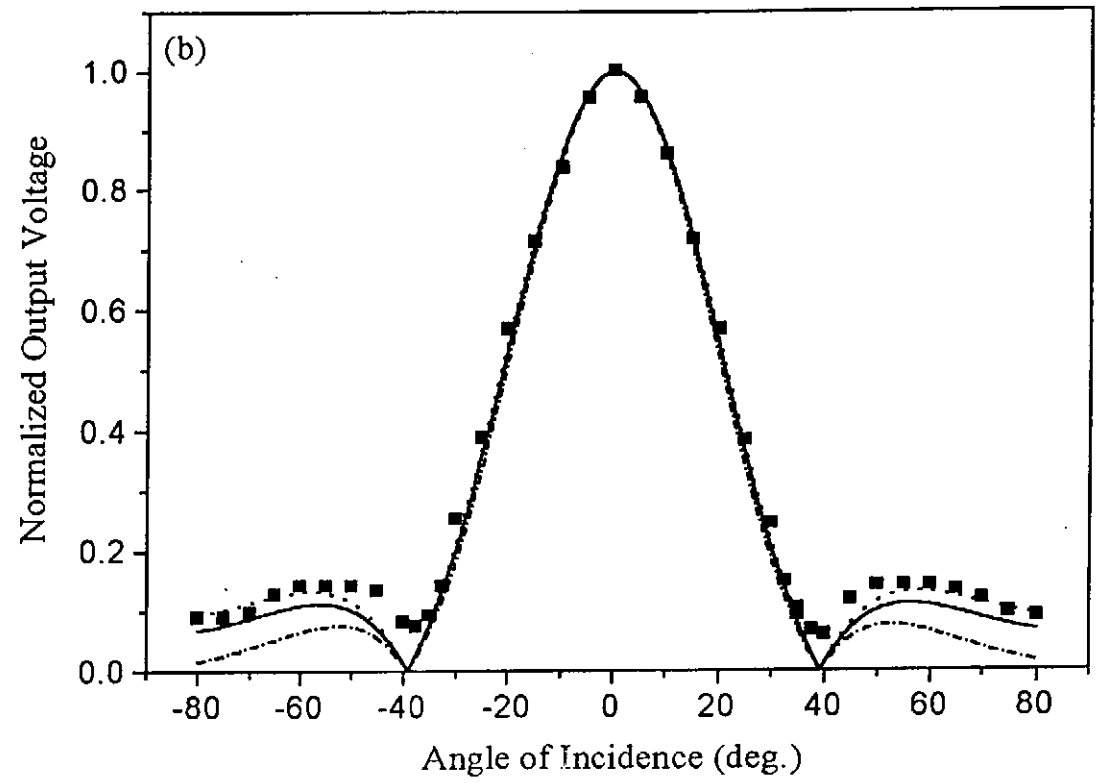

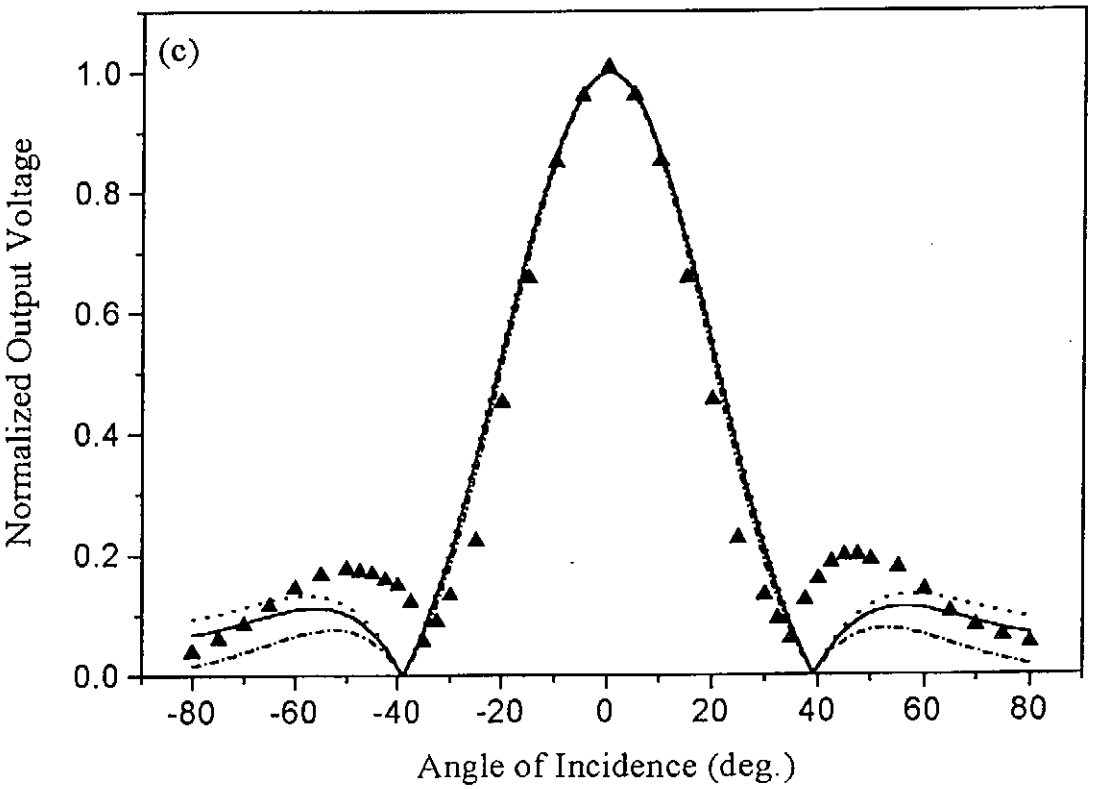

Figure 5.13 (Continued)

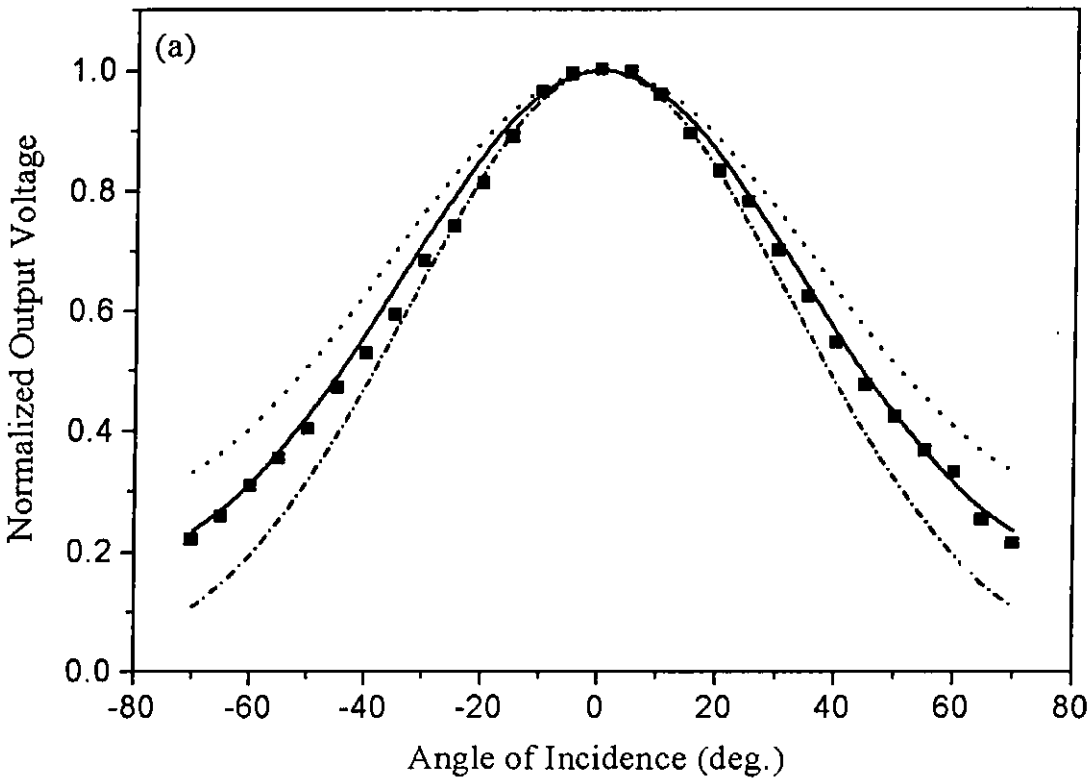

Figure 5.14 Angular response of the composite needle-type hydrophone with two phases poled in opposite directions at (a) 2.25, (b) 7.5 and (c) 10 MHz.

Theoretical values:

· · · · · : Rigid baffle model

——— : Unbaffled piston model

—·— : Soft baffle model

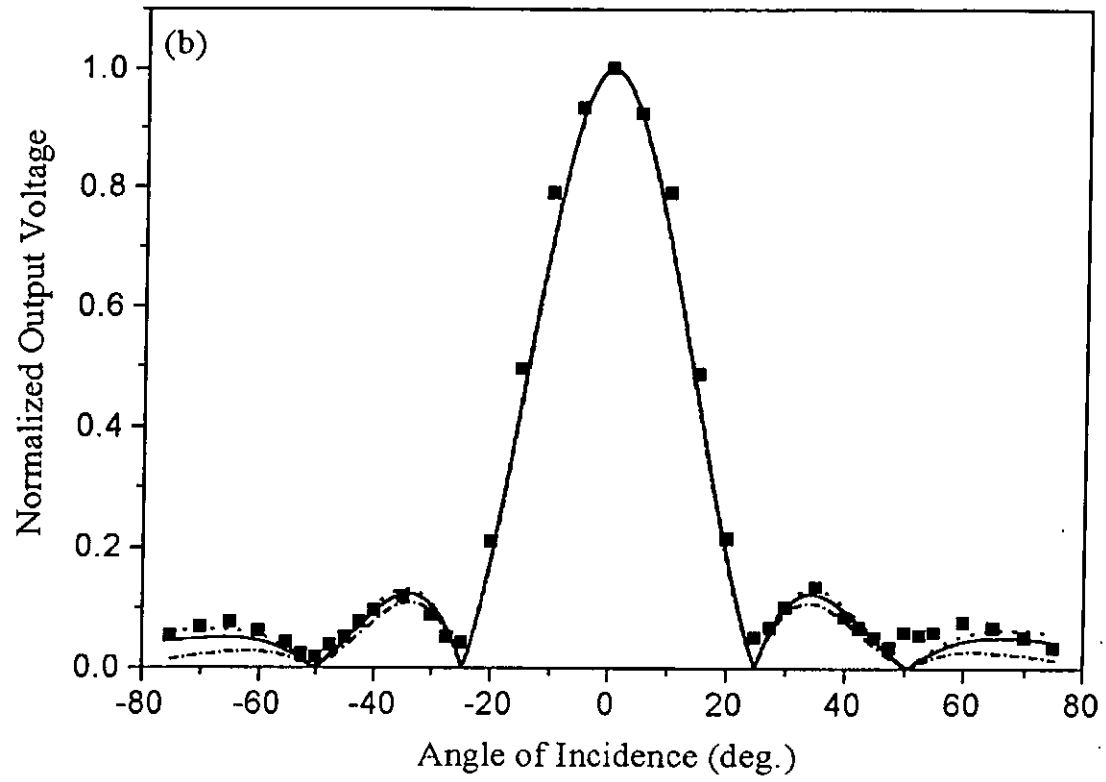

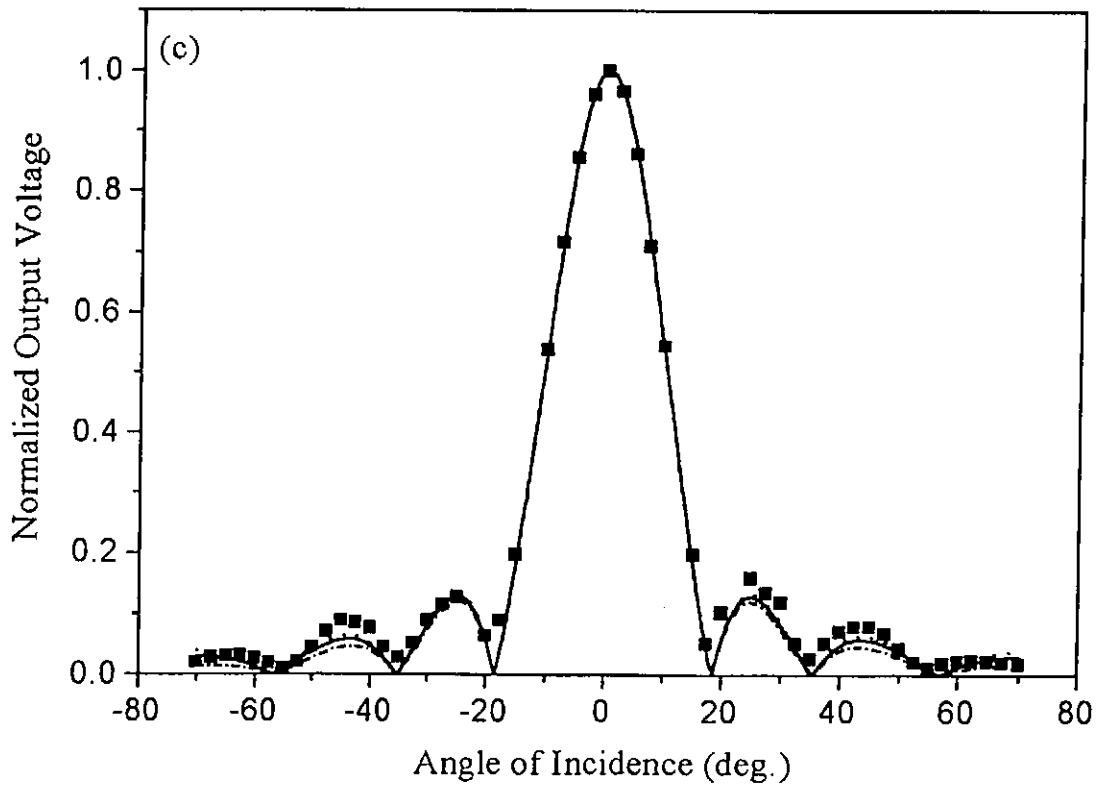

Figure 5.14 (Continued)

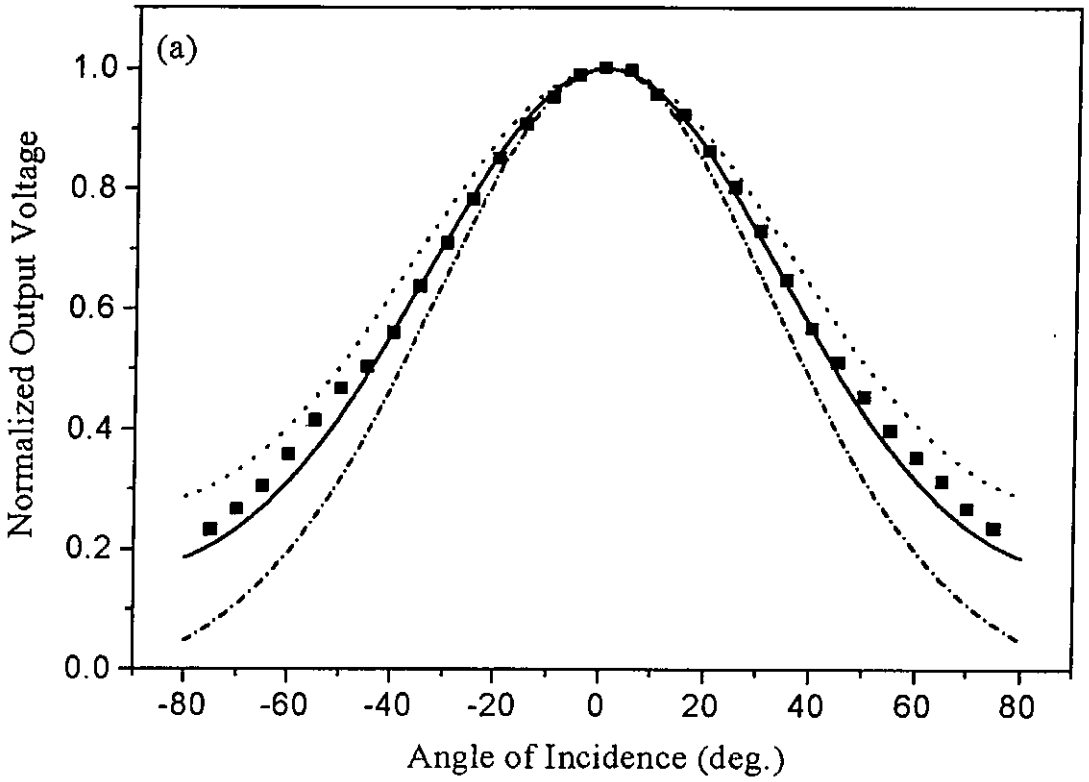

Figure 5.15 Angular response of the array element 4 at (a) 2.25, (b) 5 and (c) 10 MHz.

Theoretical values:

· · · · · : Rigid baffle model

——— : Unbaffled piston model

—·— : Soft baffle model

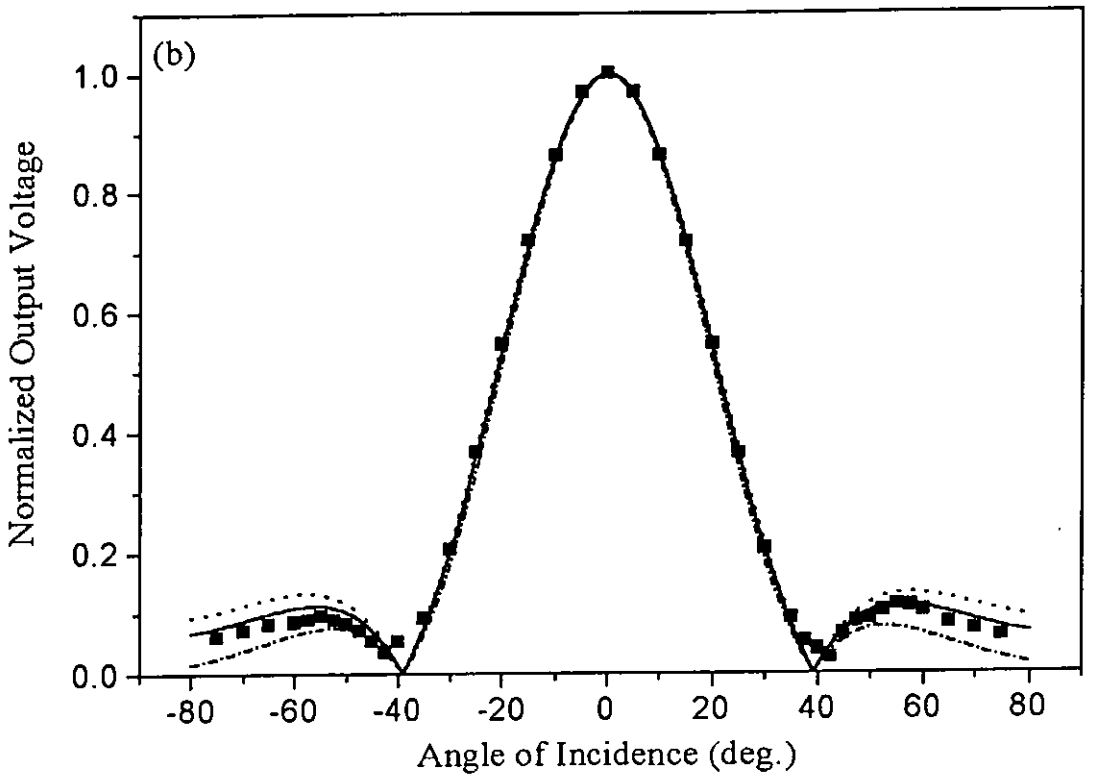

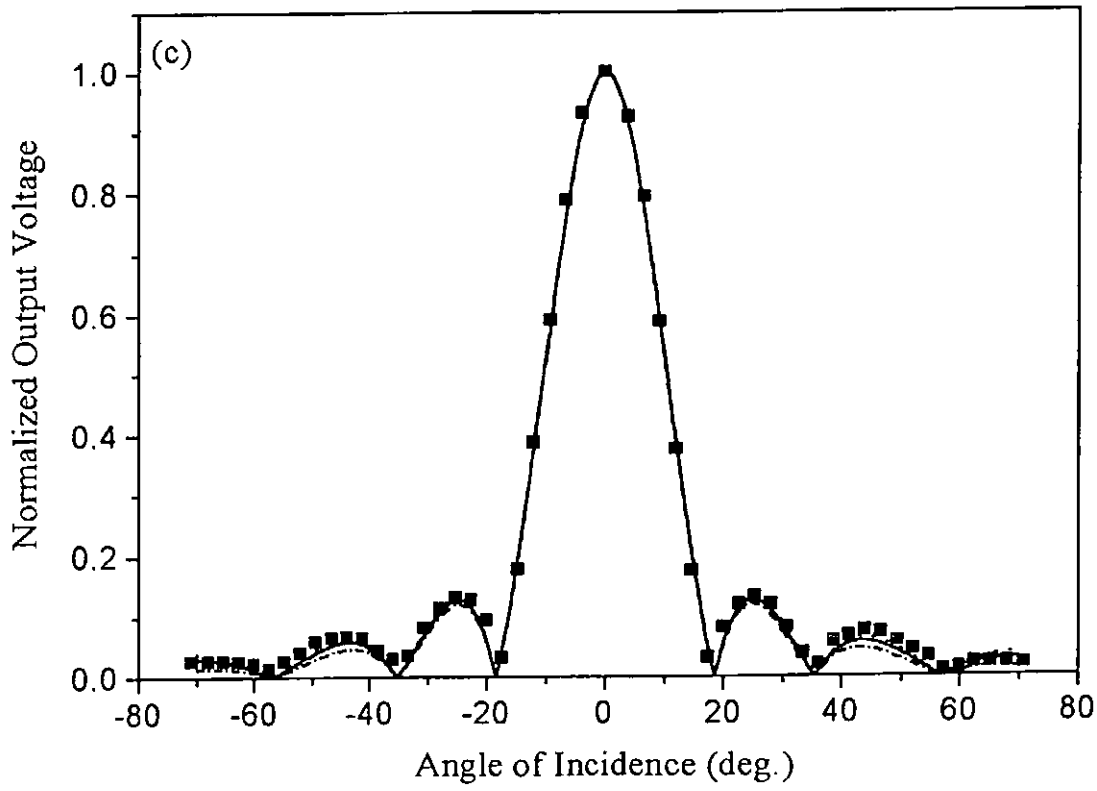

Figure 5.15 (Continued)

Table 5.2 The -3 dB and -6 dB angular response angles for the eight elements at 5 MHz.

Element	-3 dB response angle (deg.)	-6 dB response angle (deg.)
1	15.5	21.9
2	15.2	22.4
3	15.9	22.2
4	15.6	21.7
5	15.9	22.1
6	15.4	21.9
7	15.0	21.5
8	15.6	21.7

5.4 Summary

In this Chapter, needle-type hydrophones with three different materials as sensing element have been characterized: (a) PT/P(VDF-TrFE) 0-3 composite with only the ceramic phase poled, (b) PT/P(VDF-TrFE) 0-3 composite with two phases poled in opposite directions and (c) P(VDF-TrFE) copolymer. Besides, the performance of a 8-element hydrophone array using PT/P(VDF-TrFE) 0-3 composite with two phases poled in opposite directions as the sensing element has been evaluated.

The three needle-type hydrophones have good temporal resolution and flat frequency response in the frequency range of 2 and 8 MHz. By comparing the sensitivities of the three needle-type hydrophones, it is found that the sensitivity of the hydrophone is approximately proportional to the piezoelectric coefficient d_{33} of the sensing element. Such observation quite agrees with the theoretical expectation. The composite hydrophone with two phases poled in opposite directions has the highest sensitivity as it has the highest d_{33} value. As compared with the copolymer hydrophone, the sensitivity of composite hydrophone with two phases poled in opposite directions is 40 % larger.

For the hydrophone array, all the elements show good temporal resolution. The inter-element coupling in the array is not significant. The sensitivities of the eight elements are almost the same, with variations of ± 1.5 dB in the frequency

range of 2 and 8 MHz. As compared with the needle-type hydrophone with the same sensing element, the sensitivity of the array is about 2.7 times larger due to the smaller loading capacitance.

On the other hand, the angular responses of the needle-type hydrophones and the 8-element hydrophone array have been studied. The measured responses of the three needle-type hydrophones are similar. The agreement between the measured and the predicted values is good. At or above 5 MHz, the angular responses predicted by all the three models are very close. However, at lower frequency (i.e. 2.25 MHz), the difference between the three models is significant. It is found that the unbaffled piston model predicts the response more accurately than the piston in rigid or soft baffle model. The angular responses of the hydrophone array are similar to that of the needle type hydrophone. Good agreement is obtained between the measured and the predicted responses for the hydrophone array.

Chapter Six

Conclusion

The main objectives of this work are to fabricate PT/P(VDF-TrFE) 0-3 composite films with high piezoelectric but low pyroelectric activities, and to use them for fabricating piezoelectric hydrophones.

PT ceramic powder prepared by the sol-gel method has been characterized. The powder annealed at 800 °C shows typical perovskite structure and has average crystallite size of 60 nm. The particle size of the powder is about 200 nm, which is sufficiently small for fabricating homogeneous 0-3 composite films with thickness as small as 5 μm.

The PT/P(VDF-TrFE) 0-3 composite films with about 0.2 ceramic volume fraction have been prepared using the spin-coating method. In order to induce the piezoelectric and pyroelectric responses of the individual phase, the 0-3 composite must undergo a poling process. A procedure for separate poling of the ceramic and the copolymer phases of the composite is established, so the two phases are poled either in opposite directions or in the same direction. The ceramic phase is first poled under a dc field at a temperature above the ferroelectric-to-paraelectric phase transition temperature of the copolymer. The copolymer phase is then poled under an ac field at

70 °C. As the final polarization direction of the copolymer phase is determined only by the electric field direction in the last half cycle of the ac field, the polarization directions of the two phases are controlled either in opposite directions or in the same directions.

To study the effects of poling procedure on the properties of the composite, composites of four different polarization states have been prepared: (a) only the ceramic phase poled, (b) only the copolymer phase poled, (c) two phases poled in opposite directions and (d) both phases poled in the same direction. The piezoelectric and pyroelectric coefficients of the composites were measured. The results show that the piezoelectric activity of the composite is enhanced when the two phases are poled in opposite directions, but the pyroelectric activity is reduced. As compared with the copolymer, its piezoelectric response is about 30 % larger. For the composite with two phases poled in the same directions, it has reinforced pyeoelectric activity and reduced piezoelectric activity. The pyroelectric response of this composite is 30 % larger than that of the copolymer. As the composite with two phases poled in opposite directions has the highest piezoelectric response, it is feasible to use it for constructing hydrophone with good receiving response.

Needle-type hydrophones with PT/P(VDF-TrFE) 0-3 composites and P(VDF-TrFE) copolymer as sensing elements have been fabricated and characterized. It is found that the sensitivity of the hydrophone is approximately proportional to the piezoelectric response of the sensing element. The composite hydrophone with two

phases poled in the opposite directions has the highest sensitivity. The angular responses of the composite and copolymer hydrophones are similar, which agree well with the theoretical predictions. At lower frequency (i.e. 2.25 MHz), the measured response of the composite hydrophone agrees more closely with the unbaffled piston model, indicating that the sensing element of the hydrophone behaves more likely as a piston in a free space.

On the other hand, an 8-element hydrophone array has also been fabricated using the composite with two phases poled in opposite directions as the sensing element. The performance of the array has been evaluated. The array has good temporal response and flat frequency response. The inter-element coupling in the hydrophone array is not significant, and the sensitivities of the eight elements are very close. Due to its smaller electrical loading, the array shows better sensitivity than the needle-type hydrophone with the same sensing material. Similar to the needle-type hydrophone, the angular response of the array agrees well with the theoretical values, and shows better agreement with the unbaffled piston model at 2.25 and 5 MHz. With the use of an 8-channel multiplexer, such hydrophone array will be useful to acquire more information in a much shorter time by measuring the output of each element in turn.

In conclusion, fabrication of PT/P(VDF-TrFE) 0-3 composites with two phases piezoelectrically active is feasible. By poling the two phases in opposite directions, the composites attain the highest piezoelectric response and reduced sensitivity to temperature fluctuation. Using this material, one can produce high

frequency ultrasonic hydrophone with better performance as compared to that fabricated from the pure P(VDF-TrFE) copolymer.

References

Abdullah M. J. and D. K. Das-Gupta, " Electrical Properties of Ceramic/Polymer Composite", *IEEE Trans. on Electical Insulation*, Vol. 25, No.3, pp. 605-610 (1990)

Acoustic Output Measurement Standard for Diagnostic Ultrasound Equipment, AIUM/NEMA, pp.20-21 (1998)

Aindow, J. D. and R. C. Chivers, " Amplitude and Phase Directionality Measurements on Piezoelectric Ceramic Hydrophone in the Low Megahertz Frequency Range", *Acoust. Lett.*, Vol. 5, pp. 144-150 (1982)

Banno, H. and K. Ogura, " Piezoelectric Properties at Polarization Reversal Process and Coercive Force of 0-3 Composite of Polymer and Ceramic Powder Mixture PZT and $PbTiO_3$", *Jpn. J. Appl. Phys.*, Vol. 30, No. 9B, pp. 2250-2252 (1991)

Berlincourt, D. and H. H. A. Krueger, "Domain Processes in Lead Titanate Zirconate and Barium Titanate Ceramics", *J. Appl. Phys.*, Vol. 30, No. 11, pp. 1804-1810 (1959)

Birks, L. S. and H. Friedman, " Particle Size Determination from X-ray Line Broadening", *J. Appl. Phys.*, Vol. 17, pp. 687-692 (1946)

Bloomfield, P. E. and S. Preis, " Piezoelectric and Dielectric Properties of Heat Treated and Polarized VF_2/ VF_3 Copolymer", *IEEE Trans. Electrical Instul.*, Vol. EI-21, No. 3, pp. 533-537 (1986)

Blum, J. B. and S. R. Gurkovich, " Sol-Gel Derived $PbTiO_3$", *J. Mater. Sci.*, Vol. 20, pp. 4479-4483 (1985)

Byer, R. L. and C. B. Roundy, " Pyroelectric Coefficient Direct Measurement Technique and Application to a NSEC Response Time Detector", *Ferroelectrics*, Vol. 3, pp. 333-338 (1972)

Calzada, M. L., R. Sirera, F. Carmona and B. Jimenez, " Investigation of a Diop-Based Sol-Gel Process for the Preparation of Lead Titanate Materials", *J. Am. Ceram.*, Vol. 78, pp. 1802-1808 (1995)

Chan, H. L. W., A. H. Ramelan, I. L. Guy and D. C. Price, " Piezoelectric Copolymer Hydrophone for Ultrasonic Field Characterization", *Rev. Sci Instrum.*, Vol. 62, No.1, pp. 203-207 (1991)

Chan, H. L. W., P. K. L. Ng , Y. Chen and C. L. Choy, " Permittivity and Electrical Conductivity of PZT/P(VDF-TrFE) 0-3 Composites", *Ferroelectrics*, Vol. 201, pp. 225-234 (1997)

Chan, H. L. W., W. K. Chan, Y. Zhang and C. L. Choy, " Pyroelectric and Piezoelectric Properties of Lead Titanate/ Polyvinylidene Fluoride-Trifluoroethylene 0-3 Composites", *IEEE Trans. on Dielectrics and Electrical Insulat.*, Vol. 5, No. 4, pp. 505-512 (1998)

Chen, Y., H. L. W. Chan and C. L. Choy, "Pyroelectric Properties of $PbTiO_3$/P(VDF-TrFE) 0-3 nanocomposite films", *Thin Solid Films*, Vol. 323, pp. 270-274 (1998a)

Chen, Y., H. L. W. Chan and C. L. Choy, "Nanocrystalline Lead Titanate and Lead Titanate/ Vinylidene Fluoride-Trifluoroethylene 0-3 Nanocomposites", *J. Am. Ceram. Soc.*, Vol. 81, pp. 1231-1236 (1998b)

Chilton, J. A., "Electroactive Composites", *GEC Review*, Vol. 6, No. 3, pp.156-164 (1991)

Chivers, R. C., L. Bosselaar and P. R. Filmore, " Effective Area to be Used in Diffraction Correction", *J. Acoust. Soc. Am.*, Vol. 68, pp. 80-85 (1980)

Chivers, R. C. and P.A. Lewin, " The Voltage Sensitivity of Miniature Piezoelectric Plastic Ultrasonic Probes", *Ultrasonics*, Vol. 20, pp. 279-281 (1982)

Coelho, R., *Fundamental Studies in Engineering 1: Physics of Dielectrics for the Engineer*, Elsevier Scientific Publishing Co., Amsterdam, Oxford, New York, pp. 88-91 (1979)

Colbert, J. R., R. C. Eggleton and A. J. Weidner, " Intensity Calibration of Pulsed Ultrasonic Beams", *Interaction of Ultrasound and Biological Tissues (Workshop Proceedings)*, US-DHEW Publication (FDA) 73-8008 BRH/DBE 73-1, US Government Printing Office, Washington, pp. 187-192 (1973)

Cui, C., R. H. Baughman, Z. Iqbal, T. R. Kazmar and D. K. Dahlstrom, " Improved Piezoelectric Ceramic/Polymer Composites for Hydrophone Applications", *Synthetic Metals*, Vol. 85, pp. 1391-1392 (1997)

Dario, P., D. De Rossi, R. Bedini, R. Francesconi and M. G. Trivella, " PVF_2 Catheter-tip Transducers for Pressure, Sound and Flow Measurements", *Ferroelectrics*, Vol. 60, pp. 149-162 (1984)

Das-Gupta D. K. and M. J. Abdullah, " Electroactive Properties of Polymer-Ceramic Composites", *Ferroelectrics*, Vol. 87, pp. 213-228 (1988)

Davis, G. T., M. G. Broadhurst, A. J. Lovinger and T. Furukawa, " Hysteresis in Copolymer of Vinylidene Fluoride and Trifluoroethylene", *Ferroelectrics*, Vol. 57, pp. 73-84 (1984)

Delannoy, B., H. Lasota, C. Bruneel, R. Torduet and E. Bridoux, " The Infinite Planar Baffles Problem in Acoustic Radiation and Its Experimental Verification", *J. Appl. Phys.*, Vol. 50, pp. 5189-5195 (1979)

Dias, C. and D. K. Das-Gupta, " Polymer/Ceramic Composite for Piezoelectric Sensors", *Sensors and Actuators A*, Vol. 37, pp. 343-347 (1993)

Dias, C. J. and D. K. Das-Gupta, "Piezo- and Pyroelectricity in Ferroelectric Ceramic-Polymer Composites" In D. K. Das-Gupta, ed., *Ferroelectric Polymers and Ceramic/Polymer Composite*, Tran Tech Publications Ltd., Switzerland, pp. 217-249 (1994)

Dias, C., M. Simon, R. Quad and D. K. Das-Gupta, "Measurement of the Pyroelectric Coefficient in Composites Using a Temperature-modulated Excitation", *J. Phys. D: Appl. Phys.*, Vol. 26, pp. 106-110 (1993)

Furukawa, T., G. E. Johnson, H. E. Bair, Y. Tajitsu, A. Chiba and E. Fukada, "Ferroelectric Phase Transition in a Copolymer of Vinylidene Fluoride and Trifluoroethylene", *Ferroelectrics*, Vol. 32, pp. 61-67 (1981)

Furukawa, T., J. X. Wen, S. K. Y. Takashina and M. Date, "Piezoelectricity and Pyroelectricity in Vinylidene Fluoride/ Trifluoroethylene Copolymers, *J. Appl. Phys.*, Vol. 56, pp. 829-834 (1984)

Furukawa, T., K. Suzuki and M. date, " Switching Process in Composite Systems of PZT Ceramics and Polymers", *Ferroelectrics*, Vol. 68, pp. 33-44 (1986)

Galbraith, W. and G. Hayward, " Development of a PVDF Membrane Hydrophone for Use in Air-Coupled Ultrasonic Transducer Calibration", *IEEE Trans. Ultrasonics, Ferroelectrics and Frequency Control*, Vol. 45, No. 6, pp. 1549-1558. (1998)

Garn, E. and J. Sharp, "Use of Low-frequency Sinusoidal Temperature Waves to Separate Pyroelectric Currents from Nonpyroelectric Currents. Part I. Theory", *J. Appl. Phys.*, Vol. 53, pp. 8974-8879 (1982)

Han, K., A. Safari and R. E. Riman, " Colloidal Processing for Improved Piezoelectric Properties of Flexible 0-3 Ceramic-Polymer Composites", *J. Am. Ceram. Soc.*, Vol. 74 pp. 1699-1702 (1991)

Harrison, W. B., " Flexible Piezoelectric Organic Composites", *Proc. Workshop on Sonar Transducer Mat.*, P. L. Smith, R. C. Pohanka Eds., Naval Research Laboratory, 1976, pp. 257-268 (1976)

Higashihata, Y., J. Sako and T. Yagi, " Piezoelectricity of Vinylidene Fluoride-trifluoroethylene Copolymers", *Ferroelectrics*, Vol. 32, pp. 85-92 (1981)

Hill, C. R., " Calibration of Ultrasonic Beams for Biomedical Applications", *Phys. Med. Biol.*, Vol. 15, pp. 241-248 (1970)

IEEE Standard Definitions of Primary Ferroelectric Terms, ANSI/IEEE std. 180 (1986)

Ishikawa, K., K. Yorhikawa and N. Okada, " Size Effect in the Ferroelectric Phase Transition in $PbTiO_3$ Ultrafine Particles", *Phys. Rev. B: Condens. Matter*, Vol. 37, No.10, pp. 5832-5835 (1988)

Karasik, A. Ya., B. S. Rinkevichius and V. A. Zubov, " Laser Interferometry Principles" In B. S. Rinkevichius, ed., CRC Press, Inc., pp. 100-108 (1995)

Kawai, H., " The Piezoelectricity of Polyvinylidene Fluoride", *Jpn. J. Appl. Phys.*, Vol. 8, pp. 975-976 (1969)

Kholkin, A. L., Ch. Wütchrich, D. V. Taylor and N. Setter, " Interferometric Measurements of Electric Field-induced Displacements in Piezoelectric Thin Films", *Rev. Sci. Instrum*, Vol. 67, No. 5, pp. 1935-1941 (1996)

Kimura, K. and H. Ohigashi, " Generation of Very High-frequency Ultrasonic Waves Using Thin Films of Vinylidene Fluoride-Trifluoroethylene Copolymer", *J. Appl. Phys.* Vol. 61, pp. 4749-4754 (1987)

Koga, K. and H. Ohigashi, " Piezoelectricity and Related Properties of Vinylidene Fluoride and Trifluoroethylene Copolymers, *J. Appl. Phys.*, Vol. 59, pp. 2142- 2150 (1986)

Koizumi, N., N. Haikawa and H. Habuka, " Dielectric Behavior and Ferroelectric Transition of Copolymers of Vinylidene Fluoride and Trifluoroethylene", *Ferroelectrics*, Vol. 57, pp. 99-119 (1984)

Lewin, P. A., " Miniature Piezoelectric Polymer Ultrasonic Hydrophone Probes", *Ultrasonics*, Vol. 19, pp. 213-216 (1981)

Lewin, P. A. and R. C. Chivers, " Two Miniature Ceramic Ultrasonic Probes", *J. Phys. E: Sci. Instrum.*, Vol. 14, pp. 1420-1424 (1981)

Li, J. F., P. Moses, D. Viehland, "Simple, High-resolution Interferomenter for the Measurement of Frequency-dependent Complex Piezoelectric Responses in Ferroelectric Ceramics", *Rev. Sci. Instrum.*, Vol. 66, pp. 215-221 (1995)

Lovinger, L. A., " Ferroelectric Polymers", *Science*, Vol. 220, No. 4602, pp. 1115-1121 (1983)

Marra, S. P., K. T. Ramesh and A. S. Douglas, " The Mechanical and Electromechanical Properties of Calcium-modified Lead Titanate/ Trifluoroethylene 0-3 composites", *Smart Mat. Struct.*, Vol. 8, No. 1, pp.57-63 (1999)

Milne J. S. and S. H. Pyke, "Modified Sol-Gel Process for the Production of Lead Titanate Films", *J. Am. Cream. Soc.*, Vol. 74, No. 6, pp. 1407-1010 (1991)

Morse, M. P. and K. Uno Ingard, *Theoretical Acoustics*, Mc-Graw-Hill, New York, pp. 381-383 (1968)

Murphy C. E., T. Richardson and G. G. Roberts, " Thin-film Pyroelectric Inorganic/ Organic Composites", *Ferroelectics*, Vol. 134, pp. 189-194 (1992)

Newnham, R. E., D. P. Skinner and L. E. Cross, "Connectivity and Piezoelectric-Pyroelectric Composites", *Mat. Res. Bull.*, Vol. 13, pp. 525-536 (1978)

Ngoma, J. B., J. Y. Cavaille, J. Perez and F. Macchi, " Dielectric and Piezoelectric Properties of Copolymer-ferroelectric Composite", *Ferroelectrics*, Vol. 109, pp. 205-210 (1990)

Pauer, L. A., " Flexible Piezoelectric Materials", *IEEE Int'l Conv. Rec.*, pp. 1-5 (1973)

Platte, M., " A Polyvinylidene Fluoride Needle Hydrophone for Ultrasonic Applications", *Ultrasonics*, Vol. 23, pp. 113-118 (1985)

Ploss, B., B. Ploss, F.G. Shin, H.L. W. Chan and C. L. Choy, "Separate Poling of Inclusions and Matrix in PT/P(VDF-TrFE) 0-3 Composites", *Proc. 11th International Symposium on Applications of Ferroelectrics (ISAF XI)*, Montreux, Switzerland, 24-27 August, 1998, pp. 299-302 (1998)

Preston, R. C., D. R. Bacon, A. J. Livett and K. Rajendran, " PVDF Membrane Hydrophone Performance Properties and Their Relevance to the Measurement of the Acoustic Output of Medical Ultrasonic Equipment", *J. Phys. E: Sci Instrum.*, Vol. 16, pp. 786-796 (1983)

Royer, D. and E. Dieulesaint, " Optical Probing of the Mechanical Impulse Response of a Transducer", *Appl. Phys. Lett.*, Vol. 49, pp.1056-1058 (1986)

Royer, D. and V. Kmetik, " Measurement of Piezoelectric Constants Using an Optical Heterodyne Interferometer", *Electronics Lett.*, Vol. 28, pp. 1828-1830 (1992)

Sawyer, C. B. and C. H. Tower, "Rochelle Salt as a Dielectric", *Phys. Rev.*, Vol. 35, pp. 269-273 (1930)

Selfirdge, A. R., G. S. Kino and B. T. Khuri-Yakub, " A Theory for the Radiation Pattern of a Narrow-strip Acoustic Transducer", *Appl. Phys. Lett.*, Vol. 37, pp. 35-36 (1980)

Sessler, G. M., "Piezoelectricity in Polyvinylidene Fluoride", *J. Acoust. Soc. Am.*, Vol. 70, pp. 1596-1608 (1981)

Sharp, J. and E. Garn, "Use of Low-frequency Sinusoidal Temperature Waves to Separate Pyroelectric Currents from Nonpyroelectric Currents. Part II. Experiment", *J. Appl. Phys.*, Vol. 53, pp. 8980-8887 (1982)

Shombert, G. D., S. W. Smith and H. R. Gerald, " Angular Response of Miniature Ultrasonic Hydrophones", *Med. Phys.*, Vol. 9 (4), pp. 484-493 (1982)

Shotton, K. C., D. R. Bacon and R. M. Quilliam, "A PVDF Membrane Hydrophone for Operation in the Range 0.5 MHz to 15 MHz", *Ultrasonics*, Vol. 18, pp. 123-126 (1980)

Smith, A. R., " Are Hydrophones of Diameters 0.5 mm Small Enough to Characterize Diagnostic Ultrasound Equipment?", *Phys. Med. Biol.*, Vol. 34, No.11, pp. 1593-1607 (1989)

Tandon, R. P., R. Singh, V. Singh, N. H. Swami and V. K. Hans, "Ferroelectric Properties of Lead Titanate/ Polymer Composite and Its Applications in Hydrophones", *J. Mat. Sci. Lett.*, Vol. 11, pp. 883-885 (1992)

Tandon, R. P. and R. Singh, " Development and Characterisation of Composite Hydrophones", *Polymers & Polymer Composites*, Vol. 2, No. 5, pp. 287-292 (1994)

Ting, R. Y., " Evaluation of New Piezoelectric Composite Materials for Hydorphone Applications", *Ferroelectric*, Vol. 67, pp. 143-157 (1986)

Troilo, M. L., D. Damjanovic and R. E. Newnham, " Modified Lead Calcium Titanate Ceramics with a Relatively Large Dielectric Constant for Hydrophone Applications", *J. Am. Cream. Soc.*, Vol. 77, pp. 857-859 (1994)

Wang, H., Q. M. Zhang and L.E. Cross, " Piezoelectric, Dielectric, and Elastic Properties of Poly(Vinylidene Fluoride/ Trifluoroethylene)", *J. Appl. Phys.*, Vol. 74, pp. 3394-3398 (1993)

Wersing, W. K., K. Lubitz and J. Mohaupt, " Anisotropic Piezoelectric Effect in Modified $PbTiO_3$ Ceramics", *IEEE Trans. Ultrasonic, Ferroelectrics and Frequency Control*, Vol. 36 (4), pp. 424-433 (1989)

Yamada, T., T. Ueda and T. Kitayama, " Piezoelectricity of a High-content Lead Zirconate Titanate/ Polymer Composite", *J. Appl. Phys.*, Vol. 53, pp. 4328-4332 (1982)

Yamazaki, H. and T. Kitayama, " Pyroelectric Properties of Polymer-Ferroelectric Composite", *Ferroelectrics*, Vol. 33, pp. 147-153 (1981)

Zhang, Q. M., W. Y. Pan and L. E. Cross, " Laser Interferometer for the Study of Piezoelectric and Electrostrictive Strains", *J. Appl. Phys.*, Vol. 63, pp. 2492-2497 (1988)

Zhang, Q. Q., H. L. W. Chan and C. L. Choy, " Dielectric and Pyroelectric Properties of P(VDF-TrFE) and PCLT-P(VDF-TrFE) 0-3 Nanocomposite Films", *Composites: Part A*, Vol. 30, pp. 163-167 (1999)

List of Publications

Paper in Referred Journal:

H. L. W. Chan, S. T. Lau, K. W. Kwok, Q. Q. Zhang, Q. F. Zhou and C. L. Choy

" Nanocomposite Ultrasonic Hydrophones"

Sensors and Actuators A Physical, Vol. 75, pp. 252- 256 (1999).

S. T. Lau, K. W. Kwok, H. L. W. Chan and C. L. Choy

"PT/P(VDF-TrFE) Nanocomposites for Ultrasonic Hydrophone Applications"

Ferroelectrics, in press.

S. T. Lau, K. W. Kwok, H. L. W. Chan and C. L. Choy

"PT/P(VDF-TrFE) Nanocomposite Hydrophone Array", to be submitted.

Conference Presentations:

H. L. W. Chan, S. T. Lau, K. W. Kwok and C. L. Choy

PZT/P(VDF-TrFE) Nanocomposite Hydrophones for Ultrasonic Measurements

IEEE Ultrasonics Symposium (1998).

S. T. Lau, Q. F. Zhou, K. W. Kwok, H. L. W. Chan and C. L. Choy

PZT/P(VDF-TrFE) Nanocomposites for Ultrasonic Hydrophone Applications

The Tenth International Symposium on Electrets (ISE 10, 1999).